Robust Stability Assessment for Future Power Systems

by

Hung Dinh Nguyen

Submitted to the Department of Mechanical Engineering
in partial fulfillment of the requirements for the degree of

Doctor of Philosophy

at the

MASSACHUSETTS INSTITUTE OF TECHNOLOGY

February 2018

Author ..... Signature redacted
Department of Mechanical Engineering
Oct 11, 2017

Certified by ..... Signature redacted
Konstantin Turitsyn
Associate Professor
Thesis Supervisor

Accepted by ..... Signature redacted
Rohan Abeyaratne
Quentin Berg Professor of Mechanics; Graduate Officer

Robust Stability Assessment for Future Power Systems

by

Hung Dinh Nguyen

Submitted to the Department of Mechanical Engineering
on Oct 11, 2017, in partial fulfillment of the
requirements for the degree of
Doctor of Philosophy

Abstract

Loss of stability in electrical power systems may eventually lead to blackouts which, despite being rare, are extremely costly. However, ensuring system stability is a non-trivial task for several reasons. First, power grids, by nature, are complex nonlinear dynamical systems, so assessing and maintaining system stability is challenging mainly due to the co-existence of multiple equilibria and the lack of global stability. Second, the systems are subject to various sources of uncertainties. For example, the renewable energy injections may vary depending on the weather conditions. Unfortunately, existing security assessment may not be sufficient to verify system stability in the presence of such uncertainties. This thesis focuses on new scalable approaches for robust stability assessment applicable to three main types of stability, i.e., long-term voltage, transient, and small-signal stability.

In the first part of this thesis, I develop a novel computationally tractable technique for constructing Optimal Power Flow (OPF) feasibility (convex) subsets. For any inner point of the subset, the power flow problem is guaranteed to have a feasible solution which satisfies all the operational constraints considered in the corresponding OPF. This inner approximation technique is developed based on Brouwer's fixed point theorem as the existence of a solution can be verified through a self-mapping condition. The self-mapping condition along with other operational constraints are incorporated in an optimization problem to find the largest feasible subsets. Such an optimization problem is nonlinear, but any feasible solution will correspond to a valid OPF feasibility estimation. Simulation results tested on several IEEE test cases up to 300 buses show that the estimation covers a substantial fraction of the true feasible set.

Next, I introduce another inner approximation technique for estimating an attraction domain of a post-fault equilibrium based on contraction analysis. In particular, I construct a contraction region where the initial conditions are "forgotten", i.e., all trajectories starting from inside this region will exponentially converge to each other. An attraction basin is constructed by inscribing the largest ball in the contraction region. To verify contraction of a Differential-Algebraic Equation (DAE) system, I also show that one can rely on the analysis of extended virtual systems which are

reducible to the original one. Moreover, the Jacobians of the synthetic systems can always be expressed in a linear form of state variables because any polynomial system has a quadratic representation. This makes the synthetic system analysis more appropriate for contraction region estimation in a large scale.

In the final part of the thesis, I focus on small-signal stability assessment under load dynamic uncertainties. After introducing a generic impedance-based load model which can capture the uncertainty, I propose a new robust small signal (RSS) stability criterion. Semidefinite programming is used to find a structured Lyapunov matrix, and if it exists, the system is provably RSS stable. An important application of the criterion is to characterize operating regions which are safe from Hopf bifurcations.

The robust stability assessment techniques developed in this thesis primarily address the needs of a system operator in electrical power systems. The results, however, can be naturally extended to other nonlinear dynamical systems that arise in different fields such as biology, biomedicine, economics, neuron networks, and optimization.

As the robust assessment is based on sufficient conditions for stability, there is still room for development on reducing the inevitable conservatism. For example, for OPF feasibility region estimation, an important open question considers what tighter bounds on the nonlinear residual terms one can use instead of box type bounds. Also, for attraction basin problem, finding the optimal norms and metrics which result in the largest contraction domain is an interesting potential research question.

Thesis Supervisor: Konstantin Turitsyn
Title: Associate Professor

Acknowledgments

First of all, I would like to express my deep gratitude to my advisor Prof. Konstantin Turitsyn for the continuous support of not only my Ph.D. study but also my career. His guidance, thoughtfulness, and dedication were an inconceivable wellspring of support and inspiration. The profundity and expansiveness of his insight showed me the significance of applying the techniques from various fields to tackle challenging problems. Thanks to his support, I have had the opportunities of collaborating with incredible experts including Dvijotham Krishnamurthy and Zheng Zhang. Above all, I'm proud of being his student, and I wouldn't be the person I am today without him. He is truly a great advisor and "friend".

I am also very grateful for the assistance and advice provided by my doctoral committee. I would like to thank Prof. Slotine and Prof. Kirtley not only for their insightful comments and encouragement but also for the hard questions which incented me to widen my research from various perspectives. I took in new fascinating things from every meeting with Prof. Slotine, particularly about contraction analysis and nonlinear controls which reshaped my research. Prof. Kirtley guided me even before I came to MIT. I really enjoyed talking with him about practical power systems as well as academic life.

I thank my brilliant labmates and friends at MIT for the stimulating discussions, for helping me in touch times, and for all the fun we have had in the last four years. In particular, I am grateful to Petr for helping and teaching me various stuff even beyond research.

Last but not the least, I would like to express my utmost gratitude to my family, especially my wife who constantly supports me spiritually throughout my life. Thank her for giving birth to my adorable daughter. Thank both of you for making my life so special and full of joy.

Contents

List of Figures

List of Tables

Chapter 1

Introduction

Electrical systems are a critical infrastructure which provides essential services to modern societies. Even though people probably have known electricity since ancient times, the uses of electricity was very limited before Micheal Faraday discovered the principle of electricity generation based on electromagnetic induction in 1831 [38]. Since then the electricity revolution has commenced a global civilization in which electricity renovated many aspects of human's live, for instance, communication, entertainment, work, transportation, etc. Nowadays, all essential technologies, from sophisticated space stations to household fans, need electrical energy to function. Electric power systems are still and continue to be the backbone of modern life until after people can find more clean and convenient alternatives.

Designed to continuously transfer power from power plants that are typically centralized and reside in remote areas to wide-spread industrial and residential customers, power systems are undoubtedly one of the biggest and most complex man-made machines. Interconnected power systems may be extraordinarily large in size and may span across several countries or even continents. They may consist of millions of devices and components equipped with complicated hierarchical controls. That said, most of the time power systems are surprisingly stable and reliable. In US and Canada, the generally accepted Expected number of days per year of loss of load which is also known as Loss of Load Expectation (LOLE) is 1 day in 10 years [93].

1.1 Motivation

At the same time, power systems are considered both fragile and vulnerable. Over the last decades, there were several major blackouts over the world caused billions dollars worth of damage and loss of life. For example, the 2003 North American blackout contributed to 12 deaths and cost an estimated $6 billion, and the 1996 WSCC power outages cost up to $3 billion. More importantly, most major blackouts relate to instability phenomena such as voltage collapse in the 2003 North American and 2004 Athen blackout events, or small signal instability in the 1996 WSCC power outages. Instability issues have been increasingly recognized as a serious concern for the future of power systems.

There are different factors can contribute to the vulnerability of power systems and pose harsh challenges in ensuring the system stability. First, power systems, by nature, are complex nonlinear dynamical ones so to assess and maintain the system stability is challenging mainly due to the co-existence of multiple equilibria and the lack of global stability. Second, the systems are subject to various sources of uncertainties and disturbances which become especially pronounced at a high level of renewable penetration. Such uncertainties may jeopardize the system security by altering the equilibrium and the associated stability. Hence, if the issue of stability is not addressed thoroughly, the integration of renewable resources will be restricted. Third, typical power systems that are of an enormous size may consist of millions of variables; hence the operation and control problem becomes even impossible due to computational limitations and time constraints. For the same reason, many analytically elegant theories may only perform well for "small enough" systems.

Also, current stability assessment used in power system operation routines is mostly deterministic and only admits uncertainties to a limited extent. Typically, when it comes to uncertainties, the assessment will be performed on the so-called credible list consisting of a number of scenarios which are deemed most probable. This credible scenario based analysis may be competent if it engages most critical scenarios. For example, system operators can ensure N-1 security most of the time by

merely using an N-1 contingency list created based on practical experience. However, this approach is neither efficient nor effective in the case of continuous uncertainties, for example, uncertain injections, due to an infinite number of scenarios and the inability to pinpoint the most critical ones. These challenges motivated me to develop new robust feasibility and stability assessment techniques applicable to practical power systems under most common uncertainties.

1.2 Power system modeling, analysis, and stability assessment

Being a dynamical system, stability analysis of a power system inevitably involve the three fundamental questions below:

- Whether the system has (at least) an equilibrium?
- If an equilibrium exists, will it be (linearly) stable?
- If the equilibrium is (linearly) stable, whether the system is able to converge to it after transient?

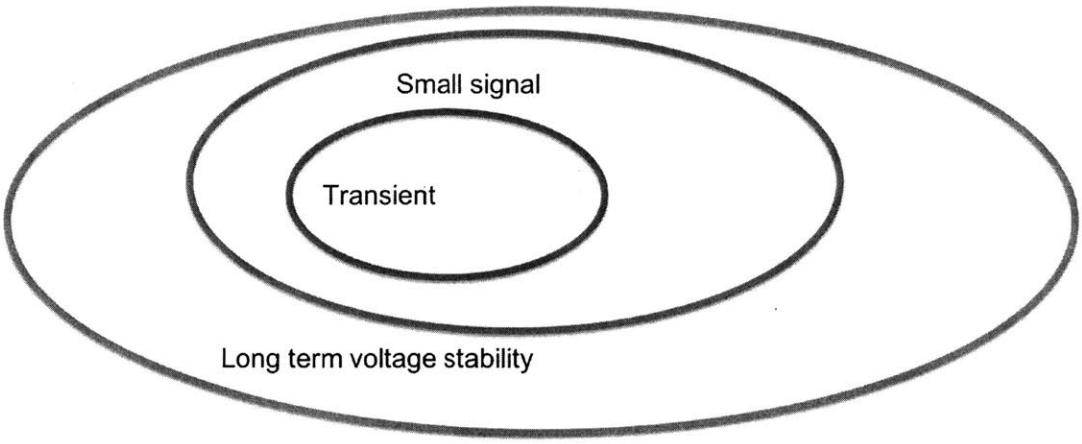

Figure 1-1: Three main types of stability

The three questions correspond to three different types of stability, i.e., long-term voltage, small-signal, and transient stability. Figure 1-1 shows the relationships among three notions of stability in which the concept associated with the inner oval implies that of the outer one. These relations can be seen by answering those questions backward.

To address these fundamental questions, we will rely on the DAE representation which consists of two following categories of equations. The first type is differential equations which describe the dynamics of dynamical components in the system, for instance, governors, generators, AVRs, FACTS, and loads, etc. The other category is algebraic equations which correspond to conservation laws, namely, Kirchoff laws. I consider a general form of DAE systems as the following.

$$\dot{\mathbf{x}} = \mathbf{f}(\mathbf{x}, \mathbf{y}), \tag{1.1}$$

$$0 = \mathbf{g}(\mathbf{x}, \mathbf{y}) \tag{1.2}$$

where $\mathbf{x} \in \mathbb{R}^{\mathbf{n}}$ and $\mathbf{y} \in \mathbb{R}^{\mathbf{m}}$ be the states and the algebraic variables. Note that the DAE system (1.1) and (1.2) can be viewed as a special case of singular perturbed systems below

$$\dot{\mathbf{x}} = \mathbf{f}(\mathbf{x}, \mathbf{y}), \tag{1.3}$$

$$\epsilon\dot{\mathbf{y}} = \mathbf{g}(\mathbf{x}, \mathbf{y}) \tag{1.4}$$

as the time constant ϵ goes to zero. In other words, DAE systems typically appear as a singular perturbation reduction of a multiscale differential system.

An important class of DAEs exclusively explored in the thesis is quadratic systems. The associated Jacobians linear in the system states offers many advantages for robust analysis, in particular, makes the proposed techniques scalable. Notably, the condition for small-signal stability can be cast as LMI problem which is supported by powerful SDP solvers. By the same token, linear programming based optimization formulation can be applied.

For a power system, a quadratic system appears naturally when rectangular representation is used, i.e., each quantity such as a nodal voltage or line current is represented by its real and imaginary parts. Nevertheless, the quadratic form is rather generic and is not restricted to rectangular form. A system in the polar coordinate, which contains trigonometric terms, can also be transformed to polynomials by introducing new variables. For example, one can introduce $x = \sin(\phi)$ and $y = \cos(\phi)$, along with extra relation $x^2 + y^2 = 1$. The new polynomials then can be further reduced to a quadratic system by, for instance, applying the theory of quadratic forms with $\mathbb{Q}$-coefficients was developed by H. Minkowski.

1.2.1 Steady state analysis

In steady state analysis, the problem of interest is to examine the equilibrium behavior of a power system where all dynamical transient already dies out. Such analysis can be simplified further by ignoring the details of the dynamical components, and at the same time, replacing those with aggregated models. Typical aggregated models are constant power, constant current, and constant impedance. By making these assumptions, one implicitly assumes that each device is equipped with an internal control which regulates the device to achieve a given reference input, for example, a fixed power consumption level. The simplified problem, which is so-called power flow problem, focuses on the interaction between the network and the aggregated components in steady state.

Power flow problem is a basic analysis typically appears in the form:

$$s_i = V_i \overline{\mathbf{YV}}, \tag{1.5}$$

if the constant power model is used, with $\mathbf{Y}$ is the admittance matrix and $\mathbf{V}$ is the nodal voltage vector. The power flow equation essentially describes the power conservation law applying to one node, or bus, of the system: the right-hand side is the total power coming out of the node. The solution to the power problem is important to other essential functions in power systems, in particular, operational planning

problems. The power flow equations are nonlinear so that they may have multiple solutions or no solution. The disappearance of solution indicates that the reference power level, which the component attempts to achieve, exceeds the maximum level dictated by the physical network, more specifically, constrained by the power transferred through the line. In practice, this leads to static voltage collapse and further, cascading blackouts. Finding such physical limit concerning power transfer becomes crucial to system operation.

It is difficult to identify such limit analytically, except for sufficient small and simple systems. In general, the limit is characterized numerically by, for instance, the notable homotopy method, Continuation Power Flow (CPF). By gradually increasing power along one direction and keep tracing the solution curve, the method can find the maximum power in such a direction. However, the maxima search is restricted to one direction, therefore, it turns out more computationally expensive or even impossible if all directions are considered in a multidimensional space. In contrast, analytic approaches provide an alternative solution with a significantly lower computational burden, thus being more efficient and appropriate approach for time-sensitive tasks.

Analytic methods can be used to certify voltage stability of a single configuration of injections (point-wise certificates [5, 89, 108]) or for a set of injections (region-wise certificates [35, 52, 71, 96]). Several advantages of the latter have been discussed in [68], including less computational costs and the ability to provide security measures.

Unfortunately, most region-wise approaches suffer from conservatism in which the characterized sets can become overly small. In recent work, Banach's fixed point theorem has been successfully applied to distribution systems and shown to construct large subsets of the stability region [7, 117, 123]. Among these, the results presented in [117] (denoted WBBP in our paper based on the authors' last names) dominate all previous results. However, the WBBP's solvability criterion requires a particular condition on the nominal point around which the solvability region approximation is constructed. In the regime where this condition is close to being violated, the estimated regions become conservative.

In Chapter 2, I do not aim to characterize analytic boundaries, but instead, I pro-

pose an optimization formulation to maximize the estimated regions. The developed technique is not only scalable but also is capable of constructing non-conservative sets of injections for which there exists a feasible solution satisfying all operational constraints.

1.2.2 Small-signal stability

In this section, I focus on small-signal stability (a.k.a linear stability, or exponential stability, or stability regarding first approximation [24]) of a dynamical system which concerns whether the system will be stable under small disturbances. By the way of explanation, small-signal stability is the local property associated with a particular equilibrium. Consider a dynamical system as the following:

$$\dot{\mathbf{x}} = A(\xi)\mathbf{x} \tag{1.6}$$

where ξ is a vector of parameters. For a given ξ, the system (1.6) is Linear Time Invariant (LTI). To check the small-signal stability of (1.6) at the 0 equilibrium, I rely on Theorem 1 below.

Theorem 1 *The following statements are equivalent.*

- *The* 0 *equilibrium is (globally) asymptotic stable (exponential stable)*
- *All eigenvalues of the system matrix A have negative real parts*
- $\forall Q \succ 0,\ Q = Q^T,\ \exists! P \prec 0,\ P = P^T\ s.t.\ A^T P + PA = -Q$

The second statement is widely used, and linear stability verification often requires an eigenvalue analysis of the system matrix.

However, if ξ is contains uncertain parameters and belongs to an uncertain set Δ, system (1.6) has a linear parameter varying (LPV) form. More importantly, if system (1.6) is resulted from linerization or virtual displacement differentiation of a quadratic system, the matrix-valued function $A(\cdot)$ is affine in parameters (in particular, the

system states), i.e.

$$A(\xi) = A_0 + \sum_i \xi_i A_i. \tag{1.7}$$

In addition, LPV system (1.6) admits an polytopic representation if the set Δ is a polytope. Such affine polytopic LPV can be used to describe power system when the operating points vary. The details will be presented in Chapter 3.

It is worth mentioning that eigenvalue analysis is not suitable for a system with uncertain parameters because the eigenvalues may behave very differently while changing the parameters. The critical eigenvalues may alter and become non-critical ones. At the same time, very varying parameters may cause any first order approximation to fail to predict or track the eigenvalues. On the other hand, the last condition which requires a solution of Lyapunov equation is more convenient. As long as one can show the existence of a symmetric definite matrix P, for example, by solving a semi-infinite LMI problem, the system will be exponential stable. In this thesis, I therefore leverage the latter condition to develop robust stability assessment.

1.2.3 Transient stability

For a transient stability problem, one needs to verify whether the system can converge to a stable equilibrium after being subject to a large disturbance. In power systems, a large disturbance is a sudden even, for instance, a line fault or generator tripped which causes large power imbalances forcing the system to move away from the pre-fault equilibrium. After the fault is cleared, normally a new balance state will be established, and it is important to certify if the system can converge to the new equilibrium. Failure to converge may place the system in a dangerous situation which is often, unfortunately, followed by a severe blackout.

Transient stability assessment is a complicated problem mainly due to the nonlinearity of power systems and the lack of the global stability. Therefore, many assumptions need to make in order to simplify the problem, most notably the voltages are fixed, and the loads' impedances are constant. These assumptions lead to

the well-known swing equations:

$$M\ddot{\theta} = P_m - P_e \tag{1.8}$$

where only the rotor angle θ is considered. The mismatch between the mechanical power P_m and the electrical power P_e will govern the generator characterized by the inertial M.

There are two main approaches currently used for transient stability assessment. The first one includes numerical techniques which verify stability via time-domain simulations. This approach is widely used because it can give illustrative results and it is considered easy to implement on most systems. However, the numerical techniques may be time-consuming and may need to rerun when some parameters or conditions change. On the other hand, the second approach, which relies on Lyapunov or energy functions, can be reused as the parameters change, and it doesn't require numerical integration. One drawback of the latter approach is that one needs to seek a good function for each system as a general form may not be available. In Chapter 3, I present a new method based on contraction analysis for assessing transient stability without a need to run time-domain simulations or to construct a tailored Lyapunov function.

1.3 Problem statement & Contributions

To response to the three fundamental issues of power system stability mentioned above and to put robust stability assessment in power system operation practice, I will consider the following problems in the scope of this thesis.

1. Characterize feasible injection sets with which the power flow problem has at least one solution satisfying all operational constraints.

2. Identify robust small-signal stability region in the system state space

3. Construct the contraction region where the initial conditions are "forgotten" in

the system state space

4. Estimate the invariant region where all trajectories if they start from inside this region will stay encompassed at all time.

5. Under which condition the system will be small-signal stable will all load dynamics.

Each problem will be addressed in details in the subsequent chapters while shining new light on three major types of stability. Novel sufficient certificate for stability (worst case scenarios), and scalable techniques for inner approximation are the main contributions of this work. In particular, they include i) developing a framework for constructing inner approximation of the OPF feasibility set based on Brouwer's fixed point theorem, ii) showing that the contraction of a DAE system can be verified through virtual extended dynamical systems which are reducible to the original one, iii) proposing scalable techniques for estimating the contraction region in different norms, iv) proposing a D-stability like condition for robust small-signal stability under uncertain load dynamics.

An important criterion to follow in this thesis is that the developed approaches must be i) as general as possible, ii) scalable/tractable, and ii) applicable to industrial graded systems. The first requirement means that no additional assumptions are made. For example, I consider the full A/C power flow equations instead of the linearized D/C ones. Also, the techniques are not restricted to either power flows or DAEs systems arising in power systems, but are applicable to any quadratic systems.

1.4 Thesis outline

The rest of the thesis is structured as follows. In Chapter 2, I propose a sufficient condition that guarantees the existence of a power flow solution. Then an optimization problem is formulated to seek the optimal feasible subsets which result in feasible power flow solutions. Next, in Chapter 3, I focus on contraction analysis for nonlinear DAE systems. The contraction in different norms and corresponding contraction

region techniques are introduced. For 2 norm, I recover the well-known quadratic stability test and propose a scalable method for solving LPV problem. In Chapter 4, I revisit the LPV problem in the context of uncertain load dynamics and propose a robust stability criterion. The last chapter is dedicated to conclusions and discussions on possible extensions and applications.

Chapter 2

OPF Feasibility Subset Estimation

This chapter aims to unravel some of the mysteries surrounding the existence of power flow solutions, in particular, when power flow problem has a feasible solution satisfying operational constraints. Based on such understanding, I propose a scalable optimization technique for estimating convex inner approximations of the power flow feasibility sets. The proposed framework relies on Brouwer fixed point theorem. The self-mapping property of fixed point form of power flow equations is certified using the adaptive bounding of nonlinear and uncertain terms. The resulting nonlinear optimization problem is non-convex, however every feasible solution defines a valid inner approximation and the number of variables scales linearly with the system size. The framework can naturally be applied to other nonlinear equations with affine dependence on inputs. Standard IEEE cases up to 300 buses are used to illustrate the scalability of the approach. The results show that the approximated regions are not conservative and cover large fractions of the true feasible domains.

2.1 Introduction

The ACOPF representation of power system forms a foundation for most of the normal and emergency decisions in power systems. Traditional ACOPF formulation targets the problem of finding the most economical generator dispatch admitting a voltage profile that satisfies operational constraints. The ACOPF is solved by

Indepent System Operators in different contexts on multiple time intervals ranging from a year for planning purposes to 5 minutes for real-time market clearing. Since it was first introduced in 1962, the OPF problem has been one of the most active research areas in power system community. Being an NP-hard problem, it still lacks a scalable and reliable optimization algorithm [13] although last years were marked by a tremendous progress in this area [22,37,69].

Relaxations of power flow equations provide a means for approximating the non-convex feasibility sets in voltage/phase domain with tractable convex envelopes. In many practically relevant situations, the optimization of the relaxed problem provides the globally optimal solution for the original problem as well. By the nature of outer approximations, convex relaxations can be naturally used for establishing certificates of insolvability of power flow equations [77] and can be naturally used to for estimation of loadability margins. At the same time, the reverse problem of establishing inner approximations of feasibility sets appears in many contexts and cannot be solved using traditional convex relaxations of the OPF. Most naturally, inner approximations of feasibility sets in power injection space can be used to assess the robustness of a given operating point to uncertainties in renewable or load power fluctuations. Similar problem formulations also appear in the context of decentralized decision making where properly shaped approximations of feasibility sets allow for independent redispatch of power resources in different areas without the need for communication or other forms of coordination between the areas.

Like many other power system problems, the original setting for construction of power flow feasibility sets was introduced by Schweppe and collaborators in late 70s [35]. The first practical algorithms based on fixed point iteration appeared in early 80s [118]. In Soviet Union, the parallel effort focused on the problem of constructing solvability sets for static swing equations [12, 110]. More recently, new algorithms based on different fixed point iterations have been proposed for radial distribution grids without PV buses [7,83,117,123], decoupled power flow models equivalent to resistive networks with constant power flows [103] and lossless power systems [101,102]. Although more general approaches that don't rely on special modeling assumptions

have been proposed in the literature [18,33,34], they typically suffer from either poor scalability or high conservativeness or both.

In this chapter I develop a novel algorithmic approach to constructing power flow feasibility domains that can be applicable to the most general formulation of power flow equations without any restrictions on the network and bus types. The size of the resulting regions is comparable to the actual feasibility domain even for large-scale models. Unlike many of the other approaches cited above the regions are not represented by a closed-form expression, but are constructed via a nonlinear optimization problem that finds the largest region in either power-injection or voltage space. This optimzation problem, although being non-convex and generally NP-hard, is a viable alternative to the purely analytic solutions. Any feasible solution of the optimization, which is guaranteed to exists establishes a region where the solution of the original power flow is guaranteed to exist and satisfy feasibility constraints. The complexity of the optimization is a constant times higher than that of the traditional optimal power flow and many of the relaxations originally developed for OPF can be potentially extended to the proposed optimization problem as well.

The structure of the rest of the chapter is the following. In section 2.2 I introduce the general form of the ACOPF and formally define the feasible set. Next, in section 2.3 I develop a solvability criterion for affine-input system based on Brouwer's fixed point theorem which is used in [10]. I also formulate an optimization problem which maximizes the inner approximation set. In section 2.4, I apply the developed solvability criterion to power flow equations in an admittance base representation, and I illustrate how to incorporate the operational constraints. Section 2.5 represents an LP relaxation of the nonlinear optimization problem in section 2.3. In the simulation section, I demonstrate the construction technique by simulating several IEEE test cases provided in MATPOWER package.

2.2 Notation and an OPF formulation

The following set of notation which will be used throughout this chapter.

$\mathbb{C}$: Set of complex numbers

$[\![\boldsymbol{x}]\!] = \text{diag}(\boldsymbol{x})$ for $\boldsymbol{x} \in \mathbb{C}^n, \overline{\boldsymbol{x}}$: Conjugate of $\boldsymbol{x} \in \mathbb{C}^n$

$\mathbf{1}$: Vector of compatible size with all entries equal to 1

$\|\boldsymbol{x}\| = \|\boldsymbol{x}\|_\infty = \max_i x_i$ for $\boldsymbol{x} \in \mathbb{C}^n$

$\|\boldsymbol{A}\| = \|\boldsymbol{A}\|_\infty = \max_i \sum_j |A_{ij}|$ for $\boldsymbol{A} \in \mathbb{C}^{n\times n}$

$$\frac{\partial f}{\partial x} = \begin{pmatrix} \frac{\partial f_1}{\partial x_1} & \cdots & \frac{\partial f_n}{\partial x_1} \\ \vdots & \vdots & \vdots \\ \frac{\partial f_n}{\partial x_1} & \cdots & \frac{\partial f_n}{\partial x_n} \end{pmatrix} \text{ for } f : \mathbb{C}^n \mapsto \mathbb{C}^n$$

$\mathcal{V}$: the graph of a system

$\mathcal{L}, \mathcal{G}$: the load and generator sets

V_k, θ_k : the voltage magnitude and angle at bus $k \in \mathcal{V}$

P_k, Q_k : the active and reactive power injecting to the network from bus $k \in \mathcal{V}$

$\mathcal{E}$: a set of unordered lines $e = (k, l) = (l, k); k, l \in \mathcal{V}$

$\text{from}(e), \text{to}(e) \in \mathcal{V}$: the sending and receiving bus of line e

i_e, I_e, s_e : the complex current and its magnitude, and power flow over line e

$x \odot y$: For $x, y \in \mathbb{R}^n$, $x \odot y \in \mathbb{R}^n$ with $[x \odot y]_i = x_i y_i$

I study a general optimal power flow problem (OPF) with the following constraints:

$$P_k + jQ_k = \sum_l V_k \overline{Y}_{kl} V_l \exp(-j\theta_e), \quad k \in (\mathcal{L}, \mathcal{G}) \tag{2.1}$$

$$V_k^{min} \leq V_k \leq V_k^{max}, \quad k \in \mathcal{L} \tag{2.2}$$

$$\theta_e^{min} \leq \theta_e \leq \theta_e^{max}, \quad e \in \mathcal{E} \tag{2.3}$$

$$P_k^{min} \leq P_k \leq P_k^{max}, \quad k \in \mathcal{G} \tag{2.4a}$$

$$Q_k^{min} \leq Q_k \leq Q_k^{max}, \quad k \in \mathcal{G} \tag{2.4b}$$

$$I_e \leq I_e^{max}, \quad e \in \mathcal{E} \tag{2.5}$$

where each bus $k \in \mathcal{V}$ of the system is characterized by a complex voltage $v_k = V_k \exp(\theta_k)$ and apparent power generation/consumption $P_k + jQ_k$. For each edge or line e connecting bus k and bus l, I define an angle difference $\theta_e = \theta_k - \theta_l$. The complex current i_e which flows through the line e has the magnitude of I_e.

The first set of equations (2.1) is the AC power flow equations which present the local power balance relation at each bus. When such power balance is achieved, the system is said to be in its steady state. The rest of the OPF constraints are operational ones which confine the voltage magnitudes, angle separations over branches, power generations, and current flows within acceptable ranges. Here I assume that all the operational requirements are box constraints, even though it is possible to extend to nonlinear ones.

In a typical OPF, the state variables can be the load voltages, generator angles, and transmitted currents. The set of control/input variables can be either the generator settings, i.e. the active power outputs and voltage reference values or the loading levels if an OPF-based load shedding problem is invoked. Even though other discrete inputs such as tap changer positions also can be incorporated in an OPF, in the scope of this thesis, I only focus on the power-related inputs, i.e. power generation and consumption. More compactly, I use the notation $\mathbf{u}$ to denote the set of inputs and use $\mathbf{x}$ to denote the others.

In the following, I formally define the main focus of the chapter, the feasible set

of the OPF problem.

Definition 2 *The feasible set of the OPF problem is the set of control variables,* $\mathbf{u}$*, with which the power flow equations* (2.1) *has at least one feasible solution which satisfies all concerned operational constraints* (2.2) *to* (2.5)*.*

Such OPF feasible set can be non-convex primarily due to the nonlinear power flow equations. As a result, the OPF becomes a non-convex optimization problem which is challenging and inefficient to solve. I therefore introduce a framework to provide "nice" search space for the OPF. In particular, I inscribe simple convex sets inside the original non-convex feasible region. To characterize the feasible set, it is essential to understand the solvability of the power flow equations.

2.3 The solvability of input-affine systems

In this section, I develop our general approach for deriving sufficient conditions for existence of solution to a nonlinear system within a certain set. Our approach applies to a broad class of nonlinear systems that satisfy two important properties: they depend affinely on the input variables, and their nonlinearity can be expressed as a product of simple nonlinearites (sin/cos/polynomial etc.) that can be bounded easily.

Consider a following set of nonlinear equations on $x \in \mathbb{R}^n$ that depend in affine way on the vector of inputs $u \in \mathbb{R}^k$ represented:

$$Mf(x) - Ru = 0 \tag{2.6}$$

Here $M \in \mathbb{R}^{n\times m}$ $R \in \mathbb{R}^{n\times k}$, and $f = [f_1, f_2, \ldots, f_m] : \mathbb{R}^n \to \mathbb{R}^m$. Assume also that I am given a *base solution* $u^\star \in \mathbb{R}^k, x^\star \in \mathbb{R}^n$ such that $Ru^\star = Mf(x^\star)$. Let

$$J(x) = M \left.\frac{\partial f}{\partial x}\right|_x, \; [J(x)]_{ij} = \sum_{k=1}^{m} M_{ik} \frac{\partial f_k}{\partial x_j}, \tag{2.7}$$

denote the Jacobian of the system of equations. Furthermore, let $J_\star = J(x^\star)$ be the Jacobian evaluated at the base solution. In the following I assume that this Jacobian

is nonsingular, and $J_\star^{-1}$ exists.

In the following paragraphs I will derive a fixed-point point representation of this system that allows for simple certification of solution existence. This solvability certificate is based on the bounds on nonlinearity in the neighborhood of the base operating point. Compact representation of the corresponding convex regions in input, state and nonlinear image spaces are introduced to facilitate our development:

Definition 3 *For any differentiable nonlinear map $f : \mathbb{R}^n \to \mathbb{R}^m$ and a base point $x^\star \in \mathbb{R}^n$ I define two linear "residual" operators $\delta f(x)$ and $\delta_2 f(x)$ as the following combinations of $f(x)$, base value $f^\star = f(x^\star)$ and base Jacobian $\partial f/\partial x|_{x^\star}$:*

$$\delta f(x) = f(x) - f^\star \tag{2.8}$$

$$\delta_2 f(x) = f(x) - f^\star - \frac{\partial f}{\partial x}\Big|_{x=x^\star} \cdot (x - x^\star) \tag{2.9}$$

These operators represent the error in the zeroeth order (constant) and first order (Jacobian based) approximation of the function $f(x)$ around $x = x^\star$. The following corollary allows us to compute the operator for the element-wise product of two nonlinear functions given the operators corresponding to each function:

Corollary 1 *For the element-wise product of two vector functions $f(x) \odot g(x)$ one has*

$$\delta_2\{f \odot g\} = \delta f \odot \delta g + \delta_2 f \odot g^\star + f^\star \odot \delta_2 g \tag{2.10}$$

Proof 1 *The proof directly follows the definitions of the two operators $\delta f(x)$ and $\delta_2 f(x)$.*

The defined residual operator allows for compact representation of the original system (9) in the fixed-point form:

$$x = x^\star + J_\star^{-1} R(u - u^\star) - J_\star^{-1} M \delta_2 f(x). \tag{2.11}$$

or, even more compactly as

$$\tilde{x} = F(\tilde{x}) = J_\star^{-1} R\tilde{u} + \phi(\tilde{x}), \tag{2.12}$$

where $\tilde{u} = u - u^\star$ denote the deviations of the variable and input vector from the base solution and $\phi(\tilde{x}) = -J_\star^{-1} M \delta_2 f(x^\star + \tilde{x})$ represents the nonlinear corrections.

Definition 4 *The admissibility polytope family $\mathcal{A}(\ell_x)$ defines the following non-empty polytope for any non-zero matrix of bounds $\ell_x = [-\ell_x^-, \ell_x^+] \in \mathbb{R}_+^{K\times 2}$:*

$$\mathcal{A}(\ell_x) = \{\tilde{x} \in \mathbb{R}^n | \pm A\tilde{x} \leq \ell_x^\pm\} \tag{2.13}$$

where $\pm A\tilde{x} \leq \ell_x^\pm$ is shorthand for the following set of inequalities:

$$\{A\tilde{x} \leq \ell_x^+, -A\tilde{x} \leq \ell_x^-\} \equiv -\ell_x^- \leq A\tilde{x} \leq \ell_x^+$$

The polytope $\mathcal{A}(\ell_x)$ will be used to establish the neigborhoods of the base operating point where the solution is guaranteed to exist. Extra conditions on ℓ_x can be then used to impose additional "feasibility" constraints on the solution, such as voltage and current bounds for power systems. To prove the existence of the solution, one needs to bound the nonlinear residual terms. Whenever the system is inside the admissibility polytope, i.e. $\tilde{x} \in \mathcal{A}(\ell_x)$, the nonlinear residual terms $\delta_2 f \in \mathbb{R}^m$ can be also naturally bounded. I assume that these bounds are formalized via another polytope family:

Definition 5 *Given $\mathcal{A}(\ell_x)$ and a base solution $x^\star$, the nonlinear map $f : \mathbb{R}^n \to \mathbb{R}^m$ satisfies the nonlinear bound polytope family $\mathcal{N}(\ell_x)$ if*

$$\tilde{x} \in \mathcal{A}(\ell_x) \Longrightarrow \delta_2 f(x^\star + \tilde{x}) \in \mathcal{N}(\ell_x) \tag{2.14}$$

A simple, though not the most general and tight nonlinear polytope family utilized

in this thesis has a simple form

$$\mathcal{N}(\ell_x) = \{z \in \mathbb{R}^m | \pm z_k \leq \delta_2 f_k^{\pm}(\ell_x)\} \tag{2.15}$$

I often drop the dependence on ℓ_x since it is implicit from the context. Given bounds of the kind above, I can derive bounds on products of nonlinearities appearing in most common representations of power flow equations:

Lemma 6 *Bounds on the products can be characterized in the following way:*

$$\begin{aligned}\delta_2^{\pm}\{f \odot g\} = &\max\{\delta f^+ \odot \delta g^{\pm}, \delta f^- \odot \delta g^{\mp}\} \\ &+ f^\star \odot \delta_2 g^{\pm} + \delta_2 f^{\pm} \odot g^\star\end{aligned} \tag{2.16}$$

which is shorthand for

$$\begin{aligned}\delta_2^{+}\{f \odot g\} = &\max\{\delta f^+ \odot \delta g^{+}, \delta f^- \odot \delta g^{-}\} \\ &+ f^\star \cdot \delta_2 g^{+} + \delta_2 f^{+} \cdot g^\star \\ \delta_2^{-}\{f \odot g\} = &\max\{\delta f^+ \odot \delta g^{-}, \delta f^- \odot \delta g^{+}\} \\ &+ f^\star \odot \delta_2 g^{-} + \delta_2 f^{-} \odot g^\star\end{aligned}$$

Our next goal is to prove the existence of solutions to (2.12) with $\tilde{x} \in \mathcal{A}(\ell_x)$. The following form of the Brouwer fixed point theorem facilitates this:

Theorem 7 *(Self-mapping condition) Suppose there exist bounds $\ell_x = [-\ell_x^-, \ell_x^+]$ such that*

$$\tilde{x} \in \mathcal{A}(\ell_x) \implies F(\tilde{x}) \in \mathcal{A}(\ell_x). \tag{2.17}$$

Then (2.12) is solvable and has at least one solution $\tilde{x} \in \mathcal{A}(\ell_x)$.

Proof 2 *Condition (2.17) ensures that F maps the compact convex set $\mathcal{A}(\ell_x)$ onto itself. Hence, by Brouwer's fixed point theorem, there exists at least one solution to (2.12) in $\mathcal{A}(\ell_x)$.*

In the above theorem, I assumed that the inputs $\tilde{u}$ are perfectly known. However, in the applications targeted by this thesis (OPF with uncertain generation or loads, for example), the inputs may not be known perfectly. In the following, I assume that the deviations of the inputs $\tilde{u}$ belong to a structured box-shaped uncertainty set $\mathcal{U}$ defined as $-\ell_u^- \leq \tilde{u} \leq \ell_u^+$ or more compactly as

$$\mathcal{U}(\ell_u) = \left\{\tilde{u} \in \mathbb{R}^L | \pm\tilde{u} \leq \ell_u^{\pm}\right\} \tag{2.18}$$

Problem Statement: Construct a region $\mathcal{U}(\ell_u) \subseteq \mathbb{R}^L$ such that

$$\mathcal{U}(\ell_u) \subseteq \mathbf{U} = \{\tilde{u} : (\exists x : \tilde{x} \in \mathcal{A}(\ell_x), \tilde{x} = F(\tilde{x}))\} \tag{2.19}$$

The following Lemma 8 and Theorem 9 establish a central result of this work:

Lemma 8 *Given the nonlinear system described by the equation* (2.12) *the admissibility and nonlinear bound polytope families* $\mathcal{A}(\ell_x)$ *and* $\mathcal{N}(\ell_x)$*, if* $\tilde{x} \in \mathcal{A}(\ell_x)$ *then the nonlinear correction term* $\phi(\tilde{x})$ *is contained in the polytope* $\mathcal{A}(\tau(\ell_x))$*, i.e.* $\phi(\tilde{x}) \in \mathcal{A}(\tau(\ell_x))$ *with* $\tau(\ell_x) = [-\tau^-(\ell_x), \tau^+(\ell_x)] \in \mathbb{R}_+^{K\times 2}$ *given by*

$$\tau^{\pm}(\ell_x) = C^+\delta_2 f^{\pm}(\ell_x) + C^-\delta_2 f^{\mp}(\ell_x) \tag{2.20}$$

where $C^+ - C^- = -AJ_\star^{-1}M$ *and* $C_{ij}^{\pm} \geq 0$.

Proof 3 *This bound generalizes the definition of a matrix* $\infty-$ *norm and follows directly from bounding the individual contributions to* $A\phi(\tilde{x})$ *with the help of the non-negativity of* $\delta_2 f^{\pm}$.

Corollary 2 *The map* $\tau(\ell_x) : \mathbb{R}_+^{K\times 2} \to \mathbb{R}_+^{K\times 2}$ *is monotone that is, if*

$$-\ell_x'^- \leq -\ell_x^- \leq \ell_x^+ \leq \ell_x'^+$$

then

$$-\tau'^- \leq -\tau^- \leq \tau^+ \leq \tau'^+.$$

The corollary 2 formalizes a trivial observation that increasing the region of variable variations can only increase the region of possible nonlinear corrections.

Theorem 9 *Given all the definitions above, assume that there exists a matrix ℓ_x, such that the matrix $\tau(\ell_x)$ as defined in the Lemma 8 satisfies $\tau^{\pm}(\ell_x) \leq \ell_x^{\pm}$. Then, for any $\tilde{u}$ such that $J_\star^{-1} R\tilde{u} \in \mathcal{A}(\ell_x - \tau(\ell_x))$ there exists at least one admissible solution $\tilde{x}^\star \in \mathcal{A}(\ell_x)$ of the equation (2.12).*

Proof 4 *The right hand side of (2.12) is contained in the polytope $\mathcal{A}(\ell_x)$, therefore the map $F(\tilde{x}) = J_\star^{-1}\tilde{s} + \phi(\tilde{x})$ maps the compact convex set $\mathcal{A}(\ell_x)$ onto itself. Thus, according to Brouwer's theorem, there exists a fixed point $\tilde{x}^\star = F(\tilde{x}^\star)$ inside $\mathcal{A}(\ell_x)$.*

Corollary 3 *The admissible solution $\tilde{x}^\star \in \mathcal{A}(\ell_x)$ is guaranteed to exists for every element $\tilde{u}$ inside a box-shaped uncertainty set $\mathcal{U}(\ell_u)$ whenever the condition*

$$\ell_x^{\pm} \geq \sigma^{\pm}(\ell_u) + \tau^{\pm}(\ell_x) \tag{2.21}$$

$$\sigma^{\pm}(\ell_u) = B^{+}\ell_u^{\pm} + B^{-}\ell_u^{\mp} \tag{2.22}$$

is satisfied with $B^+ - B^- = AJ_\star^{-1}R$ and $B_{ij}^{\pm} \geq 0$.

Proof 5 *Whenever $\tilde{u} \in \mathcal{U}(\ell_u)$, one has $-\sigma^-(\tilde{u}) \leq AJ_\star^{-1}R\tilde{u} \leq \sigma^+(\tilde{u})$, hence the inputs satisfy the conditions of Theorem 9.*

Figure 2-1 illustrates the self-mapping condition (2.21). The $\triangleright$ symbol indicates where the polytopes are.

2.3.1 Optimal certificates

There are many matrices ℓ_x and corresponding polytopes $\mathcal{A}(\ell_x)$ satisfying the conditions of the theorem 9. Each of the corresponding certificates establishes solvability of different regions in the input space. In most applications, one is interested in finding the largest region in the input space. However the definition of the region size may differ depending on the context. Below I formulate several optimization problems that

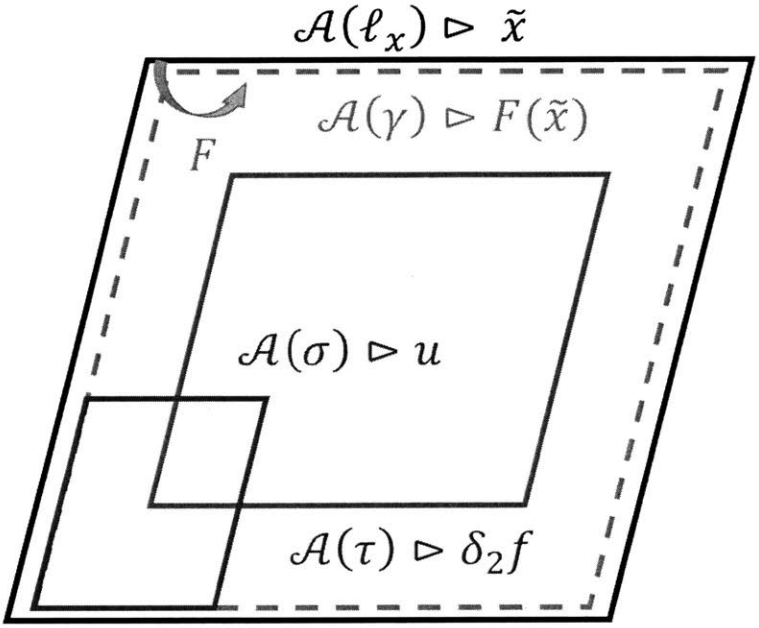

Figure 2-1: Self-mapping function for a fixed-point form

define solvability certificates that are optimal with respect to common performance specifications.

Loadability certificate

A classical problem arising in many domains, including power systems, is to characterize the limits of system loadability. In this case, the only column of the matrix R defines the stress direction, while the positive scalar u defines the loadability level. The goal of loadability analysis is to find the maximal level u for which the solution still exists. According to the corollary 3, all u satisfying $-\ell_u^- \leq u \leq \ell_u^+$ are certified to have a solution, hence the following problem formulation:

$$\max_{\ell_x, \ell_u} \ell_u^+ \tag{2.23a}$$

subject to :

$$\ell_x^\pm \geq \sigma^\pm(\ell_u) + \tau^\pm(\ell_x) \tag{2.23b}$$

with $\tau^{\pm}(\ell_x)$ and $\sigma^{\pm}(\ell_u)$ given by the equations (2.20) and (2.22) respectively. Note, that in accordance to the corollary 2, τ is a nonlinear and monotonically increasing function ℓ_x, Hence, the optimization problem is non-convex and is generally hard. On the other hand, it should be emphasized, that any solution of (2.23), even non-optimal ones defines a valid and mathematically rigorous certificate. So, the natural strategy is to solve this problem using local optimization strategies. The local search is guaranteed to produce some feasible certificate because $\ell_x = 0$ is a feasible starting point and the map $\tau(\ell_x)$ characterizes the behavior of second order residuals, and has superlinear behavior at small enough ℓ_x for the properly chosen nonlinear bounds.

Feasibility constraints The problem (2.23) can be complemented with extra constraints compliant with feasibility requirements to ensure the existence of feasible solutions. In particular, the voltage level and angle separation limits can be easily imposed with the element-wise upper bounds on the fixed point variables, i.e., $\ell_x \leq \ell_x^U$. In contrast, the reactive power generation and thermal constraints, that have a power flow representation, require bounding the fixed point map. To see this, we consider in the following a more general constraints

$$g(x) \leq 0 \tag{2.24}$$

where $g(x)$ can be represented in terms of the nonlinear power flow functions, i.e. $g(x) = Tf(x)$. Both thermal and reactive power generation constraints can be expressed in this general form with appropriate constant matrix T. Moreover, using the definition of the residual operator $\delta_2 f$, yields the below expansion.

$$\begin{aligned} g(x) &= g_\star + TL\tilde{x} + T\delta_2 f \\ &= g_\star + TLJ_\star^{-1}R\delta u + (T - TLB)\delta_2 f \end{aligned} \tag{2.25}$$

where $L = \frac{\partial f}{\partial x}|_{x_\star}$. The second equality can be derived with the help of the fixed point equation (2.12). Furthermore, let $D = TLJ_\star^{-1}R$ and $E = T - TLB$. An upper bound of the function $g(x)$ in constraint (2.24) can be estimated using ∞ norm type bound

(2.20) and (2.22). Then instead of the original feasibility constraints (2.24), one can impose the below conditions on such an upper bound.

$$D^+\ell_u^+ + D^-\ell_u^- + E^+\delta_2 f^+ + E^-\delta_2 f^- \leq -g_\star \tag{2.26}$$

Robustness certificate

In another important class of applications the goal is to characterize the robustness of a given with respect to some uncertain inputs. In power system context it could be the robustness with respect to load or renewable fluctuations. Assume, without the loss of generality that the input variable representation is chosen in a way that all the components of $\tilde{u}$ are uniformly uncertain around with uncertainty set centered at zero. In this case the goal is to find the largest value of λ, such that the for any $\tilde{u}$ satisfying $\|\tilde{u}\|_\infty \leq \lambda$ there exists a feasible solution to the original system of equations. This problem can be naturally solved by maximizing λ subject to (2.23b) and additional uniformity conditions $[\ell_u^\pm]_k = \lambda$.

Chance constraint certificates

In another popular setting one assumes some probability distribution of the uncertain inputs and aims to find a polytope that maximizes the chance of randomly sampled inputs certified to have a solution. This problem can be also naturally represented in the generic certificate optimization framework. Assume, without major loss of generality that the inputs are i.i.d. normal variables. In this case, the probability $\mathbf{P}$ of a random sample falling inside the box $\mathcal{U}(\ell_u)$ is given by

$$\log \mathbf{P}(\ell_u) = \frac{1}{2}\sum_k \operatorname{erf}\left(\frac{[\ell_u^+]_k}{\sqrt{2}}\right) - \operatorname{erf}\left(-\frac{[\ell_u^-]_k}{\sqrt{2}}\right) \tag{2.27}$$

The maximal chance certificate is established by maximizing $\log \mathbf{P}(\ell_u)$ subject to (2.23b) and any additional feasibility constraints.

2.4 OPF feasibility

In this section we apply the framework developed in previous sections to the power flow feasibility problem. There are many possible ways to represent the power flow equations in the form (4.1) amenable to the algorithm application. Moreover, the representation of the equation and the choice of nonlinear functions and their variables has a dramatic effect on the size of the resulting regions. We have experimented with a variety of formulations, most importantly traditional polar and rectangular forms of power flow equations with different choices of matrix M and function f in (4.1). In this manuscript we present only one formulation that resulted in the least conservative regions for large scale systems. This formulation is based on the admittance representation of the power flow equations and nonlinear terms associated with power lines. It can naturally deal with strong (high admittance) power lines in the system that are the main source of conservativeness for most of the formulations.

2.4.1 Admittance based representation of power flow

The power formulation discussed below is based on a non-traditional combination of node-based variables and edge based nonlinear terms. This representation is naturally constructed using the weighted incidence type matrices. Specifically, we use $y^d \in \mathbb{C}^{|V|}$ to represent the diagonal of the traditional admittance matrix, and matrices $Y^f, Y^t \in \mathbb{C}^{|\mathcal{V}|\times|\mathcal{E}|}$ as weighted incidence matrices representing the admittances of individual elements with Y^f corresponding to negative admittance of lines startign at a given bus, and Y^t to admittance of lines ending at it. Any power line with admittance y_e connecting the bus from(e) to the bus to(e) contributes to the two elements in the matrices Y^f and Y^t, specifically $Y^f_{\text{from}(e),e} = -y_e$ and $Y^t_{\text{to}(e),e} = y_e$. In this for a bus k consuming the complex current i_k, the Kirchoff Current Law takes the form

$$i_k = y^d_k v_k + \sum_e Y^f_{ke} v_{\text{to}(e)} + Y^t_{ke} v_{\text{from}(e)}. \tag{2.28}$$

Whenever the pq bus is considered with constant complex power injection s_k, one also has $\bar{i_k} = s_k/v_k$. Next, we introduce the logartithmic voltage variables as $\rho_k = \log v_k$ and $\rho_e = \rho_{\text{from}(e)} - \rho_{\text{to}(e)}$ and rewrite the power flow equations in the following form:

$$y_\nu - y_\nu^d = Y_{\nu\varepsilon}^t \mathrm{e}^{\rho_\varepsilon + j\theta_\varepsilon} + Y_{\nu\varepsilon}^f \mathrm{e}^{-\rho_\varepsilon - j\theta_\varepsilon} \tag{2.29}$$

where $y_k = \overline{s_k}/|v_k|^2$. Assuming that the base solution is given by $\rho^\star, \theta^\star$ the equations can be rewritten as

$$y_\nu - y_\nu^d = \hat{Y}_{\nu\varepsilon}^t \mathrm{e}^{\delta\rho_\varepsilon + j\delta\theta_\varepsilon} + \hat{Y}_{\nu\varepsilon}^f \mathrm{e}^{-\delta\rho_\varepsilon - j\delta\theta_\varepsilon} \tag{2.30}$$

with $\hat{Y}^t = Y^t[\![\exp(\rho_\mathcal{E}^\star + j\theta_\mathcal{E}^\star)]\!]$ and $\hat{Y}^f = Y^f[\![\exp(-\rho_\mathcal{E}^\star - j\theta_\mathcal{E}^\star)]\!]$. This equation can be further simplified to

$$y_\nu - y_\nu^d = Y_{\nu\varepsilon}^+ \cosh(\delta\rho_\varepsilon + j\delta\theta_\varepsilon) + Y_{\nu\varepsilon}^- \sinh(\delta\rho_\varepsilon + j\delta\theta_\varepsilon) \tag{2.31}$$

with the help of $Y^\pm = \hat{Y}^t \pm \hat{Y}^f$. Finally, using the $y - y^d = g - jb$ we obtain

$$\begin{bmatrix} g_\nu \\ b_\nu \end{bmatrix} = \begin{bmatrix} \mathrm{Re}(Y^+) & \mathrm{Re}(Y^-) & -\mathrm{Im}(Y^-) & -\mathrm{Im}(Y^+) \\ \mathrm{Im}(Y^+) & \mathrm{Im}(Y^-) & \mathrm{Re}(Y^-) & \mathrm{Re}(Y^+) \end{bmatrix} \cdot \begin{bmatrix} \cosh\delta\rho_\varepsilon \odot \cos\delta\theta_\varepsilon \\ \sinh\delta\rho_\varepsilon \odot \cos\delta\theta_\varepsilon \\ \cosh\delta\rho_\varepsilon \odot \sin\delta\theta_\varepsilon \\ \sinh\delta\rho_\varepsilon \odot \sin\delta\theta_\varepsilon \end{bmatrix} \tag{2.32}$$

As with the traditional power flow equations, we use $x = (\theta_{\mathcal{G}}, \theta_{\mathcal{L}}, \rho_{\mathcal{L}})$ and consider only a subset of all the equations of the form $y = Mf(x)$:

$$\begin{bmatrix} g_{\mathcal{G}} \\ g_{\mathcal{L}} \\ b_{\mathcal{L}} \end{bmatrix} = \begin{bmatrix} \mathrm{Re}(Y^{+}_{\mathcal{GE}}) & \mathrm{Re}(Y^{-}_{\mathcal{GE}}) & -\mathrm{Im}(Y^{-}_{\mathcal{GE}}) & -\mathrm{Im}(Y^{+}_{\mathcal{GE}}) \\ \mathrm{Re}(Y^{+}_{\mathcal{LE}}) & \mathrm{Re}(Y^{-}_{\mathcal{LE}}) & -\mathrm{Im}(Y^{-}_{\mathcal{LE}}) & -\mathrm{Im}(Y^{+}_{\mathcal{LE}}) \\ \mathrm{Im}(Y^{+}_{\mathcal{LE}}) & \mathrm{Im}(Y^{-}_{\mathcal{LE}}) & \mathrm{Re}(Y^{-}_{\mathcal{LE}}) & \mathrm{Re}(Y^{+}_{\mathcal{LE}}) \end{bmatrix} \cdot \begin{bmatrix} \cosh \delta\rho_{\mathcal{E}} \odot \cos \delta\theta_{\mathcal{E}} \\ \sinh \delta\rho_{\mathcal{E}} \odot \cos \delta\theta_{\mathcal{E}} \\ \cosh \delta\rho_{\mathcal{E}} \odot \sin \delta\theta_{\mathcal{E}} \\ \sinh \delta\rho_{\mathcal{E}} \odot \sin \delta\theta_{\mathcal{E}} \end{bmatrix} \tag{2.33}$$

Theorem 10 *For any $\tilde{u}$ such that $B[\![v_{min}]\!]\tilde{u} \in \mathcal{A}(\ell_x - \tau)$ there exists at least one admissible solution $\tilde{x}^* \in \mathcal{A}(\ell_x)$ of the equation* (2.29).

Proof 6 *Since $v_k \geq v_{min}$ for all bus k, the condition $B[\![v_{min}]\!]\tilde{u} \in \mathcal{A}(\ell_x - \tau)$ implies that $B\ell_x \in \mathcal{A}(\ell_x - \tau)$. This guarantees that* (2.33) *has a feasible solution, so does* (2.29).

2.4.2 Nonlinear bounds

The bounds on the individual nonlinear terms can be expressed via the following set of relation:

$$\delta^{+}_{1,2}\{\cos \delta\theta_e\} = 0 \tag{2.34a}$$

$$\delta^{-}_{1,2}\{\cos \delta\theta_e\} = \max\{1 - \cos \delta\theta^{+}_e, 1 - \cos \delta\theta^{-}_e\} \tag{2.34b}$$

$$\delta^{\pm}\{\sin \delta\theta_e\} = \sin \delta\theta^{\pm}_e \tag{2.34c}$$

$$\delta^{\pm}_{2}\{\sin \delta\theta_e\} = \delta\theta^{\mp}_e - \sin \delta\theta^{\mp}_e \tag{2.34d}$$

$$\delta^{-}_{1,2}\{\cosh \delta\rho_e\} = 0 \tag{2.34e}$$

$$\delta^{+}_{1,2}\{\cosh \delta\rho_e\} = \max\{\cosh \delta\rho^{+}_e, \cosh \delta\rho^{-}_e\} - 1 \tag{2.34f}$$

$$\delta^{\pm}\{\sinh \delta\rho_e\} = \sinh \delta\rho^{\pm}_e \tag{2.34g}$$

$$\delta^{\pm}_{2}\{\sinh \delta\rho_e\} = \sinh \delta\rho^{\pm}_e - \delta\rho^{\pm}_e \tag{2.34h}$$

Then we use Lemma 6 to bound the products.

2.5 Extension using LP relaxation

The nonlinear bounds above may cause the construction technique non-scalable. I then relax the bounds to linear ones to form an LP. The optimal solution of the LP can be fed into the original nonlinear optimization problem as a initial guess. Hereafter, I constraint all the angles to the range within $\pm\theta^U$, say $\theta^U = \pi/3$, and all logarithmic voltages ρ to $\pm\rho^U$, say $\rho^U = 1$. Let define $\delta\theta_e^m = \max\{\delta\theta_e^{\pm}\}$ and $\delta\rho_e^m = \max\{\delta\rho_e^{\pm}\}$. where I use the following inequalities for $\pm\theta \leq \theta^{\pm} \leq \theta^U \leq \pi/2$, $\theta^m = \max\{\theta^{\pm}\}$, and $0 \leq \rho \leq K \leq 1$.

$$1 - \cos(\theta) \leq (1 - \cos(\theta^U))\frac{\theta^m}{\theta^U} \tag{2.35}$$

$$\sin(x) \leq (\theta^U - \sin(\theta^U))\frac{\theta}{\theta^U} \tag{2.36}$$

$$\cosh(\rho) - 1 \leq (\cosh(\rho^U) - 1)\frac{\rho}{\rho^U} \tag{2.37}$$

$$\sinh(\rho) \leq \sinh(\rho^U)\frac{\rho}{\rho^U} \tag{2.38}$$

For product terms, we need McCormick envelopes:

$$xy \leq x^U y + xy^L - x^U y^L \tag{2.39a}$$

$$xy \leq xy^U + x^L y - x^L y^U \tag{2.39b}$$

2.6 Simulations

For our algorithm validation and simulations, I relied on transmission test cases included in the MATPOWER package, constructing the corresponding regions for all the cases up to 300 buses. While most operational constraints are provided in the test case data, the thermal limits, which mostly depend on the cable materials, temperature, and voltage levels, are not available. For simplicity, I assumes that the

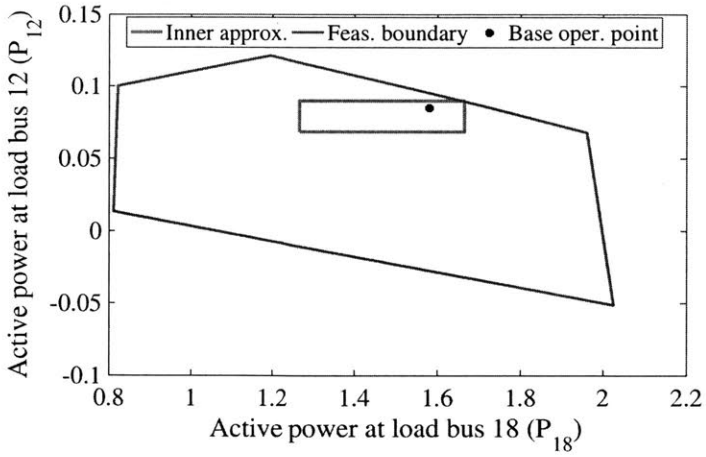

Figure 2-2: Feasibility set of an OPF for IEEE 39-bus system

maximum current level is double the corresponding value of the base case. The allowed voltage derivation range is $\pm 10\%$ around the nominal level of $1\,p.u.$, and the angle separation is limited within $-\pi/2$ and $\pi/2$ radians. I do not consider the reactive power constraints associated with the generators. In other words, I assume that the generators are capable of maintaining the terminal voltages at the reference values.

Specific choices of matrix R determine how the input variations $\tilde{u}$ enter the problem. This allows us to tailor the set of control inputs, for example, to focus on a certain dispatching/loading pattern. In the following simulations, I am interested in the inputs associated with the loading injections from a pair of non-zero load buses. For example for IEEE 39-bus system shown in Figure 2-2, the chosen pair of buses is $(18, 12)$, and the inputs are $\tilde{u}_k = P_k/V_k^2 - P_{k\star}/V_{k\star}^2$ where $k \in (18, 12)$. Moreover, for optimal certificates, I consider uniform bounds on the injection input perturbations by assuming that $\ell_u^- = \ell_u^+$. Therefore, the estimated feasible sets in the input space are hypercubes. Such hypercubes, once constructed, need to map back to the loading injection space, where the OPF actually searches for the optimal settings, by applying Theorem 10. The resulted polytopes are plotted in blue in Figures 2-2 to 2-5,

To illustrate the performance of the inner approximation technique, I plot and compare the real feasible set and the estimation. In most cases, as shown in Figures

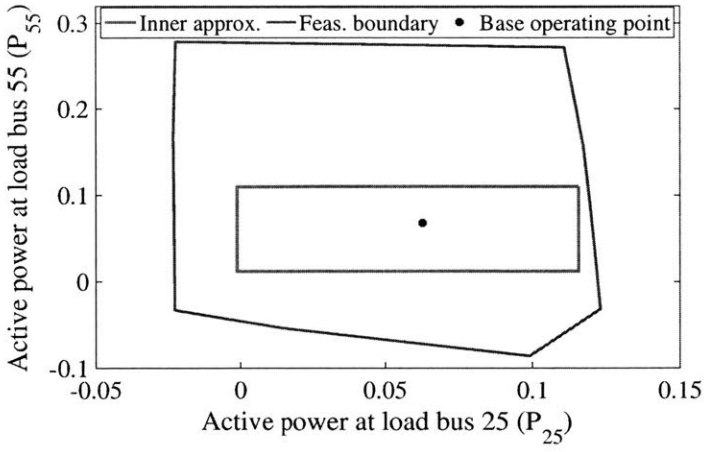

Figure 2-3: Feasibility set of an OPF for IEEE 57-bus system

2-2 to 2-5, the approximated sets cover a large fraction of the true feasible domains. Moreover, along some loading directions, the gap between the two boundaries is almost zero.

2.7 Conclusion

In conclusion, this chapter intends to develop a novel framework to estimate OPF feasible subsets. Remarkably, the proposed technique is applicable to transmission systems and more general power systems of arbitrary topology structures. The framework is based on Brouwer fixed point theorem, which is applied to polytopic regions in voltage-angle space. Unlike previous work which focuses on analytic approaches, our framework relies on nonlinear optimization procedures to find the largest sets that possess the self-mapping property. Additional constraints can be imposed on the admissible region to ensure the feasibility of the resulted solutions.

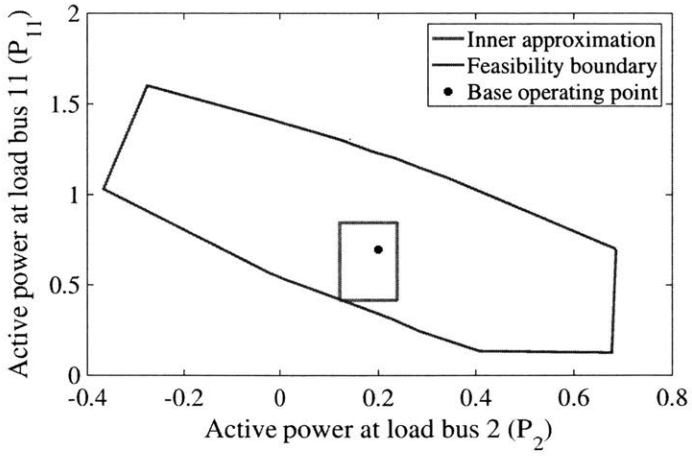

Figure 2-4: Feasibility set of an OPF for IEEE 118-bus system

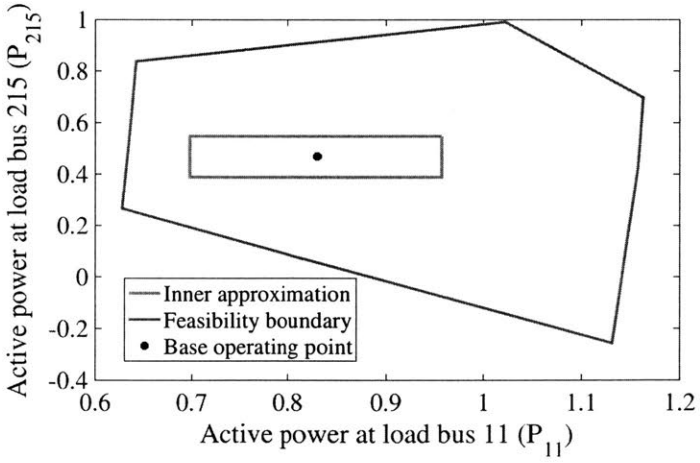

Figure 2-5: Feasibility set of an OPF for IEEE 300-bus system

Chapter 3

Attraction Basin Estimation for Nonlinear DAE Systems: Contraction Approach

This chapter studies the contraction properties of nonlinear differential-algebraic equation (DAE) systems presented in (1.1) and (1.2). A given DAE system may result from the reduction of many different "synthetic" differential ones. Here, I uncover an important property of a contracting DAE system: the reduced system always contracts faster than the corresponding synthetic system. Furthermore, there always exists a synthetic system with contraction rate arbitrarily close to that of the DAE one. Synthetic systems are useful for the analysis of attraction basins of nonlinear DAE systems. Any polynomial DAE system can be represented in quadratic form. For quadratic DAEs the Jacobian of the synthetic system is affine in the system variables. This property allows for scalable techniques for construction of the attraction basin approximations based on the uniformly negative matrix measure conditions for synthetic system Jacobian. The proposed construction algorithm is illustrated with a power system example in the context of transient stability assessment.

Associated with this work, a manuscript entitled "Contraction Analysis of Nonlinear DAE Systems" has been submitted to Transactions on Automatic Control and is currently under review.

3.1 Introduction

Differential-algebraic equations (DAE)-a generalization of ordinary-differential equations (ODE)-arise in many science and engineering problems, including networks, multibodies, optimal control, compressed fluid, etc. [99]. Typically, algebraic constraints result from multiple time-scale perturbation theory, when the fast degrees of freedom are assumed to stay on equilibrium manifold. In typical electrical and mechanical applications the algebraic relations represent the interconnection constraints, which can be considered static on the time-scales of system evolution. However, algebraic relations may be also useful for lifted representations of the purely differential systems. For instance, additional variables and relations can be used to represent any polynomial nonlinearity in a quadratic DAE form. Hence, DAE systems provide a powerful framework for studying nonlinear systems of very general structure. This work is motivated by the DAE representations of the power system models, but the results are presented in a general form.

The specific problem that motivates our study is the problem of approximating the region of attraction of DAE equilibrium points. The normal operating points of modern power systems lack global stability because of the nonlinearities naturally appearing in these systems. Characterization of the attraction region and more generally assessment of the system security, i.e. its ability to sustain all kinds of faults and disturbances, is an essential task of modern power system operations. As will be shown throughout the chapter, the contraction provides a natural framework for constructing the approximations of the attraction region for a broad range of nonlinear DAE problems, such as those arising in power systems.

Transient stability analysis is a common engineering procedure referring to the ability of the system to converge to a stable post-fault equilibrium after being subject to disturbances. The incremental stability introduced in [67] suggests an alternative way to look at the convergence of the post-fault trajectories. In the light of contraction theory, the virtual displacements of the states tend to zero as the time goes to infinity, or in other words, all the trajectories shrink and converge to the nominal

Vector norm, $\|\cdot\|$	Matrix measure, $\mu_p(M)$
$\|x\|_1 = \sum_i \|x_i\|$	$\mu_1(M) = \max_j(m_{jj} + \sum_{i \neq j} \|m_{ij}\|)$
$\|x\|_2 = (\sum_i \|x_i\|^2)^{1/2}$	$\mu_2(M) = \max_i(\lambda_i\{\frac{M+M^T}{2}\})$
$\|x\|_\infty = \max_i \|x_i\|$	$\mu_\infty(M) = \max_i(m_{ii} + \sum_{j \neq i} \|m_{ij}\|)$

Table 3.1: Standard matrix measures

one. Contraction analysis becomes a powerful tool for nonlinear analysis and control [67, 104, 105, 111]. The key property of the contraction is the preservation under different system combinations, which is advantageous in network analysis.

In this chapter I focus on the contraction analysis for nonlinear DAE systems. Specifically I develop a practical way of constructing the attraction regions by determining the relation between the contraction rates of the original DAE systems and its extension to virtual "synthetic" dynamics in differential-algebraic space. The extended system can be thought of as a virtual differential system that reduces to a given DAE after the restriction of a subset of variables to their equilibrium manifold. There can be multiple extensions of a given DAE system, each characterized by different contraction rates. However, I show that the contraction rate of the reduced system is always higher, and on the other hand, there always exists an extension with a contraction rate arbitrarily close to the original DAE system. Our results hold for the most commonly used 1, 2, and infinity norms, but can likely be extended to more general cases. I use the theoretical results to develop a scalable technique for constructing inner approximations of contraction regions from the 2 norm and infinity norm contraction metrics. I illustrate the technique with a practical example from power systems.

3.2 Contraction theory

I start this section by defining the logarithmic norm or the matrix measure. The matrix measure $\mu_p(M)$ of a matrix M is defined as $\mu_p(M) := \lim_{h \to 0^+} \frac{1}{h}(\|\mathbb{1} + hM\|_p - 1)$ following [114]. The standard matrix measures as well as vector norms are listed in Table 3.1.

In contraction analysis, I consider the deterministic systems of the form $\dot{\mathbf{x}} = f(\mathbf{x}, t)$ in $\mathbb{R}^n$ with a smooth nonlinear function f. The system is contracting in the contraction region $\mathcal{C}_p$ if the distance between two arbitrarily trajectories, starting from two different initial conditions, decay exponentially to zero. In other words, the two trajectories converge exponentially to each other. Moreover, the generalized contraction analysis often considers the distances associated with a metric $\theta(\mathbf{x})$ via a change of variables. A sufficient condition for contraction is introduced in the below theorem.

Theorem 11 *The system $\dot{\mathbf{x}} = f(\mathbf{x}, t)$ is contracting in $\mathcal{C}_p$ with respect to an invertible metric $\theta(\mathbf{x})$ if there exists a matrix measure μ such that for all $\mathbf{x} \in \mathcal{C}_\mathbf{p}$, one has $\mu_p\left(\dot{\theta}\theta^{-1} + \theta(\partial f/\partial \mathbf{x})\theta^{-1}\right) \leq -\beta$ with some $\beta > 0$.*

Proof 7 *A sketch of proof for 1, 2, and ∞ norm is shown in section 3.7(iii) in [67] (also in [95]). Below I provide a proof for more general p norm.*

To show the contraction behavior, I derive the following differential relation $\delta\dot{\mathbf{x}} = (\partial f/\partial \mathbf{x})\delta\mathbf{x}$ where $\delta\mathbf{x}$ is a virtual displacement (an infinitesimal displacement at fixed time). Define $\delta\mathbf{v} = \theta\delta\mathbf{x}$. One has $\delta\mathbf{x} = \theta^{-1}\delta\mathbf{v}$ and $\delta\dot{\mathbf{v}} = \left(\dot{\theta} + \theta(\partial f/\partial \mathbf{x})\right)\theta^{-1}\delta\mathbf{v}$ where $\dot{\theta} = (\partial\theta/\partial\mathbf{x})f(\mathbf{x}, t)$.

Let consider a Lyapunov candidate function $V = \|\delta\mathbf{v}\|_p$ which measures the distance between two different trajectories of the system. Using the same reasoning for matrix measure results introduced in [2, 115] and noting that $\limsup_{h\to 0^+} = \inf_{h\geq 0^+} \sup_{0^+\leq t\leq h}$, one takes upper Dini derivative of V to yield:

$$
\begin{aligned}
&D^+ \|\delta\mathbf{v}(t)\|_p \\
&= \limsup_{h\to 0^+} \frac{1}{h}\left(\|\delta\mathbf{v}(t+h)\|_p - \|\delta\mathbf{v}(t)\|_p\right) \\
&= \limsup_{h\to 0^+} \frac{1}{h}\left(\|\delta\mathbf{v}(t) + h\,\delta\dot{\mathbf{v}}(t)\,\delta\mathbf{v}(t) + O(h)\|_p - \|\delta\mathbf{v}(t)\|_p\right) \\
&\leq \limsup_{h\to 0^+} \frac{1}{h}\left\{\left\|1 + h\left(\dot{\theta} + \theta(\partial f/\partial\mathbf{x})\right)\theta^{-1}\right\|_p - 1\right\}\|\delta\mathbf{v}(t)\|_p \\
&= \mu_p\left(\dot{\theta}\theta^{-1} + \theta(\partial f/\partial\mathbf{x})\theta^{-1}\right)\|\delta\mathbf{v}(t)\|_p
\end{aligned}
\tag{3.1}
$$

If there exists some $\beta > 0$ *such that* $\mu_p\left(\dot{\theta}\theta^{-1} + \theta(\partial f/\partial \mathbf{x})\theta^{-1}\right) \leq -\beta$, (3.1) *leads to* $\|\delta\mathbf{v}(t)\|_p \leq \|\delta\mathbf{v}(0)\|_p exp(-\beta t)$ *for all* $t \geq 0$. *This result implies that the distance between any two trajectories will converge to zero, thus the system is contracting [67]. Q.E.D.*

3.3 Main results

As motivated by the dynamics of electrical power systems, I constrain ourselves to semi-explicit index 1 structural form as below:

$$\dot{\mathbf{x}} = \mathbf{f}(\mathbf{x}, \mathbf{y}), \tag{3.2}$$

$$0 = \mathbf{g}(\mathbf{x}, \mathbf{y}). \tag{3.3}$$

In this representation, vector $\mathbf{x} \in \mathbb{R}^n$ corresponds to dynamic state variables, $\mathbf{y} \in \mathbb{R}^m$ refers to algebraic variables (whose dynamics is assumed to be fast/instantaneous relative to the dynamics of the state variables). For this class of systems, it is impossible to obtain equivalent ODEs.

For convenience, reduction techniques are widely used to eliminate the algebraic variables. Yet this practice may prohibit one from exploring the underlying structure of the DAE form. To that end a number of works in the literature concentrate on the original systems rather than the reduced ones, for instant, in the context of stability analysis of the descriptor form as below:

$$E\dot{\mathbf{z}} = \mathbf{h}(\mathbf{z}), \tag{3.4}$$

with $\mathbf{z}^T = [\mathbf{x}^T, \mathbf{y}^T]$, $\mathbf{h}^T = [\mathbf{f}^T, \mathbf{g}^T]$ and E being a diagonal $\mathbb{R}^{(n+m)\times(n+m)}$ matrix with $E_{ii} = 1$ for $i \leq n$ and $E_{ii} = 0$ otherwise [8, 65, 72, 119].

For any given differential state $\mathbf{x}$ the equation (3.3) may have multiple or no solutions for $\mathbf{y}$. In engineering and natural systems that motivate this study, disappearance of all the solutions is usually an indicator of inappropriate modeling that

should be fixed accordingly, typically by introducing the fast dynamics of the algebraic states in the model. I don't consider this scenario in our work, and I assume that for every $\mathbf{x}$ there exists at least one solution $\mathbf{Y}(\mathbf{x})$ of the algebraic system of equations (3.3). For every solution branch I can naturally define the domain $\mathbf{x} \in \mathcal{R}$ where such a solution exists and can be tracked via homotopy/continuation procedure. This domain is characterized by non-singularity of the algebraic Jacobian:

$$\mathcal{R} = \left\{ \mathbf{x} : \ \det \left(\frac{\partial \mathbf{g}}{\partial \mathbf{y}} \Big|_{\mathbf{y}=\mathbf{Y}(\mathbf{x})} \right) \neq 0 \right\}. \tag{3.5}$$

I restrict our analysis only to such a domain associated with a specific solution branch. For a system of differential-algebraic equations (3.2), (3.3) I introduce the Jacobian defined as

$$J(\mathbf{x}, \mathbf{y}) = \begin{bmatrix} \partial \mathbf{f}/\partial \mathbf{x} & \partial \mathbf{f}/\partial \mathbf{y} \\ \partial \mathbf{g}/\partial \mathbf{x} & \partial \mathbf{g}/\partial \mathbf{y} \end{bmatrix}. \tag{3.6}$$

To simplify the notations I also define its restriction to the algebraic manifold (3.3) as follows:

$$J(\mathbf{x}, \mathbf{Y}(\mathbf{x})) = \begin{bmatrix} A & B \\ C & D \end{bmatrix}. \tag{3.7}$$

One of the primary goals of this chapter is to provide a characterization of the contraction and invariant regions in the state space of a DAE system. I formally define the contraction domains $\mathcal{C}_p$ as set of differential states $\mathbf{x}$ for which there exists an invertible metric $\theta(\mathbf{x}) \in \mathbb{R}^{n \times n}$ such that the differential equation $\dot{\mathbf{x}} = \mathbf{f}(\mathbf{x}, \mathbf{Y}(\mathbf{x}))$ is locally contracting with respect to this metric with some rate $\beta > 0$. Given that for any infinitesimal displacement $\delta\mathbf{x}$ we have $\delta\mathbf{y} = -D^{-1}C\delta\mathbf{x}$ the standard contraction arguments presented in [67, 105] lead to the following Proposition.

Proposition 1 *The DAE system* (3.2) (3.3) *is contracting with respect to the metric* $\theta(\mathbf{x})$ *in the domain* $\mathcal{C}_p$ *if for all* $\mathbf{x} \in \mathcal{C}_p$ *one has* $\mu_p(F_r) \leq -\beta$ *with some* $\beta > 0$ *and*

$$F_r = \dot{\theta}\theta^{-1} + \theta(A - BD^{-1}C)\theta^{-1}. \tag{3.8}$$

The term $\dot{\theta}$ in (3.8) represents the derivative of the metric along the trajectory and is formally defined for DAE systems as

$$\dot{\theta} = \left(\frac{\partial \theta}{\partial \mathbf{x}}\right)^T \mathbf{f}(\mathbf{x}, \mathbf{Y}(\mathbf{x})). \tag{3.9}$$

The proof of Proposition 1 directly follows that of Theorem 11 by using the relation $\partial f/\partial \mathbf{x} = A - BD^{-1}C$.

The proof of proposition 1 directly follows from the contraction analysis for dynamical system presented in [67]. The matrix F_r appears naturally from the dynamic equation on $\delta\mathbf{v} = \theta\delta\mathbf{x}$ given by $\dot{\delta\mathbf{v}} = F_r\delta\mathbf{v}$. Hereafter I refer to F_r as the *generalized reduced Jacobian matrix.*

The standard contraction theory arguments suggest that for any two trajectories $\mathbf{x}_1(t), \mathbf{x}_2(t)$ that both remain within the contraction region $\mathcal{C}_p$ during the interval $[t_1, t_2]$ satisfy $d(\mathbf{x}_1(t_2), \mathbf{x}_2(t_2)) \leq d(\mathbf{x}_1(t_1), \mathbf{x}_2(t_1)) \exp(-\beta(t_2 - t_1))$ where d is the distance associated with the metric θ. The assumption that both of the trajectories stay within the contraction region is critical for this result and can be verified only after showing the existence of an invariant domain $\mathcal{I}_p \subset \mathcal{C}_p$ satisfying:

$$\mathbf{x}(t) \in \mathcal{I}_p \Longrightarrow \forall t' \geq t : \quad \mathbf{x}(t') \in \mathcal{I}_p. \tag{3.10}$$

Constructing invariant regions is usually a difficult aspect of applying contraction theory to systems which are not globally contracting. One straightforward strategy for constructing invariant regions exists for systems that have an equilibrium point $\mathbf{x}_\star$ inside the contraction domain satisfying $\mathbf{f}(\mathbf{x}_\star, \mathbf{Y}(\mathbf{x}_\star)) = 0$. In this case, any ball $\mathcal{B}_r = \{\mathbf{x} : d(\mathbf{x}, \mathbf{x}_\star) \leq r\}$ that lies within the contraction region $\mathcal{C}_p$ defines an invariant region, i.e. $\mathcal{B}_r \subset \mathcal{C}_p \Longrightarrow \mathcal{B}_r \subset \mathcal{I}_p$. By construction, such a ball also provides an inner approximation for the attraction region of $\mathbf{x}_\star$ and can be naturally used in a variety of practical applications such as security assessment of power systems [81]. In this I develop a general framework for constructing such invariant regions for a broad class of nonlinearities, and I present a specific power system example in sections 3.4. The

key challenge in using the function F_r directly is its highly nonlinear nature. Even for simple polynomial nonlinearities of $\mathbf{f}, \mathbf{g}$ the function F_r involves an inversion of the matrix $D(\mathbf{x})$. From a practical perspective, it is therefore desirable to formulate conditions equivalent to contraction as defined in Propostion 1 that do not involve any inversions of matrices A, B, C, D which are nonlinearly dependent on $\mathbf{x}$. In order to achieve this goal I derive equivalent representation of the contraction condition that doesn't require elimination of the local variables and is more suitable for analysis. I introduce the *generalized unreduced Jacobian matrix* as follows:

$$F = \begin{bmatrix} F_r + \theta R^T C \theta^{-1} & \theta R^T D \rho^{-1} \\ Q^T C \theta^{-1} & Q^T D \rho^{-1} \end{bmatrix}. \tag{3.11}$$

The generalized unreduced Jacobian F depends on the metric θ defined as in the previous discussion, another metric ρ associated with the $\mathbf{y}$ variable and two auxiliary matrices $Q \in \mathbb{R}^{m \times m}$ and $R \in \mathbb{R}^{m \times n}$. By selecting specific auxiliary matrices, i.e. $R = D^{-T} B^T$ and $Q = \rho^T$, one can recover the standard generalized unreduced Jacobian, $[\![\theta, \rho]\!] J(\mathbf{x}, \mathbf{Y}(\mathbf{x}))[\![\theta^{-1}, \rho^{-1}]\!]$.

Formally, this new Jacobian matrix may be associated with a virtual synthetic ODE representation of the original system of the form

$$\dot{\delta \mathbf{v}} = F_r \delta \mathbf{v} + \theta R^T (C \theta^{-1} \delta \mathbf{v} + D \rho^{-1} \delta \mathbf{u}), \tag{3.12}$$

$$\dot{\delta \mathbf{u}} = Q^T (C \theta^{-1} \delta \mathbf{v} + D \rho^{-1} \delta \mathbf{u}). \tag{3.13}$$

where $\delta \mathbf{u} = \rho \delta \mathbf{y}$ and so the expression $C \theta^{-1} \delta \mathbf{v} + D \rho^{-1} \delta \mathbf{u} = C \delta \mathbf{x} + D \delta \mathbf{y} = 0$ defines the algebraic manifold. Whenever the dynamics of $\delta \mathbf{u}$ can be considered fast, the restriction of the $\delta \mathbf{u}$ variables to their equilibrium manifold results in the original DAE systems. Therefore, this representation provides a family of synthetic representations that reduce to the same original system. It will be shown that this representation is useful for characterization of the contraction and invariant regions. It is worth mentioning that there are different ways to represent F. To analyze the relationship between the original system and the extended ones, the form of (3.11) is more con-

venient because the generalized unreduced Jacobian, F, can be represented in terms of the reduced one, F_r. However, this representation is not suitable for constructing a contraction region since F_r consists of highly nonlinear terms induced by the inversion operation. Instead, one should use the other forms of F, for example, (3.31) for 2 norm, and (3.40) for 1 and infinity norms which do not contain F_r, but linearly variable-dependent terms.

The key property important for the analysis is defined in the following relation:

$$\begin{aligned} F\delta\mathbf{w} &= \begin{bmatrix} F_r + \theta R^T C\theta^{-1} & \theta R^T D\rho^{-1} \\ Q^T C\theta^{-1} & Q^T D\rho^{-1} \end{bmatrix} \begin{bmatrix} \theta\delta\mathbf{x} \\ \rho\delta\mathbf{y} \end{bmatrix} \\ &= \begin{bmatrix} F_r\theta\delta\mathbf{x} \\ 0 \end{bmatrix} + \begin{bmatrix} \theta R^T(C\delta\mathbf{x} + D\delta\mathbf{y}) \\ Q^T(C\delta\mathbf{x} + D\delta\mathbf{y}) \end{bmatrix}. \end{aligned} \tag{3.14}$$

where we have introduced the new variables vector $\delta\mathbf{w} \triangleq \begin{bmatrix} \delta\mathbf{v} \\ \delta\mathbf{u} \end{bmatrix}$. This observation allows us to formulate the following central results of this work.

3.3.1 Forward theorems: from virtual extended systems to reduced ones

Lemma 12 *Define*

$$\gamma = \left\| \begin{bmatrix} \delta\mathbf{v} + hF_r\delta\mathbf{v} \\ \delta\mathbf{u} \end{bmatrix} \right\|_p - \left\| \begin{bmatrix} \delta\mathbf{v} \\ \delta\mathbf{u} \end{bmatrix} \right\|_p - (\|\delta\mathbf{v} + hF_r\delta\mathbf{v}\|_p - \|\delta\mathbf{v}\|_p)$$

where $h > 0$. Then for all $p \geq 1$, $\gamma \geq 0$ if the following condition holds.

$$\left\| \begin{bmatrix} \delta\mathbf{v} + hF_r\delta\mathbf{v} \\ \delta\mathbf{u} \end{bmatrix} \right\|_p - \left\| \begin{bmatrix} \delta\mathbf{v} \\ \delta\mathbf{u} \end{bmatrix} \right\|_p \leq 0. \tag{3.15}$$

The proof of Lemma 12 is as the following. For fixed $\delta\mathbf{v}$ and $hF_r\delta\mathbf{v}$, γ depends solely on $\delta\mathbf{u}$. Taking partial derivative of γ with respect to $|\delta\mathbf{u}_j|$ using the definition of p

norm for a vector, i.e. $\|\mathbf{v}\|_p = (\sum_i |v_i|^p)^{1/p}$, yields the following:

$$\frac{\partial \gamma}{\partial |\delta \mathbf{u}_j|} = |\delta \mathbf{u}_j|^{p-1} \left(\left\| \begin{bmatrix} \delta \mathbf{v} + hF_r \delta \mathbf{v} \\ \delta \mathbf{u} \end{bmatrix} \right\|_p^{1-p} - \left\| \begin{bmatrix} \delta \mathbf{v} \\ \delta \mathbf{u} \end{bmatrix} \right\|_p^{1-p} \right). \tag{3.16}$$

On the other hand, the assumption $p \geq 1$ leads to $1 - p \leq 0$. This together with (3.15) and (3.16) concludes $\frac{\partial \gamma}{\partial |\delta \mathbf{u}_j|} \geq 0$ for all $j = 1, \ldots, m$. In other words, γ is indeed a monotonically increasing function with respect to the absolute value of each entry $\delta \mathbf{u}_j$. Moreover it can be seen that γ vanishes when $\delta \mathbf{u} = 0$. Therefore for any non-zero $\delta \mathbf{u}$, γ is non-negative.

For infinity norm one can prove the non-negativity of the partial derivatives $\frac{\partial \gamma}{\partial |\delta \mathbf{u}_j|}$ by taking the limit as p goes to infinity and exploiting the assumption presented by (3.15). Alternatively γ can be directly evaluated using the matrix measure expression associated with infinity norm listed in Table 3.1.

With Lemma 12 I introduce the first central result as the following.

Theorem 13 *For the system $\dot{\mathbf{x}} = \mathbf{f}(\mathbf{x}, \mathbf{Y}(\mathbf{x}))$ and metric function $\theta(\mathbf{x})$, and contracting extended system F with $\mu_p(F) < 0$ characterized by the matrices Q, R, ρ, the following relation holds:*

$$\mu_p(F_r) \leq \mu_p(F) \nu_p(H). \tag{3.17}$$

in which $S = \rho D^{-1} C \theta^{-1}$, $H = \begin{bmatrix} 1 \\ S \end{bmatrix}$, and

$$\nu_p(H) = \min_{\|v\|_p = 1} \|Hv\|_p . \tag{3.18}$$

Note that for invertible H, one has $\nu_p(H) = 1 / \|H^{-1}\|_p$.

Proof 8 *The matrix induced norm definition $\|M\| = \max_{\|v\|=1} \|Mv\|$ implies that for each positive scalar h, there exists $\delta \mathbf{v}_h$ with $\|\delta \mathbf{v}_h\|_p > 0$ satisfying the following equality:*

$$\frac{\|\delta \mathbf{v}_h + hF_r \delta \mathbf{v}_h\|_p - \|\delta \mathbf{v}_h\|_p}{h \|\delta \mathbf{v}_h\|_p} = \frac{\|\mathbb{1} + hF_r\|_p - 1}{h}. \tag{3.19}$$

The logarithmic norm is then defined as

$$\mu_p(F_r) = \lim_{h\to 0} \frac{\|\delta \mathbf{v}_h + hF_r\delta \mathbf{v}_h\|_p - \|\delta \mathbf{v}_h\|_p}{h\,\|\delta \mathbf{v}_h\|_p}. \tag{3.20}$$

Lemma 1 implies that this expression can be also rewritten as

$$\mu_p(F_r) \leq \lim_{h\to 0} \frac{\left\|\delta \mathbf{w}_h + h\begin{bmatrix} F_r\delta \mathbf{v}_h \\ 0 \end{bmatrix}\right\|_p - \|\delta \mathbf{w}_h\|_p}{h\,\|\delta \mathbf{v}_h\|_p}. \tag{3.21}$$

On the other hand, applying the property defined by (3.14) *we have that*

$$\begin{aligned} &\delta \mathbf{w}_h + h\begin{bmatrix} F_r\delta \mathbf{v}_h \\ 0 \end{bmatrix} \\ &= \delta \mathbf{w}_h + hF\delta \mathbf{w}_h - h\begin{bmatrix} \theta R^T(C\delta \mathbf{x}_h + D\hat{\delta \mathbf{y}}_h) \\ Q^T(C\delta \mathbf{x}_h + D\hat{\delta \mathbf{y}}_h) \end{bmatrix} \\ &= \delta \mathbf{w}_h + hF\delta \mathbf{w}_h \end{aligned} \tag{3.22}$$

where $\delta \mathbf{x}_h = \theta^{-1}\delta \mathbf{v}_h$ *and* $\hat{\delta \mathbf{y}}_h = -D^{-1}C\delta \mathbf{x}_h$. *Combining* (3.21) *and* (3.22), *we have that*

$$\begin{aligned} \mu_p(F_r) &\leq \lim_{h\to 0} \frac{\|\delta \mathbf{w}_h + hF\delta \mathbf{w}_h\|_p - \|\delta \mathbf{w}_h\|_p}{h\,\|\delta \mathbf{v}_h\|_p} \\ &= \lim_{h\to 0} \frac{\|\delta \mathbf{w}_h + hF\delta \mathbf{w}_h\|_p - \|\delta \mathbf{w}_h\|_p}{h\,\|\delta \mathbf{w}_h\|_p} \frac{\|\delta \mathbf{w}_h\|_p}{\|\delta \mathbf{v}_h\|_p}. \end{aligned} \tag{3.23}$$

By definition

$$\delta \mathbf{w}_h = \begin{bmatrix} \delta \mathbf{v}_h \\ \delta \mathbf{u}_h \end{bmatrix} = H\delta \mathbf{v}_h, \tag{3.24}$$

so $\|\delta \mathbf{w}_h\|_p \geq \nu_p(H)\,\|\delta \mathbf{v}_h\|_p$, *and by combining this with the assumption* $\mu_p(F) < 0$, *I*

can rewrite (3.23) *as the following*

$$\mu_p(F_r) \leq \lim_{h\to 0} \frac{\|\delta \mathbf{w}_h + hF\delta \mathbf{w}_h\|_p - \|\delta \mathbf{w}_h\|_p}{h\,\|\delta \mathbf{w}_h\|_p} \nu_p(H)$$
$$\leq \mu_p(F)\nu_p(H). \tag{3.25}$$

Q.E.D.

The purpose of introducing H is to show an important property of a DAE system: if an extended system is contracting, the reduced system is also contracting, but with a faster rate. As a result, the contraction rate of the synthetic system can be used as a lower bound of the reduced one. Note that even though H still involves a matrix inversion, if the contraction rate of the reduced system is not of primary interest, there is no need for an explicit construction. An example of this is the contraction region approximation procedure in section 3.4.

The below corollary of Theorem 13 provides the explicit expression of $\nu_p(S)$ with $p = 2$.

Corollary 4 *(2* ***norm****) Assuming that all assumptions of Theorem 13 are satisfied, the contraction rate associated with the reduced system can be bounded as below*

$$\mu_2(F_r) \leq \mu_2(F)\sqrt{1 + \sigma^2_{\min}(S)} \tag{3.26}$$

in which $\sigma_{\min}(S)$ denotes the minimal singular value of the matrix S.

The proof of Corollary 4 follows from Theorem 13 and note that for $p = 2$, we have that $\nu_2(H) = \sqrt{1 + \min_{\|v\|=1} \|Sv\|_2^2} = \sqrt{1 + \sigma^2_{\min}(S)}$.

3.3.2 Converse theorems

Theorem 14 *(2* ***norm****) For a contracting system $\dot{\mathbf{x}} = \mathbf{f}(\mathbf{x}, \mathbf{Y}(\mathbf{x}))$ and metric function $\theta(\mathbf{x}, t)$ with $\mu_2(F_r) < 0$ and any $\epsilon > 0$ there exists an extended system F characterized by the matrices Q, R, ρ contracting with the contraction rate satisfying $\mu_2(F) \leq \mu_2(F_r)/(1 + \epsilon)$.*

Proof 9 *This theorem can be proven by explicit construction of the matrices Q, R, ρ, which ensures fast enough contraction of F. The matrix ρ is chosen to be small enough, so that $\sigma^2_{\max}(S) \leq \epsilon$ and $R = \eta D^{-T}\rho^T\rho D^{-1}C\theta^{-1}$, $Q = -\eta D^{-T}\rho^T$, where $\eta = -\mu_2(F_r)/(1+\sigma^2_{\max}(S))$. This choice of R and Q ensures that the symmetric part of F is block-diagonal, so the following inequality follows from* (3.14)*:*

$$\begin{aligned}
\delta\mathbf{w}^T F \delta\mathbf{w} &= \begin{bmatrix}\theta\delta\mathbf{x}\\ \rho\delta\mathbf{y}\end{bmatrix}^T \begin{bmatrix}F_r + \eta S^T S & 0\\ 0 & -\eta\mathbb{1}\end{bmatrix}\begin{bmatrix}\theta\delta\mathbf{x}\\ \rho\delta\mathbf{y}\end{bmatrix}\\
&= \delta\mathbf{v}^T\left(F_r + \eta S^T S\right)\delta\mathbf{v} - \eta\|\delta\mathbf{u}\|^2\\
&\leq \left(\mu_2(F_r) + \eta\sigma^2_{\max}(S)\right)\|\delta\mathbf{v}\|^2 - \eta\|\delta\mathbf{u}\|^2\\
&= -\eta\|\delta\mathbf{w}\|^2 + \left(\eta + \mu_2(F_r) + \eta\sigma^2_{\max}(S)\right)\|\delta\mathbf{v}\|^2\\
&= -\eta\|\delta\mathbf{w}\|^2. \qquad (3.27)
\end{aligned}$$

Since this inequality holds true for any $\delta\mathbf{w}$, I conclude that $\mu_2(F) \leq -\eta \leq \mu_2(F_r)/(1+\epsilon)$.

The counterpart of Theorem 14 for 1 norm and ∞ norm are presented below.

Theorem 15 *(1 **norm and** ∞ **norm**) For a contracting system $\dot{\mathbf{x}} = \mathbf{f}(\mathbf{x}, \mathbf{Y}(\mathbf{x}))$ and metric function $\theta(\mathbf{x}, t)$ with $\mu_p(F_r) < 0$ and any $\epsilon > 0$ there exists an extended system F characterized by the matrices Q, R, ρ contracting with the contraction rate satisfying $\mu_p(F) \leq \mu_p(F_r)(1-\epsilon)$ where $p = 1, \infty$.*

Proof 10 *Similar to proof 9 we need to construct an appropriate tuple of matrices Q, R, ρ. Below I only present ∞ norm, but 1 norm can be considered in the same way. Choosing $R = 0$, $Q = \mu_\infty(F_r)D^{-T}\rho^T$, and metric ρ small enough so that $\|S\|_\infty \leq \epsilon$, leads to a diagonally dominant matrix F below:*

$$F = \begin{bmatrix}F_r & 0\\ \mu_\infty(F_r)S & \mu_\infty(F_r)\mathbb{1}\end{bmatrix}, \qquad (3.28)$$

then we have the following relation:

$$\begin{aligned}\mu_\infty(F) &= \max\{\mu_\infty(F_r), \\ &\qquad \max_{n+1\le i\le n+m}\{\mu_\infty(F_r) + \sum_{j=1}^{n} |\mu_\infty(F_r)S_{ij}|\}\} \\ &\le \max\{\mu_\infty(F_r), \mu_\infty(F_r) + |\mu_\infty(F_r)|\,\|S\|_\infty\} \\ &\le \mu_\infty(F_r)(1-\epsilon). \end{aligned} \tag{3.29}$$

Q.E.D.

3.3.3 Relation to other works

In this section I first discuss the relation to linear stability of DAE systems. The DAE systems have been studied extensively under "descriptor" forms [8, 65, 72, 106, 119] as well as singular systems in [113]. In fact if there exists a matrix Z that satisfies the Lyapunov inequality (3.32) in section 3.4 with $J_\star$ at an equilibrium $\mathbf{z}_\star$ and $\beta = 0$, then the descriptor system is asymptotically stable. Theorem 14 not only suggests that the existence of such matrix Z is indeed the sufficient condition for linear stability, but also provides an explicit construction of the certificate. The relation between the two notions of contraction and linear stability is further discussed below.

Contraction analysis and linear stability are closely related for autonomous systems. As discussed in section 3.4.3 if there exists a stable equilibrium that lies within a ball-like invariant region inscribed in the contraction region, all the trajectories of the systems starting inside the ball will shrink towards each other and merge to the nominal trajectory associated with the equilibrium; hence, the system is linearly stable at such equilibrium. In other words, if the system is linear stable at a particular equilibrium, there exists a contraction region centered at the equilibrium. This is true for ODEs as observed in [6]. The converse theorems 14 and 15 provide an explicit construction for DAEs.

From the contraction and linear stability comparability, the inner approximated contraction region constructed below in section 3.4 is indeed a robust linear stability

region in the variable space associated with the nominal operating point. Speaking of robust linear stability region, any equilibrium, if it exists and lies in such region, is a linearly stable one. Moreover as motivated by applying contraction analysis to the power systems which can be represented in DAE form, incremental stability implies convergence and vice versa. For the distinctions between the two concepts, interested readers can refer to [4, 94].

Singularly perturbed systems are also related to DAE systems as the time constant $\epsilon \to 0$. [9, 111] revisit some key results of singular perturbations using contraction tools, where the fast and slow sub-systems are assumed to be partially contracting. Our approach here, on the other hand, doesn't require the systems to be partially contracting in the algebraic variable $\mathbf{y}$. In comparison to the key theorems from [9, 111], our results provide explicit conditions on the Jacobian matrices that can be applied to any system. However, to our knowledge, neither of our previously reported results on contraction of singularly perturbed systems dominate each other.

With respect to the contraction condition, the condition introduced in [23] can be recovered under our framework when ϵ goes to 0, as follows. Consider the standard singular perturbation system:

$$\dot{x} = f(x, y, t),\ \epsilon\dot{y} = g(x, y, t),\ \epsilon \geq 0. \tag{3.30}$$

Assume that the system (3.30) is partially contracting in x and in y with respect to transformation metrics θ and ρ. For simplicity let the transformation metrics be constant. Let's consider a Lyapunov function $V = \left\|[\theta\delta\mathbf{x}\ \rho\delta\mathbf{y}]^T\right\|$ then the system (3.30) is contracting if the generalized Jacobian $F_{sing} = \begin{bmatrix} \theta A\theta^{-1} & \theta B\rho^{-1} \\ \rho C\theta^{-1}/\epsilon & \rho D\rho^{-1}/\epsilon \end{bmatrix}$ has a uniform negative matrix measure. Therefore if I select $Q = \rho^T/\epsilon$, $R = D^{-T}B^T$, then $F_{sing} = F$. This implies that the central theorem 13 applies to the DAE system associated to the system (3.30).

In [67], a similar class of systems was analyzed, where the linear constraints were imposed on the differential systems. The key conclusion that contraction of the orig-

inal unconstrained flow implies local contraction of the constrained flow is consistent with our results. However, apart from being constructive, our results also don't directly follow from the observations made in [67] as in our case the contraction of the synthetic system is not restricted to the algebraic manifold.

3.4 Inner approximation of contraction region

In this section I constraint ourself to the class of DAE systems which can be represented by quadratic equations in variables $\mathbf{z}$. As a result the Jacobian J depends linearly on $\mathbf{z}$. As identifying the real contraction region is challenging and even impossible in many practical situations, I introduce two scalable techniques for constructing inner approximations of the contraction region centered at a given equilibrium: an LMI formulation for 2 norm, and a robust linear programing for 1 and infinity norms. The approximated region has its merits of determining transient stability in electrical systems as shown in the application section.

Proposition 2 *The DAE system* (3.2) *and* (3.3) *is contracting in the contraction region $\mathcal{C}_p$ if there exists transform $\theta(\mathbf{x}, t)$ such that $\exists \beta > 0$, $\forall \mathbf{x} \in \mathcal{C}_p$, $\mu_p(F) \leq -\beta$.*

Proof 11 *$\mu_p(F_r)$ is negative follows from Theorem 13. The definition of contraction region in* (3.8) *then concludes the proof.*

An important application of Proposition 2 is to construct the contraction region by analyzing the extended systems. In the following subsections I present the construction for both 2 and infinity norms.

3.4.1 Inner approximation in 2 norm and LPV problem

Since the generalized unreduced Jacobian matrix introduced in (3.11) is not suitable for LMI formulation, I rewrite the Jacobian in more convenient form as below with a constant metric θ, $R = \tilde{R} + D^{-T}B^T$ and $Q = \tilde{Q}$, and $\rho = \mathbb{1}$ so that the system

contracts in $\mathbf{y}$ with respect to the identity metric:

$$\begin{aligned}\delta\mathbf{w}^T F \delta\mathbf{w} &= \begin{bmatrix}\delta\mathbf{x}\\ \delta\mathbf{y}\end{bmatrix}^T \begin{bmatrix}PA+\tilde{R}^TC & \tilde{R}^TD+PB\\ \tilde{Q}^TC & \tilde{Q}^TD\end{bmatrix}\begin{bmatrix}\delta\mathbf{x}\\ \delta\mathbf{y}\end{bmatrix}\\ &= \delta\mathbf{z}^T Z^T J(\mathbf{z})\delta\mathbf{z},\end{aligned} \tag{3.31}$$

with a lower block diagonal auxiliary matrix $Z = \begin{bmatrix}P & 0\\ \tilde{R} & \tilde{Q}\end{bmatrix}$. Such matrix Z also is used in linear stability assessment for descriptor systems. This is discussed in details in section 3.3.3. With the new representation, the problem of solving $\mu_2(F) \leq -\beta$ reduces to the following Lyapunov bilinear inequality in Z and $J(\mathbf{z})$:

$$Z^T J(\mathbf{z}) + J(\mathbf{z})^T Z \preceq -\beta\mathbb{1}. \tag{3.32}$$

LPV problem Note that the Jacobian matrix is affine in states, i.e. $J(\mathbf{z}) = J_\star + \sum_k z_k J_k$. Hence, if the states belong to a compact set, the equality (3.32) is a semi-infinite LMI problem: find a matrix Z such that (3.32) holds true for all states in this compact set [10, 11]. One can then rely on a relaxation scheme which particularly is a relaxation of affine parameter-dependent LMI to transform the semi-infinite problem into finite ones [11, 100]. However, from a power engineering perspective this approach has two main drawbacks: i) such compact set may not be available, and ii) even if the set of states is given, solving the resulted finite LMI problems associated with a large-scale power system may be computationally prohibited.

I therefore consider a different problem: for a given nominal matrix Z, find a set of states which satisfies the inequality (3.32). This iterative approach, which often applies to bilinear problems, can be implemented in the following 2-step procedure. First, for a fixed point, say the equilibrium $\mathbf{z}_\star$ which without loss of generality can be assumed zero, one sets $J(\mathbf{z}) = J_\star$ then solves (3.32) for Z. Let $Z_\star$ be the solution of the first step, then the metric θ can be determined as the Cholesky decomposition of P.

Next I fix $Z = Z_\star$, perturb the system around its equilibrium $\mathbf{z}_\star$, and then iden-

tify an acceptable perturbation region. For any fixed Z the equation (3.32) defines a spectrahedral region where the system is provably contracting. The invariant region around equilibrium point could have been constructed by inscribing the ball (ellipsoid) associated with the metric θ, ρ inside this region. However, inscription of ellipsoids inside spectrahedra is a NP-hard problem not scalable to the large power systems. Instead, I propose an alternative procedure, where I construct an intermediate polytopic region inscribed in a spectrahedron in which I inscribe the contracting ball.

The polytopic region is constructed in the variable space in which $Z_\star$ is the common matrix satisfying (3.32) for all inner points. Particularly, we need to find variations $\mathbf{z}$ satisfying the following LMI:

$$J(\mathbf{z})^T Z_\star + Z_\star^T J(\mathbf{z}) + \beta \mathbb{1} \preceq 0. \tag{3.33}$$

Note that (3.33) holds at the equilibrium. This leads to the following:

$$Z_\star^T J_\star + J_\star^T Z_\star + \beta \mathbb{1} = -U^T U \preceq 0. \tag{3.34}$$

Moreover for non-singular U one can symmetrize (3.33) by multiplying on the left and the right by U^{-T} and U^{-1}, respectively. As a result we have that

$$-1 + \sum_k U^{-T} z_k (Z_\star^T J_k + J_k^T Z_\star) U^{-1} \preceq 0. \tag{3.35}$$

For each coefficient matrix J_k, using SVD decomposition, yields the following:

$$U^{-T}(Z_\star^T J_k + J_k^T Z_\star)U^{-1} = \sum_h \lambda_{kh} e_{kh} e_{kh}^T. \tag{3.36}$$

Then it's sufficient to conclude that (3.35) holds if the following condition satisfies:

$$\sigma_{max}\left(\sum_k z_k \sum_h \lambda_{kh} e_{kh} e_{kh}^T\right) \leq 1, \tag{3.37}$$

which then can be formulated as the following:

$$\begin{aligned}
&\max_{\|v\|_2=1} \sum_k z_k \sum_h \lambda_{kh} (v^T e_{kh})^2 \\
&\leq \max_{k,h} \left[|z_k \lambda_{kh}| \sigma_{max} \left(\sum_{l,h} e_{lh} e_{lh}^T \right) \right] \\
&\leq 1. \qquad (3.38)
\end{aligned}$$

A box-type bound of the variation z_k can be estimated as

$$\max |z_k| \leq \frac{1}{(\max_h |\lambda_{kh}|)\sigma_{max}(\sum_{l,h} e_{lh} e_{lh}^T)}, \qquad (3.39)$$

which defines the bounds on each variable variation z_k thus identifying the inner approximated contraction region. It can be seen that the explicit bound defined by (3.39) depends on the uniform upper-bound of the contraction rate β and matrix $Z_\star$. The bounds become more conservative for a large value of β. Since there is an infinite number of choices of $Z_\star$ satisfying $\mu_2(Z_\star^T J_\star) \leq -\beta$, it's essential to understand which $Z_\star$ would correspond to the least conservative bounds. The bounds obtained from (3.39) can be also improved by deploying a better estimated upper bound in (3.42).

3.4.2 Inner approximation in 1 and infinity norms

A similar inner approximated contraction region can be also constructed based on 1 and infinity norms. To verify contraction, $\mu_p(F) < 0$, both norms require diagonally dominant generalized Jacobian, so the associated constructions are alike. Below I present only the procedure for infinity norm.

Closely following the reasoning used for the construction for 2 norm, we need to exclude the high nonlinear terms in the generalized Jacobian. By choosing $\tilde{R} = D^{-T} B^T$ and $Q^T = \rho$, we have the standard unreduced generalized Jacobian:

$$F = \begin{bmatrix} \theta A \theta^{-1} & \theta B \rho^{-1} \\ \rho C \theta^{-1} & \rho D \rho^{-1} \end{bmatrix}. \qquad (3.40)$$

An important property of this representation is that, for fixed metrics, the generalized Jacobian is linear in states. This fact allows us to proceed with the two-step procedure.

In the first step, for a fixed point $z_\star$, we need to find the nominal metrics $\theta_\star$ and $\rho_\star$ which make the generalized Jacobian diagonally dominant, thus $\mu_\infty(F) < 0$. In general, finding such metrics is not trivial. One possible approach is to make the two off-diagonal submatrices vanish at the nominal point. In particular, for the upper right submatrix with B term, I can select a metric θ which has a sufficiently small infinity norm. The lower left submatrix associated with C term will become zero if I replace the algebraic variable perturbations, δy, with mixed variables $\delta\tilde{y} = C_\star \delta x + D_\star \delta y$ where $C_\star = C|_{z=z_\star}$ and $D_\star = D|_{z=z_\star}$. The algebraic relations can be reduced to $-\delta\tilde{y} = 0$, thus yielding a new generalized Jacobian which is of the form $F = \begin{bmatrix} F_r & 0 \\ 0 & -\mathbb{1} \end{bmatrix}$. A natural following step is to find a metric θ with which F_r is negatively diagonally dominant. If the system is overdamped, the Schur complement of the Jacobian, $J_r = A - BD^{-1}C$, has only negative real eigenvalues, and is thus diagonalizable. The metric θ then can be simply chosen to consist all eigenvectors of J_r. Moreover, for the new form of F, all invertible metrics ρ would work, but for simplicity, let ρ be an identity metric.

Once the metrics are obtained, I continue with the second step where I fix the metrics and perturb the states. The admissible range of state perturbations which maintains negative $\mu_\infty(F)$ defines an inner approximation of the contraction region. As many practical engineering systems require all physical quantities to be in compliance with specified operational constraints, I propose to use box constraint construction. I shall inscribe a box inside the spectrahedron by allowing some variability to the coordinates

$$\underline{z_k} \leq z_k \leq \overline{z_k} \tag{3.41}$$

in all the directions $k = 1, \ldots n + m$. The following robust linear programing is

formulated to certify that the box region indeed lies in the contraction region.

$$\begin{aligned} \underset{v}{\text{minimize}} \quad & \gamma \\ \text{subject to} \quad & \max_{\underline{z_k} \le z_k \le \overline{z_k}} (F_{ii}) + \sum_{j \neq i} \zeta_{ij} \le \gamma \quad i = 1, \dots n+m \\ & \max_{\underline{z_k} \le z_k \le \overline{z_k}} (-F_{ij}) - \zeta_{ij} \le 0 \quad i, j = 1, \dots n+m \\ & \max_{\underline{z_k} \le z_k \le \overline{z_k}} (F_{ij}) - \zeta_{ij} \le 0 \quad i, j = 1, \dots n+m \end{aligned} \tag{3.42}$$

where ζ_{ij} associates with the absolute value of the off-diagonal entry F_{ij}, $i \neq j$. If the optimal value of the objective function in (3.42) is negative, the box is certified.

3.4.3 Invariant set construction

In this section I describe the procedure for constructing an invariant set $\mathcal{I}_2$ that lies in the contraction region $\mathcal{C}_2$.

Assume that an inner approximation of the contraction region, $\mathcal{C}_2$, constructed from section 3.4 is a convex region defined by a set of linear inequalities $e_i^T \mathbf{x} \le b_i$, for $i = 1, \dots, 2(n+m)$, and the equilibrium $\mathbf{x}_\star = 0$. e_i is a unit vector with the non-zero element either $+1$ or -1 due to the box-type constraints. $b_i > 0$ represents the bound on the variation along each direction, and b_i is set to infinity if the corresponding G_k vanishes. The linear transformation with metric θ prompts a corresponding contraction region in $\mathbf{v}$ space, i.e. $\mathcal{C}_{2\mathbf{v}} = \{\mathbf{v} | e_i^T \theta^{-1} \mathbf{v} \le b_i\}$, for $i = 1, \dots, 2(n+m)$. Then to construct an invariant set I find the largest Euclidean ball centered at the equilibrium where $\mathbf{v}_\star = \theta \mathbf{x}_\star = 0$ that lies in $\mathcal{C}_{2\mathbf{v}}$. The problem can be formulated as the following LP:

$$\begin{aligned} \underset{r}{\text{maximize}} \quad & r \\ \text{subject to} \quad & q_i(r) \le b_i; \quad r \ge 0 \quad i = 1, \dots, 2(n+m) \end{aligned} \tag{3.43}$$

where the constraints be

$$\begin{aligned} q_i(r) &= \sup_{\|u\| \leq 1} e_i^T \theta^{-1}(v_\star + ru) \\ &= r \left\| e_i^T \theta^{-1} \right\|_2 . \end{aligned} \tag{3.44}$$

(3.44) follows from the Cauchy-Schwarz inequality, i.e. for a nonzero vector x, the vector u satisfying $\|u\|_2 \leq 1$ that maximizes $x^T u$ is $x/\|x\|_2$. It also can be seen that the LP (3.43) admits the optimal solution $r_{max} = \min_i \{b_i / \left\| e_i^T \theta^{-1} \right\|_2\}$.

3.5 Transient stability of power systems

In this section I demonstrate how the developed techniques can be applied to the problem of constructing inner approximations of the contraction regions applicable to transient stability analysis of power systems modeled in DAE forms.

3.5.1 Large-disturbance stability

Large disturbance stability or transient stability is defined as the ability of the system to maintain synchronism after being subject to major disturbances such as line failures or loss of large generators or loads. Unstable systems will exhibit large angle separation or voltage depression which lead to system disintegration [60]. The objective of transient analysis is to determine whether the system can converge to a feasible post-fault stable equilibrium for a given pre-fault stable operating point and a trajectory along which the system evolves during the fault, the so-called fault-on trajectory. Assuming that all operational constraints or feasibility conditions, and stability conditions are satisfied at the post-fault equilibrium, I then go into the convergence of the post-fault trajectory.

There are two main approaches to transient stability analysis including time-domain simulations and energy based or direct methods [19]. An alternative based on inner approximated contraction region is then proposed. This doesn't require intensive computation efforts like the time-domain approach while still providing a

reasonably non-conservative stability region in the state space. As long as the initial point of the post-fault trajectory lies inside such region, the convergence to post-fault stable equilibrium is guaranteed.

The salient features of the contraction approach include scalibility, online analysis facilitation, and it does not require tailored energy function construction. The heaviest computational tasks are solving Lyapunov inequalities and SVD decomposition, which even of large scale problems, are ready to be solved with existing algorithms in regular processors. The contraction approach also allows the analysis be free from post-fault trajectory numerical integration which is time consuming and prevents online assessment. The third feature makes a key distinction between the contraction approach and the direct methods. Indeed the direct methods rely on energy function construction which doesn't have a general form in lossy networks and there is a need for finding critical energy levels based on which a stability region is identified. The contraction approach, on the other hand, just requires the transform θ and ρ under which the system is contracting. Once the transform is found through solving Lyapunov inequalities a corresponding sub-region of the contraction region can be constructed.

It's worth mentioning that the inner approximated contraction region is also a robust linear stability region so that the post-fault equilibrium is stable if it is an interior point. By construction the feasibility of the constructed region is easily validated as well. More importantly based on the inner approximated region one can either gain insight about the system stability "degree" or preliminarily compute "sufficient" critical clearing time ($sCCT$) which is more strict than the actual CCT, the maximum allowed fault-on duration. Hence if the fault is cleared before $sCCT$, the fault-on trajectory won't escape or exit the invariant region and the post-fault trajectory will converge to a post-fault stable equilibrium inside the invariant region. For more details on CCT one can refer to [19, 61].

3.5.2 A 2-bus system

The applications of approximating the contraction region are discussed above. In this section I illustrate the procedure by constructing one for a two-bus system as shown in Figure 3-1 [112]. The 2-bus system includes one slack bus, and one generator

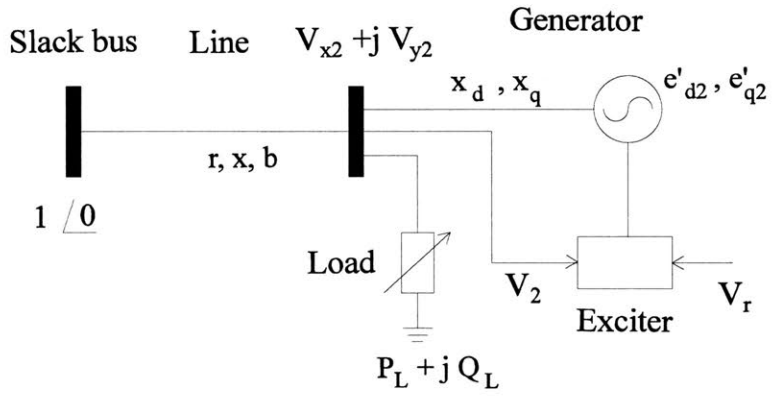

Figure 3-1: A 2-bus system

bus with a load residing at the same bus. The slack bus voltage is specified, i.e. $V_1 = 1.04\angle 0$. The generator, modeled with a high order generator model, maintains the voltage at bus 2 and generates active power at specific levels, i.e. $V_2 = 1.025\,p.u.$ and $P_G = 0.8\,p.u.$. The load consumes fixed amount of powers, $P_L = 1.63\,p.u.$ and $Q_L = 1.025\,p.u.$. Note that hereafter I use r to denote the line resistance.

The sets of differential equations $\dot{\mathbf{x}} = f(\mathbf{x}, \mathbf{y})$ which describe the dynamics of the generator are listed below. The details are introduced in [75].

$$
\begin{aligned}
T'_{d0}\frac{d}{dt}e'_{q2} &= -e'_{q2} - (x_d - x'_d - \frac{T''_{d0}}{T'_{d0}}\frac{x''_d}{x'_d}(x_d - x'_d))i_{d2} + (1 - \frac{T_{AA}}{T'_{d0}}V_2),\\
T''_{d0}\frac{d}{dt}e''_{q2} &= -e''_{q2} + e'_{q2} - (x'_d - x''_d - \frac{T''_{d0}}{T'_{d0}}\frac{x''_d}{x'_d}(x_d - x'_d))i_{d2} + \frac{T_{AA}}{T'_{d0}}V_2,\\
T'_{q0}\frac{d}{dt}e'_{d2} &= -e'_{d2} + (x_q - x'_q - \frac{T''_{q0}}{T'_{q0}}\frac{x''_q}{x'_q}(x_q - x'_q))i_{q2},
\end{aligned}
$$

$$
\begin{aligned}
T''_{q0}\frac{d}{dt}e''_{d2} &= -e''_{d2} + e'_{d2} + (x'_q - x''_q - \frac{T''_{q0}}{T'_{q0}}\frac{x''_q}{x'_q}(x_q - x'_q))i_{q2},\\
\frac{d}{dt}\sin\delta'_2 &= 2\pi f_n \cos\delta'_2(-1+\omega_2),\\
M\frac{d}{dt}\omega_2 &= p_m - i_{d2}v_{d2} - i_{q2}v_{q2} - D(-1+\omega_2).
\end{aligned} \tag{3.45}
$$

Algebraic equations, $g(\mathbf{x},\mathbf{y}) = 0$, are composed of the relations describing the generator, the network, and the load, that can be stated as follow:

$$
\begin{aligned}
0 &= -e''_{q2} + x''_{d2}i_{d2} + v_{q2},\\
0 &= -e''_{d2} - x''_{q2}i_{q2} + v_{d2},\\
0 &= -v_{q2} + \cos\delta'_2 v_{x2} + \sin\delta'_2 v_{y2},\\
0 &= -v_{d2} + \sin\delta'_2 v_{x2} - \cos\delta'_2 v_{y2},\\
0 &= (\cos\delta'_2)^2 + (\sin\delta'_2)^2 - 1,\\
0 &= \cos\delta'_2 i_{q2} + i_{d2}\sin\delta'_2 + \frac{bv_{y2}}{2} + \frac{rV_1}{r^2+x^2}\\
&\quad - \frac{xv_{y2}}{r^2+x^2} - P_L v_{x2} - Q_L v_{y2},\\
0 &= -\cos\delta'_2 i_{d2} + i_{q2}\sin\delta'_2 - \frac{rv_{y2}}{r^2+x^2}\\
&\quad - \frac{rV_1}{r^2+x^2} + Q_L v_{x2} - P_L v_{y2},\\
0 &= v_2^2 - v_{x2}^2 - v_{y2}^2.
\end{aligned} \tag{3.46}
$$

For the 2-bus system, the set of variables includes 6 states, $\mathbf{x} = [E'_{q2}, E''_{q2}, E'_{d2}, E''_{d2}, \sin(\delta'_2), \omega_2]^T$, and 8 algebraic variables, $\mathbf{y} = [i_{d2}, i_{q2}, V_{d2}, V_{q2}, V_2, V_{x2}, V_{y2}, \cos(\delta'_2)]^T$, where the subscript 2 indicates bus number 2. The system parameters are given as the following: $T'_{d0} = 0.6$, $T''_{d0} = 0.02$, $x_q = 0.8958$, $x'_q = 0.1969$, $x''_q = 0.1$, $T'_{q0} = 0.535$, $T''_{q0} = 0.02$, $M = 12.8$, $D = 20$, $T_{AA} = 0.002$, $p_m = P_G$, $r = 0.01938$, $x = 0.05$, $b = 0.0528$, $f_n = 60$. All parameters are in *p.u.* except time constants in seconds and frequency in Hertz.

A dynamic simulation and analysis package is developed in Mathematica 10.3.0.0 taking PSAT dynamic models [75] as the input. I also use CVX in MATLAB for

solving Lyapunov inequalities.

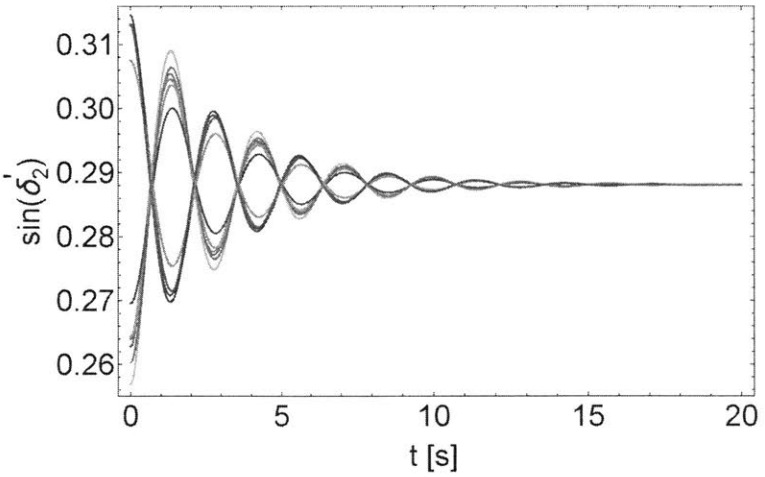

Figure 3-2: The state $\sin(\delta_2')$ of the generator simulated to 20 s

As shown in Figure 3-2, the system will converge to the nominal equilibrium if the gaps between the initial values of states, i.e. $\sin\delta_2'$ in this case, and the nominal values do not exceed the maximum distance that corresponds to the maximum radius r_{max} and the metric θ as discussed in the invariant set construction in section 3.4.3.

Figure 3-3 shows the contraction region in state space which is an ellipsoidal region corresponding to the ball-like invariant set as discussed in section 3.4. The convergence of all inner trajectories confirms that if the system starts from inside the ball, the corresponding trajectory is contained at all times. This can be interpreted as the following: if the post-fault equilibrium and the initial point of the post-fault trajectory both are a part of the region inside the ball, the system is transient stable. It also can be seen that the constructed invariant region touches the approximated contraction region boundary which associates with the state $\sin\delta_2'$. By assigning non-uniform weights to variables $\mathbf{z}$ in (3.42), the invariant region can be stretched along other directions as well.

In addition to 2 norm, I present the contraction results for infinity norm. As discussed in section 3.4.2, I consider an overdamped system. The new system is almost identical to the above 2-bus system, except for the synchronous machine inertial and the damping coefficient, i.e. $M = 4$ and $D = 200$. Figure 3-4 shows the evolutions

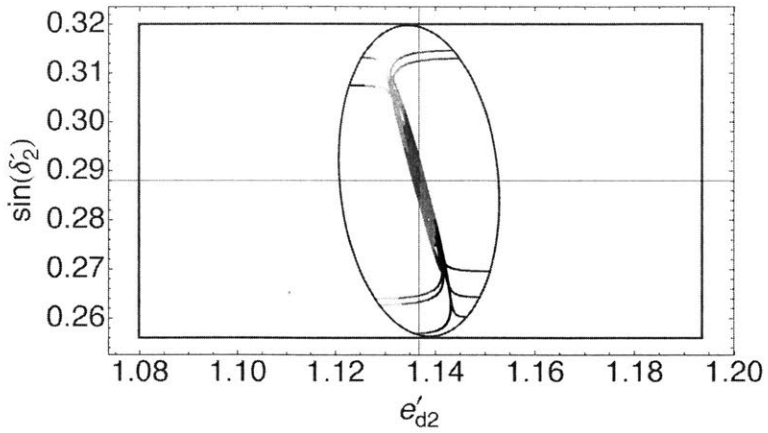

Figure 3-3: The ellipsoidal invariant region

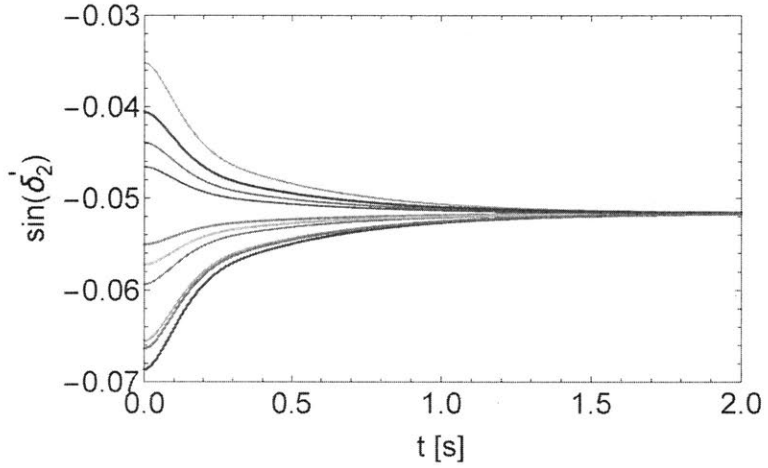

Figure 3-4: The state $\sin(\delta_2')$ of the generator simulated to $2\,s$ in an overdamped system

of the state $\sin(\delta_2')$ up to $2\,s$ starting from different initial conditions. Figure 3-5 illustrates a blue polytopic invariant region, the largest "ball" in infinity norm inside the contraction sub-region which is in brick brown. It can be seen that all trajectories starting from inside this ball will stay encompassed and eventually converge to the stable equilibrium.

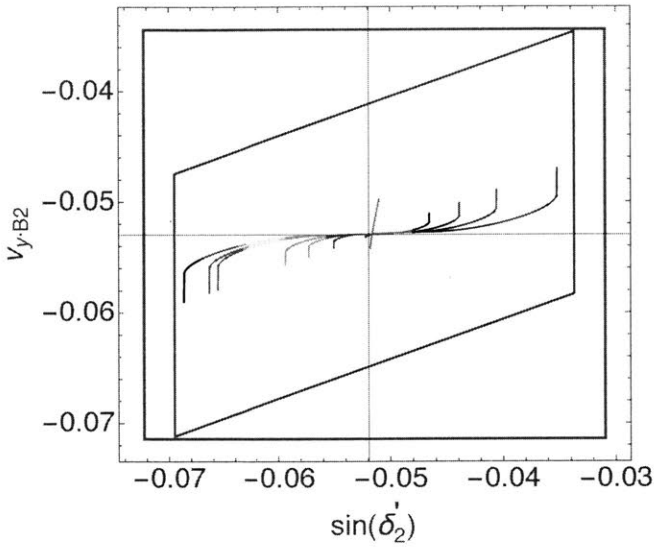

Figure 3-5: A polytopic invariant region

3.6 Conclusion

In this chapter the contraction properties of Differential-Algebraic Systems were characterized in terms of the contracting properties of the synthetic Jacobian representing the virtual differential system that reduces to a given DAE under singular perturbation theory analysis. I established the relations between the contraction rates of the extended ODE and reduced DAE systems and used these relations to develop a systematic technique for constructing inner approximations of the attraction region for quadratic DAE systems.

Chapter 4

Robust Small-Signal Stability Assessment for Load Dynamics Uncertainty

Dynamic response of loads has a significant effect on system stability and directly determines the stability margin of the operating point. Inherent uncertainty and natural variability of load models make the stability assessment especially difficult and may compromise the security of the system. I propose a novel mathematical "robust stability" criterion for the assessment of small-signal stability of operating points. Whenever the criterion is satisfied for a given operating point, it provides mathematical guarantees that the operating point will be stable with respect to small disturbances for any dynamic response of the loads. The criterion can be naturally used for identification of operating regions secure from the occurrence of Hopf bifurcation. Several possible applications of the criterion are discussed, most importantly the concept of Robust Stability Assessment (RSA) that could be integrated in dynamic security assessment packages and used in contingency screening and other planning and operational studies.

4.1 Introduction

Loss of stability of power systems usually results in some of the most dramatic scenarios of power system failure and has played an important role in most of the recent blackout. The dynamic of response of loads affects the voltage and to lesser extend angular stability in most important way [60]. The loads affect the overall system behavior and may lead to loss of stability because of insufficient damping [76]. Typically the loss of stability of the system occurs via Hopf bifurcation [14, 21, 29], when some part of the upper branch of the nose curve becomes unstable. The load response was shown to play a major role in this scenario for example in [30, 88, 97, 112]. Hereafter, whenever I mention stability, I mean small-disturbance stability that associates with a particular operating point.

Loads, by definition, represent an aggregate of hundreds or thousands of individual devices such as motors, lighting, and electrical appliances [50]. Load modeling has been a subject of intensive research for several decades [23, 49, 56, 74, 122]; however, it is still a rather open subject. Even though some certain types of loads such as aluminum or steel plant, and pumped hydroelectric storage are considered as well-identified ones [51]; due to its natural complexity and uncertainty, load dynamics, in general, may be never known completely in operational planning, operation, and control [44, 45]. The lack of knowledge about the dynamic characteristic of each individual component due to poor measurements, modeling, and exchange information, as well as the uncertainties in components/customers behaviors via switching events contribute to load uncertainties. Hence, loads are the main source of uncertainty [44] that undermines the accuracy of the power dynamic models used by system operators all over the world.

Incorporation of the uncertainty into existing models is essential for improving the system security usually defined as the ability of the system to withstand credible disturbances/contingencies while maintaining power delivery services continuity [80, 86]. The future power systems will likely be exposed to higher levels of overall stress and complexity due to penetration of renewable generators, and more intelligent loads,

deregulation of the system, and introduction of short-time scale power markets. Secure operation of these systems will necessarily require the operator to track the voltage stability boundary with new generation of security assessment tools providing comprehensive, fast and accurate assessment [85]. This work addressed the need in "robust" security assessment tools that can provide security guarantees even in the presence of modeling uncertainty.

In [26, 28, 31], several techniques were developed that rely on transversality conditions for quantifying the distance to various types of bifurcation including Hopf bifurcation in multidimensional parameter space. These techniques ensure robust stability of the equilibrium associated with nominal parameter Λ_0. Although they could be naturally extended to an uncertainty in small subspace of parameters, there extension to situations when the space of uncertain parameters has high dimension. In this chapter, I provide robust stability certificate in multidimensional space of certain system parameters. Unlike the works mentioned above I do without tracking the most dangerous direction, rather I indicate whether such directions exist or not. Hence, I do not attempt to find the unstable points associated with some certain critical parameters.

The existence of robust stability certificate and whole region of operating points that are certified to be robust stable provides new practical alternatives for dealing with load dynamics uncertainty. It has been noted in [32] that traditional "voltage collapse" instability is not affected by the load dynamics as it corresponds to saddle-node bifurcation, where the equilibrium point disappears altogether. At the same time for the more common Hopf bifurcation it was argued in [13] that sensitivity analysis of the system trajectories may provide enough information to assess the risks associated with common disturbances. Moreover, whenever the system operates in the robust stability regime, the stability can be certified even without knowing the dynamic characteristics of the load altogether. The stability of the system can be certified simply by analyzing the static characteristics of the loads in combination with well-understood dynamic models of generators. In this sense, I argue that accurate modeling of the loads is essential only when the system operates in the intermediate

regimes of the nose curves or the PV curves, between the robust stability region and the saddle-node bifurcation on the nose tip.

The structure of the chapter and the main contributions are summarized below. After introducing our modeling assumptions in 4.2.2 I derive the novel robust stability criterion in section 4.3. Then, I propose a practical algorithm RSA for robust stability certification. In section 4.5 I perform various simulations with several test cases from 2-bus system to WSCC 3-machine, 9-bus system and the IEEE 39-bus New England system to illustrate the concept of robust stability and RSA. The dynamic simulations are implemented in SystemModeler 4.0 and the computations are performed in Mathematica 10 and with the help of CVX program, a package for convex programming. Then in section 4.4 I discuss the proposed applications of the algorithm, and possible extensions to other kinds of uncertainty. Finally, the non-certified robust stability region is discussed in section 4.6.

4.2 Voltage stability and load dynamics

4.2.1 Voltage stability

While the power system operates in stressed heavily loaded regime it may be prone to subject to voltage stability problems. The secure operating region is confined by voltage stability boundary. As a common practice, static voltage stability criteria is widely used by system operators [120, 121]. Moreover, it has been argued that static analysis is preferred over dynamic approach [78]. At the same time it has been reported in many works that Hopf bifurcation may destabilize the system before it reaches the static stability limits [14].

Under some particular conditions, Hopf bifurcation may not occur [20] but typically, Hopf bifurcation determines the stability margins of most common systems [14] when the system exhibits Hopf bifurcation before it reaches the saddle-node bifurcation point or the tip of the nose curve. This situation can happen in the quasi-stable Hopf bifurcation region shown in Figure 4-1. The term quasi-stability used in power

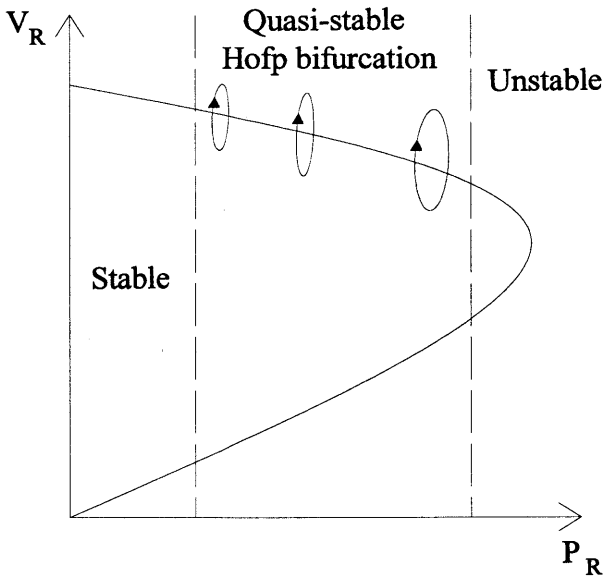

Figure 4-1: Qualitative visualization of Hopf bifurcation [58]

engineering is related to the oscillatory behavior of the system that is observed after the occurrence Hopf Bifurcation [58]. Detecting the loadability limits associated with the bifurcation is a much more complicated problem in comparison to the static stability analysis associated with the saddle-node bifurcation [1, 27, 124]. Some realistic examples of finding Hopf bifurcation point can be found in [51] and related works. In this context, the key contribution of this work is an alternative approach based on robust stability. Whenever the robust criterion criterion is satisfied, the system is mathematically guaranteed that Hopf bifurcation cannot occur.

4.2.2 Dynamic load modeling

The stability of any operating point and the position of the Hopf bifurcation on the nose curve depends on the dynamical behavior of loads on individual buses. Traditional models of load dynamics are based on combination of differential and algebraic equations for the load state. In steady state the loads can be characterized by their static characteristics $P^s(V,\omega)$ and $Q^s(V,\omega)$ which describe the dependence of the active and reactive power consumption levels P, Q on the load bus voltage level V

and system frequency ω. The dynamic state of the loads is typically characterized by single state variable x that represents the internal state of the system, for example the average slip of the induction motors. Whenever the composition of the loads on a single bus is highly heterogeneous, it may be represented by a parallel interconnection of several components characterized by different models. At any moment of time the load consuming active power P and reactive power Q can be characterized by the effective conductance $g = P/V^2$ and susceptance $b = Q/V^2$. The first order dynamic model for the conductance representing the dynamics of the internal state of the load can be than written in a general form as:

$$\dot{g} = F(g, V, \omega) \tag{4.1}$$

The right hand side of this equation is not arbitrary and should have the equilibrium point corresponding to the steady state characteristic of the load. Hence whenever the active power consumption is equal to steady rate, so $P = gV^2 = P^s(V, \omega)$, the right hand side of (4.1) should vanish, so $F(P^s(V, \omega)/V^2, V, \omega) = 0$. Any function F that satisfies this relation can be rewritten as $F = \tau^{-1}(P^s(V, \omega) - gV^2)$. In this form, the factor τ generally depends on voltage and frequency and can be interpreted as instant relaxation rate of the load. Whenever the load is stable when connected to an infinite slack bus, the factor τ can be trivially shown to be positive, so $\tau > 0$. The same mathematical form and analysis also apply to the load susceptance.

This discussion allows us to conclude that for the purposes of small-signal stability studies the first order models of the loads can be represented as

$$\tau_{gk}\dot{g_k} = -(g_k V_k^2 - P_k^s), \tag{4.2}$$

$$\tau_{bk}\dot{b_k} = -(b_k V_k^2 - Q_k^s). \tag{4.3}$$

Here the index k runs over all load buses in the system, the factors τ_{gk}, τ_{bk} represent the uncertainties in the dynamic models, that can be also interpreted as relaxation time. The factors P_k^s and Q_k^s represent the voltage dependent static characteristic of

the loads.

This type of load model is also introduced in [88, 107, 109], typically for thermostatic loads. However as we have argued in [82] this model can naturally be used to represent the standard models for thermostatically controlled loads, induction motors, power electronic converters, aggregate effects of otherwise unmodelled distribution Load Tap Changer (LTC) transformers etc. The static loads can be also naturally modeled within this framework by taking the limit $\tau_{gk} \to 0$. Obviously, the range of time constants is wide, ranging is from cycles to minutes and can introduce a lot of uncertainty in the modeling process.

I finish this section by comparing the model to the two other classical load models. Equations (4.2) are just another form of the traditional dynamic load models introduced originally in [42, 56]:

$$\dot{P}_d + f(P_d, V) = g(P_d, V)\,\dot{V} \tag{4.4}$$

Here P_d is the instantaneous power, that is denoted by $p_k = g_k V_k^2$ in our notations and V is the bus voltage magnitude, referred to as V_k in equations (4.2). The more specific form of these equations, known as exponential recovery model was introduced in [42, 56]:

$$T_p\,\dot{P}_d + P_d = P_s(V) + k_p(V)\,\dot{V} \tag{4.5}$$

I can recover the model (4.4) from equation (4.2) by taking the derivative of $g_k|V_k|^2$. This results in the following expression:

$$\dot{p_k} + \frac{p_k - P_k^s(V_k)}{\tau_{g\,k}} V_k^2 = 2\frac{p_k}{V_k}\frac{d}{dt}V_k \tag{4.6}$$

Another equivalent model was introduced in [122] and [63]:

$$T_p\frac{dx}{dt} = P_s(V) - P;\; P = x\,P_t(V) \tag{4.7}$$

$$T_q\frac{dy}{dt} = Q_s(V) - Q;\; Q = y\,Q_t(V) \tag{4.8}$$

where x is the state; subscript s and t indicate steady state and transient values, respectively; $P_t(V) = V^\alpha$, $P_s(V) = P_0 V^a$; $Q_t(V) = V^\beta$, $Q_s(V) = Q_0 V^b$. This model is equivalent to (4.2), (4.3) with $x = g_k$ and $y = b_k$ when $\alpha = \beta = 2$.

The proposed load model can naturally represent the most common types of loads, such as induction motors, thermostatically controlled loads. Hence, I believe that the form of the load model is rather general and can be used in a variety of practically relevant problems.

For example, below I show how the induction motor model can be embedded in our generic modeling framework. The induction motor depicted in Figure 4-2 can be

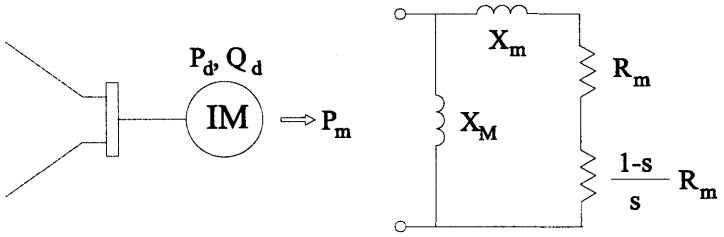

Figure 4-2: Induction motor load model [42]

described as [42]:

$$\dot{s} = \frac{1}{I\omega_0^2}\left(\frac{P_m}{1-s} - P_d\right) \tag{4.9}$$

where s is the motor slip, ω_0 is the base frequency, I is the rotor moment of inertia, P_m is the mechanical power, and P_d is the electric power given by

$$P_d = \frac{V^2 R_m s}{R_m^2 + X_m^2} = V^2 h(s) \tag{4.10}$$

Since $P_d = h(s) V^2$, from (4.10), I can represent the motor as the dynamic inductance with

$$g = h(s) \tag{4.11}$$

In normal operating regime, this relation can be also reversed so that $s = h^{-1}(g)$.

Differentiation of the two sides of (4.11) with respect to time yields the following expression:

$$\dot{g} = \alpha \frac{dh}{ds}(\frac{P_m}{1-s} - g V^2) \tag{4.12}$$

where $\alpha = \frac{1}{Iw_0^2}$. As long as s can be expressed in terms of g I reproduce the general form (4.1). Similar approach can be applied to most of the other types of loads, like thermostatically controlled loads, static loads behind Under-Load Tap Changers (ULTCs), and certainly the static loads which are described in more detail in Appendix in [81].

From (4.11) and (4.12), the induction motor load can be modeled in the form of (4.1). More importantly, the proposed dynamic load model not only is convenient for static analysis even in non-conventional power flow regime [82] but also satisfies all fundamental requirements for load models in voltage stability studies which are mentioned in [79].

4.3 Stability theory

In this section I address the question of the small-signal stability of an operating point by first reviewing the classical stability criteria applied to the problem of voltage stability of modern power system models in subsection 4.3.1 and then introduce the central result of the chapter: robust stability criterion in 4.3.2.

4.3.1 Linear stability

Consider again the nonlinear differential algebraic equations (1.1) and (1.2). Moreover, for convenience, one can decompose the state variables two sets, i.e. generator $\mathbf{x}_\mathcal{G} \in \mathbb{R}^{n_\mathcal{G}}$ and load states $\mathbf{x}_\mathcal{L} \in \mathbb{R}^{n_\mathcal{L}}$. Here $n_\mathcal{L}$ and $n_\mathcal{G}$ are the total number of states associated with loads and generators, respectively. Also, I assume that the subset of algebraic variables y represents the bus voltages, including the voltages on load buses. Under the assumptions above it is possible to represent (1.1) and (1.2) in terms of $\mathbf{x}_\mathcal{G}$

and $\mathbf{x}_{\mathcal{L}}$ as:

$$\dot{\mathbf{x}_{\mathcal{G}}} = \mathbf{f}^{\mathcal{G}}(\mathbf{x}_{\mathcal{G}}, y) \tag{4.13}$$

$$\dot{\mathbf{x}_{\mathcal{L}}} = \mathcal{T}^{-1}\mathbf{f}^{\mathcal{L}}(\mathbf{x}_{\mathcal{L}}, y) \tag{4.14}$$

$$0 = \mathbf{g}(\mathbf{x}_{\mathcal{G}}, \mathbf{x}_{\mathcal{L}}, y) \tag{4.15}$$

where $\mathcal{T}$ is a diagonal matrix with the size of $n_{\mathcal{L}} \times n_{\mathcal{L}}$ whose diagonal entries are the time constants of corresponding loads as introduced in (4.2); $\mathbf{f}^{\mathcal{G}}$ and $\mathbf{f}^{\mathcal{L}}$ are the functions associate with the sets of generators and the loads, respectively. Note, that in this representation the functions $\mathbf{f}^{\mathcal{G}}, \mathbf{f}^{\mathcal{L}}$ and G can be assumed to be known and all the uncertainty is aggregated in the matrix $\mathcal{T}$. This assumption is reasonable in the situations when the network characteristics are known, generator models are verified and static load characteristics are understood better than their dynamic response which is the case in practical situations. Note, also, that in the equations (4.13) and (4.14) there is no direct coupling between the dynamics of generators and loads, as the individual load components interact only indirectly via algebraic bus voltage variables.

Small signal stability can be characterized by considering the linearized version of the equations for the deviations of state and algebraic variables from their equilibrium values.

$$\begin{bmatrix} \delta\dot{\mathbf{x}}_{\mathcal{G}} \\ \delta\dot{\mathbf{x}}_{\mathcal{L}} \\ 0 \end{bmatrix} = \begin{bmatrix} \mathbf{f}^{\mathcal{G}}_{\mathbf{x}_{\mathcal{G}}} & \mathbf{f}^{\mathcal{G}}_{\mathbf{x}_{\mathcal{L}}} & \mathbf{f}^{\mathcal{G}}_{y} \\ \mathcal{T}^{-1}\mathbf{f}^{\mathcal{L}}_{\mathbf{x}_{\mathcal{G}}} & \mathcal{T}^{-1}\mathbf{f}^{\mathcal{L}}_{\mathbf{x}_{\mathcal{L}}} & \mathcal{T}^{-1}\mathbf{f}^{\mathcal{L}}_{y} \\ \mathbf{g}_{\mathbf{x}_{\mathcal{G}}} & \mathbf{g}_{\mathbf{x}_{\mathcal{L}}} & \mathbf{g}_{y} \end{bmatrix} \begin{bmatrix} \delta\mathbf{x}_{\mathcal{G}} \\ \delta\mathbf{x}_{\mathcal{L}} \\ \delta y \end{bmatrix} \tag{4.16}$$

where the subscripts of $\mathbf{x}_{\mathcal{G}}$, $\mathbf{x}_{\mathcal{L}}$, and y indicate the partial derivatives with respect to the corresponding states and variables. Away from saddle-node bifurcation the algebraic variables δy can be eliminated from (4.16) yielding

$$\begin{bmatrix} \delta\dot{\mathbf{x}}_{\mathcal{G}} \\ \delta\dot{\mathbf{x}}_{\mathcal{L}} \end{bmatrix} = A \begin{bmatrix} \delta\mathbf{x}_{\mathcal{G}} \\ \delta\mathbf{x}_{\mathcal{L}} \end{bmatrix} = \begin{bmatrix} \mathbf{f}^{\mathcal{G}}_{\mathbf{x}_{\mathcal{G}}} - \mathbf{f}^{\mathcal{G}}_{y} G_{y}^{-1} G_{\mathbf{x}_{\mathcal{G}}} & -\mathbf{f}^{\mathcal{G}}_{y} G_{y}^{-1} G_{\mathbf{x}_{\mathcal{L}}} \\ -\mathcal{T}^{-1}\mathbf{f}^{\mathcal{L}}_{y} G_{y}^{-1} G_{\mathbf{x}_{\mathcal{G}}} & \mathcal{T}^{-1}(\mathbf{f}^{\mathcal{L}}_{\mathbf{x}_{\mathcal{L}}} - \mathbf{f}^{\mathcal{L}}_{y} G_{y}^{-1} G_{\mathbf{x}_{\mathcal{L}}}) \end{bmatrix} \begin{bmatrix} \delta\mathbf{x}_{\mathcal{G}} \\ \delta\mathbf{x}_{\mathcal{L}} \end{bmatrix}$$

This expression can be more conveniently decomposed as $A = \Lambda J$ in the following

form

$$A = A_{\mathcal{T}} \triangleq \begin{bmatrix} \mathbb{1} & 0 \\ 0 & \mathcal{T}^{-1} \end{bmatrix} \begin{bmatrix} J_{\mathcal{GG}} & J_{\mathcal{GL}} \\ J_{\mathcal{LG}} & J_{\mathcal{LL}} \end{bmatrix}. \tag{4.17}$$

where $\mathbb{1}$ is the identity matrix of size $n_{\mathcal{G}} \times n_{\mathcal{G}}$.

The key advantage of this decomposition is the separation of the matrix A in an uncertain diagonal matrix $\mathcal{T}$ and the Jacobian matrix J that does not depend on the uncertain load time constants, and depends only on the properties of the steady state equilibrium point defined in load and generator variables.

Notably, for load models considered in this work the second row depends only on the steady-state behavior of the load, i.e. it can be computed given the load levels and voltage/frequency dependence of the steady-state active and reactive power consumption.

According to the Lyapunov direct method, the system described by $\dot{x} = Ax$ is stable if and only if there exist a symmetric positive definite matrix $Q = Q^T \succ 0$ such that

$$QA + A^T Q \prec 0 \tag{4.18}$$

where superscript T is used for transpose operator. However, existence of a Q matrix for a given A merely implies the system stability for some specific load dynamics. In the next section, I introduce the concept of robust stability that guarantees the stability of the system stability for any load time constant uncertainty, i.e. any positive definite diagonal matrix Λ.

4.3.2 Robust stability

As discussed previously, in this work, I assume that the operator has reliable information about the generator models and settings, and the corresponding Jacobian matrix row $J_{\mathcal{G}}$ is available for analysis. At the same time, I assume that the grid model and all the algebraic equations characterized by G are known with high accuracy. For the load model I assume that the matrices $\mathbf{f}^{\mathcal{L}}_{\mathbf{x}_{\mathcal{L}}}$ and $\mathbf{f}^{\mathcal{L}}_{y}$ describing the static characteris-

tics of loads are known with high accuracy, however the matrix $\mathcal{T}$ representing the dynamic response is not. The goal of robust stability certificate is to guarantee that the operating point is stable for any positive definite $\mathcal{T} \succ 0$.

It is important to distinguish between two categories of load uncertainties, i.e. load level uncertainty and load dynamic uncertainty. The former relates to load level fluctuations due to various factors such as individual consumer behavior or variations in the production output of DGs. This type of uncertainty is considered in [16, 44, 46, 47, 87]. On the other hand, load dynamic uncertainty concerns the unpredictability of the dynamic response of the load to small fluctuation in voltage and frequency. In this work, I only focus on the latter type of uncertainty and do not discuss the uncertainty in load variations assuming that the operating point is known. However, the regions of robust stability can be also used to account for uncertainty in load consumption levels.

There are many sources of uncertainty in load dynamics. Apart from the natural uncertainty related to composition of power consumption devices, the level of uncertainty may increase dramatically in coming years when more small scale generators, i.e. DGs, are integrated to the systems, especially on the distribution level. When the penetration level becomes very high the traditional static voltage stability may be insufficient to assess the system security [82, 84]. On the other hand, the approach proposed in this work is valid, at least for non-synchronous DGs that can be modelled as a negative loads with dynamics in the form of (4.2) and (4.3).

The robust stability criterion developed in the thesis is directly linked to the concept of D-stability [55, 57] that are extended to model the uncertainty in a subset of state variables.

In the following theorems I denote the set of positive definite matrices of size $n \times n$ as $\mathbb{P}_n$ and set of diagonal positive definite matrices of size $n \times n$ as $\mathbb{D}_n$. The following theorem is central to the robust stability certification of power systems.

Theorem 16 *Assume that there exists block-diagonal positive definite block diagonal*

matrix Q, such that

$$Q = \begin{bmatrix} Q_{\mathcal{G}} & 0 \\ 0 & Q_{\mathcal{L}} \end{bmatrix}, \tag{4.19}$$

with positive definite matrix $Q_{\mathcal{G}} \in \mathbb{P}_{n_{\mathcal{G}}}$ and diagonal positive definite matrix $Q_{\mathcal{L}} \in \mathbb{D}_{n_{\mathcal{L}}}$ that satisfies

$$QA_{\mathcal{T}} + A_{\mathcal{T}}^T Q \prec 0 \tag{4.20}$$

for some $\mathcal{T} > 0$. In this case the system is robust stable, i.e. in other words, for any diagonal $\tilde{\mathcal{T}} \in \mathbb{D}_{n_{\mathcal{L}}}$ there exists $\tilde{Q} \succ 0$ such that $\tilde{Q}A_{\tilde{\mathcal{T}}} + A_{\tilde{\mathcal{T}}}^T \tilde{Q} \prec 0$

Proof 12 *Consider the matrix $\tilde{Q} = \tilde{Q}^T = Q\mathcal{T}\tilde{\mathcal{T}}^{-1}$. Due to block-diagonal structure of Q we have $\tilde{Q}A_{\tilde{\mathcal{T}}} = QA_{\mathcal{T}}$ and at the same time $A_{\tilde{\mathcal{T}}}^T \tilde{Q} = A_{\mathcal{T}}^T Q$, so $\tilde{Q}A_{\tilde{\mathcal{T}}} + A_{\tilde{\mathcal{T}}}^T \tilde{Q} = QA_{\mathcal{T}} + A_{\mathcal{T}}^T Q \prec 0$.*

Note, that the condition (4.20) first reported in the framework of D-stability [55, 57] only establishes a sufficient criterion for robust stability. To our knowledge no computationally tractable necessary and sufficient criteria reported for D-stability have been reported in the literature. The only exception is the set of results on the so-called positive matrices [59] for which the existence of diagonal Lyapunov function is a necessary condition for stability. Positive matrices are characterized by negative off-diagonal components. The question of whether they can be used to describe power system dynamics is interesting and worth exploring, but is outside of the scope of this study.

The problem of checking whether the block diagonal matrix Q exists for given $A_{\mathcal{G}}$, $A_{\mathcal{L}}$ and $\mathcal{T}$ is easy and can be accomplished by solving the following semi-definite programming (SDP) problem.

$$\begin{aligned} &\max_{Q} \rho \\ \text{subject to: } &QA_{\mathcal{T}} + A_{\mathcal{T}}^T Q + \rho \mathbb{1} \prec 0 \\ &Q \succ 0 \\ &\mathrm{tr}(Q) = 1. \end{aligned} \tag{4.21}$$

Here the optimization is carried over the matrices Q with structure defined in (4.19). The condition $\mathrm{tr}(Q)$ fixes the overall normalization of the Lyapunov function. Whenever the resulting value ρ is positive the system is guaranteed to be robust stable. The complexity of this procedure is polynomial in the size of the system. In recent years mathematically similar procedures have been successfully applied in the context of optimal power flow approaches [54, 62], and more recently for power system security assessment purposes [77]. It has been shown in a number of chapters, that even large scale systems admit fast analysis with SDP algorithms [64].

However, from (4.14), one can see that the proposed robust stability criterion requires the equilibrium to be independent on uncertain parameters, for example the time constants of the loads. Fortunately, the standard control systems in generators and other components normally satisfy this requirement. This can be seen by looking at the equations for the system equilibrium point, like load flow equations and observe that they don't depend on the dynamic time constants of governors, AVR and loads.

In this work I illustrate the approach by considering the load dynamic uncertainties. In real power systems, the dynamics of generators and Flexible AC Transmission Systems (FACTS) devices are also the sources of uncertainties [3, 15, 61, 116]. The generators and the system uncertainties cause much difficult in designing effective Power System Stabilizer (PSS) and other controllers [17, 36]. As mentioned before, as long as these uncertainties do not alter the system equilibrium, the proposed robust stability criterion can be applied to access the system stability. In this case, all known dynamic components can be grouped in set $\mathcal{G}$ and unknown dynamic ones can be classified in set $\mathcal{L}$.

4.4 Proposed applications

In this section I discuss the possible applications of the mathematical techniques explained above.

4.4.1 Dynamic Security Assessment (DSA)

DSA are used to analyze the security of power systems and assess various types of stabilities such as voltage stability in Voltage Stability Assessment (VSA) and transient stability which is assessed in Transient Stability Assessment (TSA). The configuration of the DSA integrated into the Energy Management System (EMS) is discussed in details in [80]. Depending on the purpose of the assessment and the time-scale of the function of interest, the input of DSA may be different. Typical DSA assess the stability of a given operating state determined either from Supervisory Control and Data Acquisition (SCADA) or Phasor Measurement Unit (PMU) measurement tools or constructed in framework of scenario analysis for planning or operation purposes. Being a fundamental component of DSA toolbox, the main goal of VSA is to certify pre- and post-contingency voltage stability and calculate the voltage stability margin. The contingency set typically includes major equipment outages such as generator, transformer, line tripping. $N-1$ security set is normally of interest [39, 80, 98].

Brute-force accounting for load dynamics and other uncertainties in traditional VSA is computationally expensive due to large number of scenarios that need to be analyzed. An alternative proposed here and discussed in more details in section 4.4.2 is based on the worst case scenario analysis and relies only on the analysis of static characteristics of the loads and well-understood dynamic characteristics of the generators. Hence it eliminates the need for computationally expensive dynamic simulations and stochastic Monte Carlo approached to modeling the uncertainty.

Typically, the objective of the DSA module is to assess the system stability margins and its behavior in major contingencies. At the input, the DSA module admits a scenario which includes: i) a power flow base case which describes a snapshot of the system conditions; ii) dynamic data of the system; iii) set of critical disturbances. The output from the DSA module is composed of the system stability and corresponding margins. The work [48] describes DSA in more details from the perspectives of both traditional approaches in off-line analysis as well as intelligent system (IS) based one for on-line assessments.

It is worth to distinguish the two main classes of security assessment, i.e. Static Security Assessment (SSA) and DSA. SSA concerns whether the operating constraints are satisfied, i.e. whether the post-contingency voltage lies within the acceptable range, whereas DSA looks for the system stability. In some cases, acceptable voltage levels may imply that the system is stable. However, in general, this relationship is not such simple. Therefore, the system stability needs to be assessed thoroughly in the framework of DSA.

4.4.2 Robust Stability Assessment

The algorithms developed in this work can form the foundation of a potentially more powerful technique that I call Robust Stability Assessment (RSA). Specifically I propose to use RSA to develop the fast screening phase of VSA in an online DSA that is required to be fast enough to either automatically or manually choose the proper remedial control actions. For an effective and powerful VSA, the accuracy and the speed of computation are the two most crucial and challenging issues. As previous mentioned, the accuracy of VSA is affected due to uncertainties. RSA is able to eliminate such errors. Moreover, the fast algorithm of RSA is extremely helpful to speed up the program, especially when it relies on deterministic method that exhaustively screens contingency and searches for secure limits. Even for intelligent system based VSA, RSA is still able to help to remove a significant number of possibilities. The efficiently computational aspect of the proposed algorithm can be easily scale to bulk systems which is impossible for traditional dynamic approaches while rendering the meaning of dynamic stability assessment.

Within this approach in RSA, the stability is certified not for a single mathematical model of a system, but rather for the whole set of systems defined by different realizations of uncertain elements. The key steps required for performing the Robust Stability Assessment are explained below:

1. **Input** The input of RSA is an equilibrium configuration of the system characterized by the levels of load consumption, network model, and dynamic model

of the generators.

2. **Initialization** On the initialization stage the algorithm defines the model of the system by introducing the uncertain model of the load. In the simplest approach the load buses are modeled as time dependent impedances as discussed in section 4.2.2. In the framework of more advanced approaches it may be reasonable to separate the actual loads into static components, well-defined dynamic ones (like aluminum smelters) and finally the uncertain dynamic loads. Only the uncertain components should be incorporated in the $\mathbf{x}_{\mathcal{L}}$ part of the dynamical system descriptions, whereas all the other components should be modeled as known ones and described by the vector $\mathbf{x}_{\mathcal{G}}$.

3. **Linearization** The dynamic model of the system is linearized and the matrix $A_{\mathcal{T}}$ is calculated for some arbitrarily chosen load relaxation time constants matrix $\mathcal{T}$. As explained in previous section the choice of initial $\mathcal{T}$ does not have any effect on the outcome of the analysis.

4. **Optimization** The Semi-Definite Programming problem (4.21) is solved for the constructed matrix $A_{\mathcal{T}}$. Whenever the resulting value ρ is positive the equilibrium point is certified to be robust stable, i.e. it is provably stable for any matrix $\mathcal{T}$.

5. **Direct Analysis** As the condition $\rho > 0$ from (4.21) is only sufficient but not necessary, whenever the result of optimization results in negative ρ, nothing can be said about the stability of the system. The user of RSA has to rely on other probabilistic or deterministic techniques to assess the probability of having stable system given the uncertainty in load dynamics.

RSA can be naturally incorporated in several planning and operational studies that are described below.

4.4.3 RSA for deterministic stability assessment

One specific application of the RSA approach is the deterministic stability assessment that is regularly performed during power system operation. At any moment of time, the system operators need to know the following [80].

1. Whether the current state is secure
2. Whether the system will remain secure after the next several minute changes
3. If the system is insecure, what countermeasures need to be carried out

The general deterministic stability assessment answers these questions via the following sequence of steps [73]:

1. Develop the power flow base cases for the study
2. Select the contingency set
3. Select parameters in the expected operating range
4. Identify security constraint violations
5. Find the security boundary
6. Construct the comprehensive reports like plots or tables by combining all the security boundaries

Robust stability technique naturally fits in this process without any adjustments to the logic. The key advantage of the RSA is its ability to certify the stability and security of the system even in the presence of dynamic uncertainty naturally expressed as parameter ranges in step 3) above. The proposed robust stability criterion is compatible with both off-line and on-line security assessments in the presence of uncertainties. Moreover, it may also provide additional benefits for implementing real-time and distributed security assessment schemes which are still the main challenge to the current technologies [39]. In this framework, the assessment has to be performed without

access to full model of external entities, and the operator may represent the dynamic response of these entities via equivalent models with uncertain time-constants. Such a scheme is more robust to communication system malfunctions and potentially reduces the requirements to throughput and latency of sensing, communication and computation components. In some cases, large enough robust stability region can be directly applied in operation procedures and used as secure regimes that are displayed to the operators. Moreover, as mentioned before, RSA can access the system dynamic stability simply based on static analysis (power flow) and well-understood dynamic components, the dynamical secure regimes can be constructed in advance. Specific demonstration of the usage of robust stability in VSA is presented in section 4.5.2 where I examine the $N-1$ contingency set of WSCC 3-machine, 9-bus system.

4.4.4 Security Indicator

The optimization problem (4.21) can be used not only to certify the stability of a given point but also to estimate the stability margin. Indeed, the value of ρ is naturally interpreted as the worst case rate of decay of the Lyapunov function defined by x^TQx and can be thus viewed as the worst case stability margin. The security indicator defined by ρ can be used for risk monitoring purposes and can assist the system operators in designing the preventive control strategies. In the latter it is natural to optimize for control actions that ensure some minimal level of worst-case stability margin.

With additional research effort invested it should be possible to modify the security indicator defined by ρ from (4.21) in a way that it's value reflects the probabilities of system losing stability in the presence of random factors, such as renewable generators. To achieve this goal it is necessary to study the sensitivity of matrix A with respect to random factors, and modify the term $\rho\mathbb{1}$ in a way that certificate that bounds ρ from below can be interpreted in probabilistic way, i.e. probability of system losing stability bounded from above.

4.4.5 Stability constrained Planning and Optimization

RSA and security indicator discussed in section 4.4.4 can be also used for planning and dispatch purposes in the framework of stability or security constrained optimization. In this case the security indicator can be used as one of the optimization objectives or constraints. As closed form expression for ρ does not exist, the corresponding optimization needs to rely on some iterative heuristics, like genetic algorithms. The algorithms may need to be complemented with direct approaches as described for example in [28, 70, 71, 91].

4.5 Simulations

In this section I report the results of application of the Robust Stability Certification to several common models of power systems. Moreover, RSA technique does not explicitly address the question of feasibility of the operating point, although it could be trivially extended with any kinds of voltage and current constraints. As these constraints depend on the operating point, and not on the dynamic equations, they can be checked separately from the small signal stability. Whenever the small-signal stability of the operating point needs to be analyzed, and RSA technique allows to assess stability even in the presence of load modeling uncertainty. As a matter of fact, in contingency analysis, it is essential to assess the system stability even when the voltage levels are unacceptable according to normal operating conditions.

4.5.1 A 2-bus system

The rudimentary 2-bus system shown in Figure 4-3 is adopted from [112] and is extended with the dynamic model of the loads. The generator consists of an internal voltage source behind the transient reactance and an IEEE Type 1 exciter. In this work, I do not consider angle dynamics but focus solely on voltage dynamics, although the extension to more general models is trivial. The set of differential equations

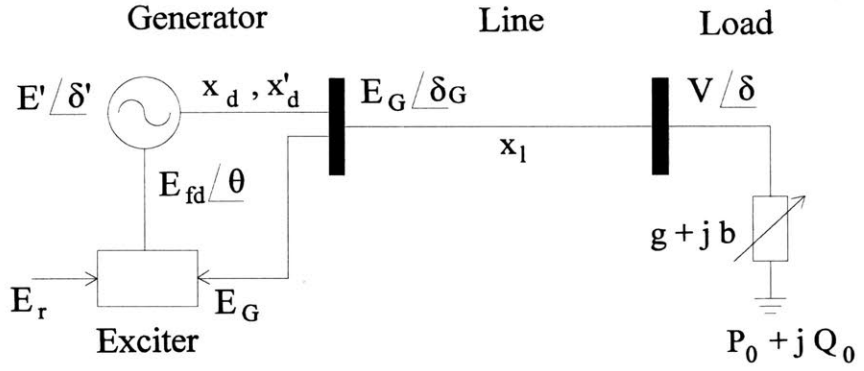

Figure 4-3: A rudimentary system [112]

describing the generator dynamics are the same as described in [112] or [97]:

$$T'_{d0}\dot{E}' = -\frac{x_d}{x'_d}E' + \frac{x_d - x'_d}{x'_d}E_G\cos(\delta_G - \delta') + E_{fd} \tag{4.22}$$

$$T\dot{E}_{fd} = -E_{fd} - K(E_G - E_r) \tag{4.23}$$

where x_d and x'_d are the equivalent direct axis reactance and transient direct axis reactance; T'_{d0} is the direct axis transient open circuit time constant; $E'\angle\delta'$ is the internal source voltage; $E_G\angle\delta_G$ is the terminal voltage; E_R is the reference voltage; E_{fd} is the exciter output voltage (generator field voltage); K and T are the gain and integral time constant associated with exciter PI control. Generator models are described in details in [61, 90, 92]. The dynamics of the load is described by (4.2):

$$\tau\dot{g} = -(gV^2 - P_0) = -(p - P_0), \tag{4.24}$$

$$\tau\dot{b} = -(bV^2 - Q_0) = -(q - Q_0). \tag{4.25}$$

where τ is the load time constant, $\tau = \tau_g = \tau_b$; V is the voltage magnitude at the load bus; $P_0 = P^S$ and $Q_0 = Q^S$ are the desired demand levels that I assume to be constant and not depending on the voltage; p and q are the instantaneous power consumptions of the load. For the rudimentary system, the set of state variables includes 4 states, i.e. $x = [E', E_{fd}, g, b]^T$ which can be decomposed into 2 state vectors $\mathbf{x}_\mathcal{G} = [E', E_{fd}]^T$ and $\mathbf{x}_\mathcal{L} = [g, b]^T$. Moreover, the diagonal matrix constituted by the time constants of

the loads is $\mathcal{T} = \text{diag}(\tau, \tau)$. The relations (4.23) and (4.24) form the set of differential equations.

Algebraic equations, $G(x, y) = 0$ are composed of relation describing the generator, the network, and the load can be stated as follow:

$$0 = \frac{E'E_G}{x'_d}\sin(\delta_G - \delta') + \frac{E_G V}{x_l}\sin(\delta_G - \delta) \tag{4.26}$$

$$0 = \frac{1}{x'_d}(E_G^2 - E_G E'\cos(\delta_G - \delta')) \tag{4.27}$$

$$+ \frac{1}{x_l}(E_G^2 - E_G E\cos(\delta_G - \delta)) \tag{4.28}$$

$$0 = \frac{VE_G}{x_l}\sin(\delta - \delta_G) + p \tag{4.29}$$

$$0 = \frac{1}{x_l}(V^2 - E_G E\cos(\delta - \delta_G)) + q \tag{4.30}$$

$$p = gV^2 \tag{4.31}$$

$$q = bV^2 \tag{4.32}$$

The internal voltage source angle is used as the reference, i.e. $\delta' = 0$. The system parameters are given as the following: $T'_{d0} = 5$; $E_r = 1$; $x_d = 1.2$; $x'_d = 0.2$; $T = 0.39$; $K = 10$; $x_l = 0.1$. All parameters are in $p.u.$ except time constants in second and scalar gain K.

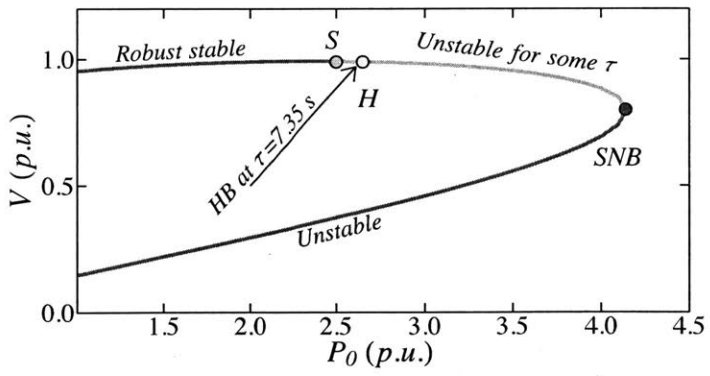

Figure 4-4: Robust stability illustration for rudimentary system

In Figure 4-4 I show the results of stability analysis of different points on the nose

curve. The system is shown to be robust stable up to point S where $P_0 = 2.51\,p.u.$ at the upper branch of the nose curve of $\cos\phi = 0.98$. Saddle-node bifurcation (SNB) corresponding to voltage collapse occurs at $P_0 = 4.2\,p.u.$. The section of the upper branch between S and SNB cannot be certified to be robust stable, and can be numerically shown to be unstable for some load time constant τ at every point. For example, at point H where $P_0 = 2.6\,p.u.$, the system exhibits Hopf bifurcation (HB) with $\tau = 7.35\,s$. The eigenvalues of matrix A at point H are shown on figure 4-5.

For the rudimentary system, the lower branch of the PV is unstable for most of load dynamics.

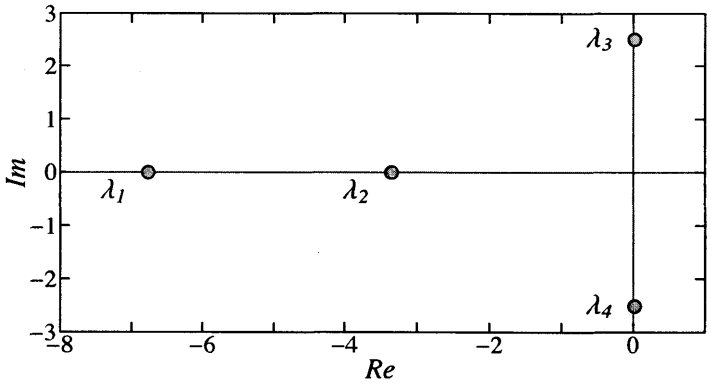

Figure 4-5: The eigenvalues of A matrix of rudimentary system encountering Hopf bifurcation

4.5.2 The WSCC 3-machine, 9-bus system

The WSCC 3-machine, 9-bus system with all the parameters is plotted in Figure 4-6. Bus 1 is the slack bus, and bus 2 and 3 are PV buses with specified the active power outputs and the magnitude of voltages at the terminals. Three PQ loads are connected to 3 substations residing at buses 5, 6, and 8. The base power is $S_{base} = 100\,MVA$. I assume that load bus 8 works with a constant power factor, i.e. $\cos\phi_8 = 0.894$. All branches and transformers data are described in Appendix in [81].

To characterize the stability of the system I increase the load at bus 8 while keeping the other parameters fixed. The system is robust stable up to point S where

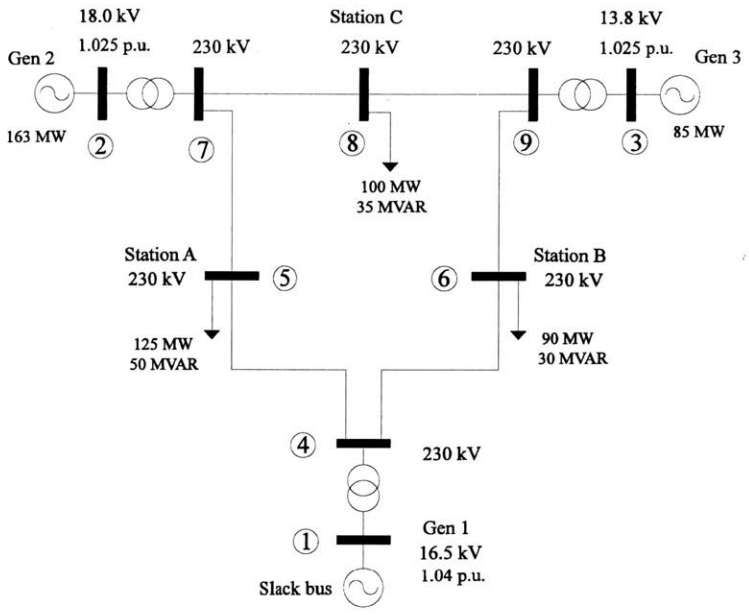

Figure 4-6: The WSCC 3-machine, 9 bus system [97]

$P_8 = 3.0\,p.u.$. The region from S to SNB where saddle-node bifurcation happens at $P_8 = 3.5\,p.u.$, the system may become unstable for some time constants. For example, fixed time constant of load 5 and 6 to be equal $1\,s$, the system encounters Hopf bifurcation at point H_1 where $P_8 = 3.36\,p.u.$, $\tau_8 = 15.57\,s$, or at point H_2 where $P_8 = 3.45\,p.u.$, $\tau_8 = 11\,s$. Voltage oscillation that corresponds to point H_2 is shown in Fig. 4-8.

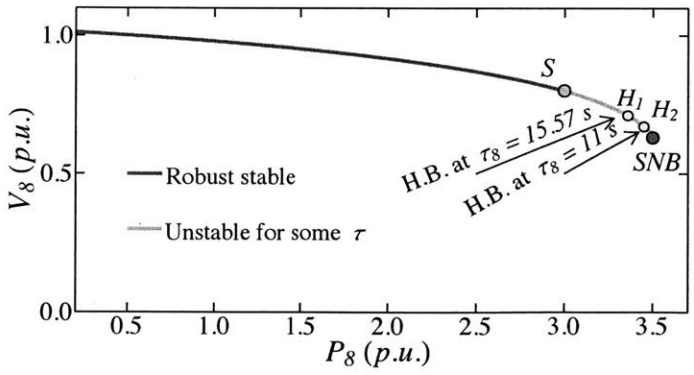

Figure 4-7: Robust stability illustration for WSCC 3-machine, 9-bus system

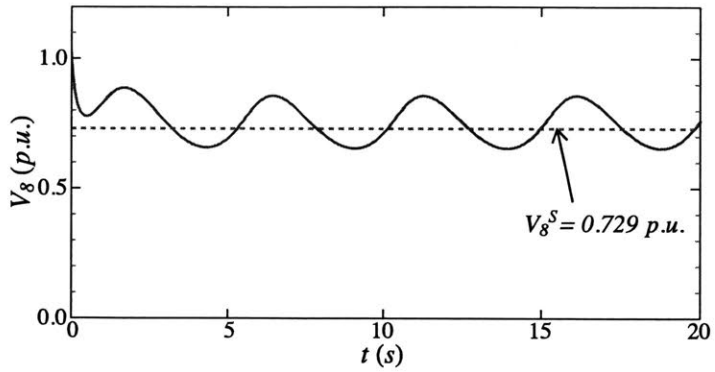

Figure 4-8: Oscillatory voltage instability with the WSCC 3-machine, 9-bus system at H_2 where $P_8 = 3.45\,p.u.$ and $\tau_8 = 11\,s$

In Figure 4-7, V_8^S is the voltage level when the system is stable for the same level of power consumption, i.e. $P_8 = 3.45\,s$ but with smaller time constant, say $\tau_8 = 9\,s$. For less uncertain systems, i.e. when load buses 5 and 6 have fixed $\tau_g = \tau_b$, point S may extent to higher level of active power at bus 8, $P_8 = 3.1\,p.u.$. This observation is true for more general situations, i.e. the less uncertainty presents in the system, the more stable the system is.

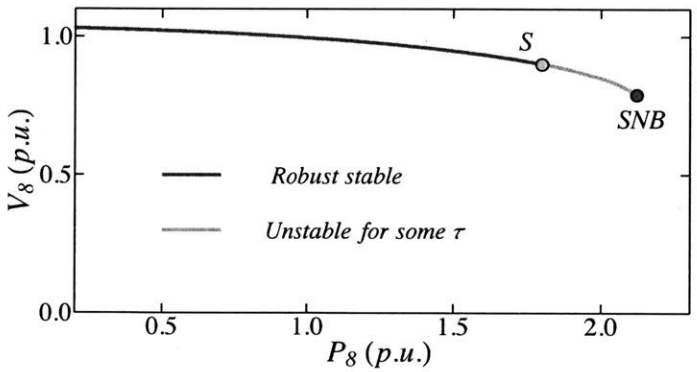

Figure 4-9: Robust stability illustration for WSCC 3-machine, 9-bus system, correlated loading condition

Also, I consider a more realistic loading scenario with correlated loading condition. I consider the case when $P_5 = P_6 = P_8$ and $Q_5 = Q_6 = Q_8$. Again, the PV

curve shown in Figure 4-9 indicates the robust stability region in blue where $P_8 \leq 1.86\,p.u.$ and the yellow region, from point S to SNB, where the system may become unstable for some instant relaxation times of the loads. Figure 4-9 resembles Figure 4-7 where no correlated loading scenario is considered. They differ only in loading conditions at the robust stable point, S, and the saddle-node bifurcation. The lower critical loading conditions are observed because the power transferred through power lines increases faster when all buses are loaded at once. Different correlated loading scenarios considered but not reported in the thesis were characterized by qualitatively similar results as shown in either Figure 4-7 or Figure 4-9. In the follow-up section 4.5.3 I also report similar studies with more realistic economic load dispatch scheme that accounts for distribution of the load increase between different generators [97]. The behavior observed in that scenario is also qualitatively similar.

RSA for WSCC 3-machine 9-bus system

As mentioned before, in this subsection I demonstrate the application of robust stability applied to RSA within $N-1$ security assessment. Different from off-line assessment in which an exhaustive list of contingencies is assessed, here I only consider a set of most dangerous contingencies. This practice, indeed, is more suitable for online assessment. The subset of considered contingencies may include the lines with large power flows or the lines that are connected to low voltage buses [66]. The base case power flow is chosen as shown in Figure 4-6 except for load bus 8, where $P_8 = 1.8\,p.u.$, $Q_8 = 0.5\,p.u.$. For the WSCC 3-machine 9-bus system, all the voltage levels are close to $1\,p.u.$. Therefore, I rely on the total MVA power flows through the line to determine the most dangerous ones.

Table 4.1: Contingency analysis summary table

Line trip	$1-4$	$2-7$	$7-8$	$9-3$
Case I	Stable	Stable	Stable	Stable
Case II	Limit Cycle	Stable	Stable	Stable
Case III	Unstable	Unstable	Limit Cycle	Stable
RSA	NRS	NRS	NRS	RS

There are two different situations in contingency analysis, i.e. with uncertainty or without uncertainty. When there is no uncertainty in the model, consider 3 different cases of fixed time constants at bus 5, 6, and 8; i.e. $\tau_5 = \tau_6 = \tau_8 = \tau$, and $\tau = 1\,s$ in Case I, $\tau = 5\,s$ in Case II, $\tau = 10\,s$ in Case III. The absolute values of the instant relaxation time are not important because the actual set of the time constants of the loads may vary over time and may be different from bus to bus. Therefore, the 3 cases are used merely to demonstrate the performance of robust stability analysis. In contrast, I use RSA in the presence of uncertainty. For each dangerous contingency and such time constants, the system stability is assessed as shown in Table 4.1.

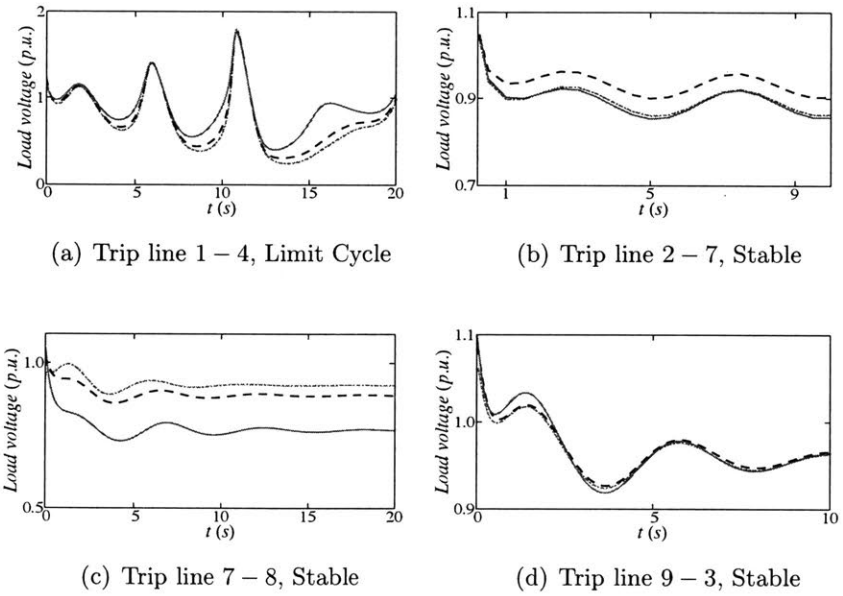

(a) Trip line $1-4$, Limit Cycle

(b) Trip line $2-7$, Stable

(c) Trip line $7-8$, Stable

(d) Trip line $9-3$, Stable

Figure 4-10: The load voltage evolutions in time-domain simulations in contingency analysis for Case II, $\tau = 5\,s$

In Table 4.1, for RSA results, RS and NRS imply robust stable and non robust stable, respectively. One can observe that if the system is robust stable, for example when line $9-3$ is tripped, the non-uncertain stability assessment also indicates that the system is stable in all cases. In contrast, if the system is not robust stable according to RSA results, there exists some cases or some set of instant relaxation times cause the system unstable. This happens when either line $1-4$ or $2-7$ is

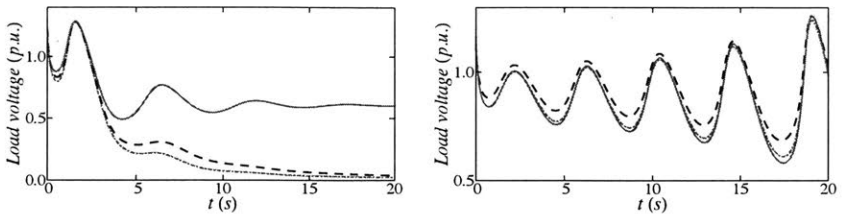

(a) Trip line $1-4$, Unstable

(b) Trip line $2-7$, Unstable

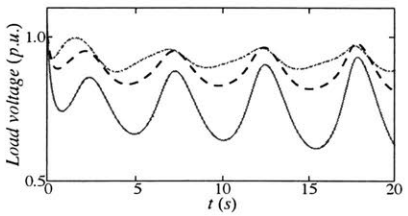

(c) Trip line $7-8$, Limit Cycle

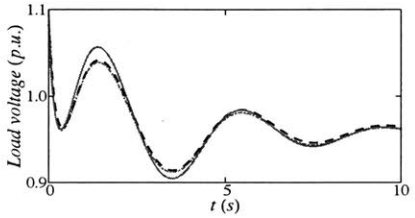

(d) Trip line $9-3$, Stable

Figure 4-11: The load voltage evolutions in time-domain simulations in contingency analysis for Case III, $\tau = 10\,s$

disconnected. Moreover, in two considered cases, the system is stable if the line $7-8$ is tripped. For this contingency, RSA result indicates that the system is non-robust stable. In fact, the system is unstable with $\tau_5 = \tau_6 = 1\,s$ and $\tau_8 > 14\,s$ where the load voltage at bus 8 collapses around $t = 60\,s$.

In considered situations, limit cycles (LC) appear in Case II with line $1-4$ tripping and in Case III with line $7-8$ tripping. The system will exhibit voltage oscillations which are unexpected and dangerous because they may limit the power transfers and induce stress in the mechanical shafts [97]. In such cases, RSA also indicates that the system is non-robust stable or potentially unstable.

The contingency analysis results, for example in Case II and Case III, can also be represented with time-domain simulations as in Figure 4-10 and Figure 4-11 where the red dash-dot, black dash, and blue solid trajectories correspond to the load voltages at bus 5, 6, and 8, respectively. For $\tau = 5\,s$ and tripping the line $1-4$, the system encounters Hopf bifurcation and the voltages keep oscillating but never go beyond the range from $0.2\,p.u.$ to $1.8\,p.u.$. Also, for $\tau = 5\,s$ and tripping the line $2-7$, the

system is stable but very lightly damped. The voltages settle around $t = 800\,s$ which indicates that the system is close to Hopf bifurcation point. The first 20-second and 10-second evolutions of the load bus voltages when tripping the line $1-4$ and $2-7$ for Case II are presented in Figure 4-10(a) and Figure 4-10(b), respectively. Moreover, for Case III, the line $2-7$ is tripped, the voltage at the load bus 8 collapses around $t = 80\,s$; hence the system is unstable. Figure 4-11(b) shows the first 20-second time evolution of the unstable voltage trajectory.

However, RSA does not require any time-domain simulation, thus reduces the need of storages and the time consuming. In addition, RSA does not provide the margin to SNB or particular bifurcation points, instead RSA provides another type of stability margin i.e. robust stability margin which measures the distance between the current operating point to the robust stability boundary. For example, for the contingency case in which the line $9-3$ is tripped, the security indicator discussed in section 4.4.4, $SI = \rho = 0.004$, indicates that the system will work close to the robust stability boundary after the contingency. Hence, a slight change in parameters will cause the system move to the non-robust stable region where it may become unstable. In contrast, the contingency cases with the line $2-7$ tripping, even though the system is non-robust stable, the security SI is very small, i.e. $SI = \rho = -3.4 \times 10^{-5}$. If appropriate control is applied, the system will be secure in the robust stability region. In this sense, RSA with SI can help the system operators in designing emergency controls.

As aforementioned, it may be impossible to determine the actual values of the instant relaxation times of the loads. Without making any assumption about the load responses, RSA is recommended to run first to screen the most dangerous contingency set. If the RSA certifies that the system is robust stable, no further action is needed; otherwise, deeper analysis or other probabilistic-based assessments such as Monte Carlo simulations are required. Therefore, if RSA is used as the very first screening, the whole process of contingency analysis is expedited.

4.5.3 IEEE 39-bus New England system

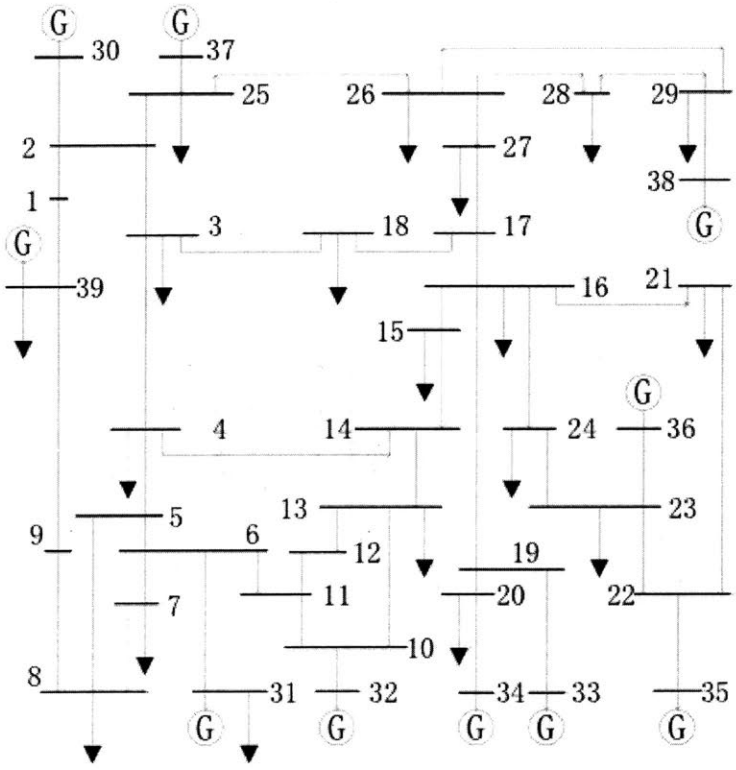

Figure 4-12: The New England system

In this section, I illustrate the concept of robust stability with the IEEE 39-bus New England system. The configuration of the system is shown in Figure 4-12. All generators are identical and have the same set of parameters as the following: $T'_{d0} = 10\,s$; $x_d = 1.0\,p.u.$; $x'_d = 0.2\,p.u.$; $T = 0.39\,s$; $K = 10$. Other system parameters are adopted from [53]. In the considered scenario, all the loads have the same power factor, i.e. $\cos(\phi) = 0.9$ lagging; the load bus 29 is chosen as the reference load and other load levels are increased with the correlated loading factor k_c, i.e. $P_i = k_c P_{29}$, where $i \in \mathcal{L}$, $i \neq 29$. I will consider the situation with identical load power consumptions or $k_c = 1$. The load increments were picked up by evenly distribution among all generators.

For the given scenario, the robust stability of the New England system is illustrated in Figure 4-13 which is similar to that of the rudimentary system and WSCC 3-

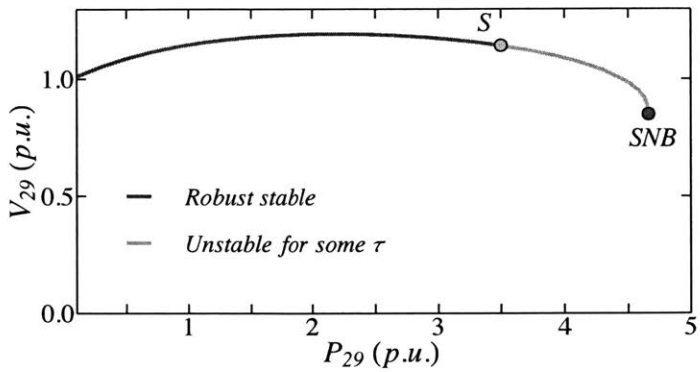

Figure 4-13: Robust stability illustration for the New England system, correlated loading condition $k_c = 1$

machine, 9-bus system. The system is robust stable up to point S where $P_{29} = 3.5\,p.u.$. SNB occurs near $P_{29} = 4.67\,p.u.$. Therefore, the margin from S to SNB is around 25.05%.

I also considered another loading scenario where the base loading levels are adopted from [53]. Then for each load the power factor is kept unchanged while all the load consumptions are scaled with the same scalar factor $k_c > 0$. In this scenario, SNB happens at $k_c = 3.0$ and the system is robust stable up to $k_c = 1.2$. This means that the system can become unstable at some loading level that is above 20% of the normal operating condition. Moreover, the margin from S to SNB is 60%.

4.6 Investigation of the non-certified robust stability region

In Figure 4-4, 4-7, 4-9, and 4-13, the non-certified robust stability regions are in yellow and lie between the robust stable point S and the saddle-node bifurcation point SNB. Different from the robust stability region, the non-robust stability one is mostly affected by the load dynamic uncertainty. The system dynamics and behavior may be very different and complicated because of more pronounced nonlinearity. When

the system is stressed or is subject to disturbances, the system is likely to operate in those regions. Therefore, it is important to explore the non-robust stability regions which may help the system operators to have better understanding of the system. I will address two important questions in this section, i.e. which parameter determines the robust stable point S and how the system behaves in the non-certified robust stability region.

4.6.1 Robust stable point S

The position of point S as well as the robust stability region characterizes the level of "robustness" of the system. For the same configuration, the size of robust stability region might vary from case to case, from scenario to scenario.

Effect of loading levels

I reconsider the scenario with correlated loading condition, i.e. $P_5 = P_6 = k_c P_8$ and $Q_5 = Q_6 = k_c Q_8$ where k_c is the correlation factor. Table 4.2 illustrates how the system loading levels affect the robust stability region. The margin in % measures the distance between point S and SNB compares to the maximum loading level corresponding to SNB.

Table 4.2: Effect of loading levels on S

k_c	0.5	1	2	4
S (*p.u.*)	2.70	1.86	1.07	0.55
SNB (*p.u.*)	3.10	2.16	1.22	0.65
Margin (%)	12.90	13.89	12.30	15.38

From Table 4.2, one can see that an increase in the correlation loading factor resulted in an decrease in the maximum loading level where SNB happens. However, increasing k_c may not necessarily lead to the change in the robust stable point S in such a way that extends the margin between S and SNB.

Effect of load power factors

Various power factors were considered in Table 4.3. One can see that as the load power factors change from lagging to leading, the relative distance between the robust stable point S and SNB increases. This means that the more lagging the power factor is, the wider the robust stable region becomes. Therefore, injecting more reactive powers into the network may shorten the robust stability region relatively.

Table 4.3: Effect of power factor on S

power factor	0.5 *lag*	0.9 *lag*	1.0	0.9 *lead*	0.5 *lead*
S (*p.u.*)	0.95	1.86	2.30	2.40	2.20
SNB (*p.u.*)	1.00	2.16	2.74	3.35	4.80
Margin (%)	5.00	13.89	16.06	28.36	54.17

Effect of exciter gain K

The model of exciter is described in (4.23). In this section, effect of exciter gain K is analyzed in Table 4.4. As observed in [97], the sufficient increase of the exciter gain may lead to instability even for normal loading level. With robust stability analysis, I now can determine at which loading level the exciter gain cannot affect the system stability by considering K as an uncertain parameter.

Table 4.4: Effect of exciter gain K on S

K	5	10	20	30	40	50
S (*p.u.*)	1.60	1.80	1.86	1.87	1.96	1.97
SNB (*p.u.*)	2.16	2.16	2.16	2.16	2.16	2.16
Margin (%)	25.93	16.67	13.89	13.43	9.26	8.79

As expected, the changing in K does not affect the maximum loading level at SNB point. However, surprisingly, an increase in K tends to extend the robust stable region as pushing point S closer to SNB point. When K goes to infinity, point S does not change much and the system is robust stable up to circa $P_8 = 2.00\,p.u.$. This indicates that exciter gain may affect the system stability in a rather complicated manner which depends on the interactions between exciters and generators with other dynamic devices/components; as well as depends on the considered conditions/scenarios.

4.6.2 The system behavior in the region between S and SNB

Since dynamic voltage stability is normally studied by monitoring the eigenvalues of the linearized system [97], I investigate how these factors alter the system eigenvalues in the s-plane. The rudimentary system results are demonstrated as below.

Effect of loading levels

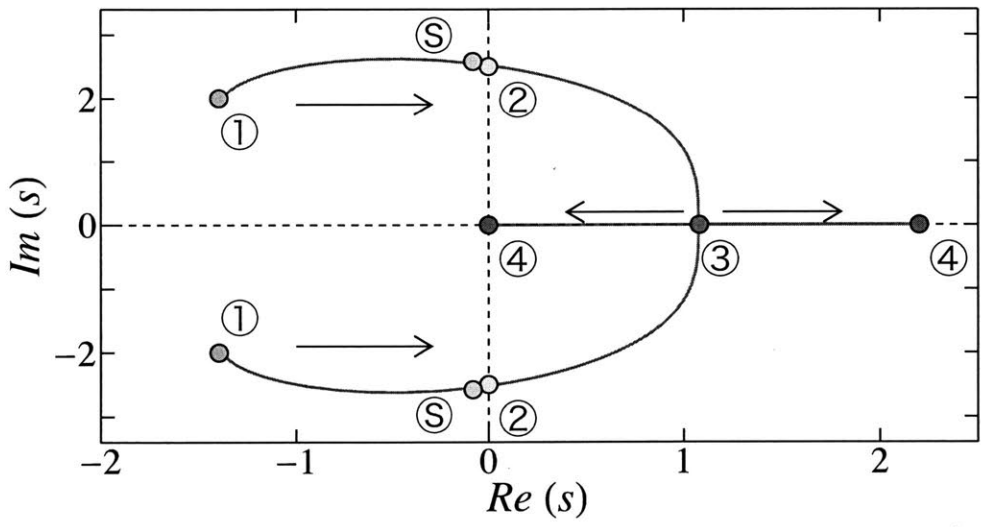

Figure 4-14: Critical eigenvalue trajectory under the load changes in the rudimentary system, $\tau = 7.35\,s$

For $\tau = 7.35\,s$, the trajectory of the critical eigenvalue pair, ①-Ⓢ-②-③-④, is plotted in Figure 4-14 as the load power increases from zero to the maximum loading level. Note, that the enclosed alphanumerics indicate that the corresponding eigenvalues belong to the same system matrix which is related to the same power level consumption P_0. In Figure 4-14, the pair of critical eigenvalues starts at ① with zero power level consumption and move to the right half plane in the s-plane. When the trajectory crosses the imaginary axis at ② where $P_0 = 2.6\,p.u.$, the system encounters Hopf bifurcation. This is also illustrated at point H in Figure 4-4. The eigenvalues

associated with the power level at robust stable point S in RSA are marked with Ⓢ which is close to ②. As the load power continues increasing, the two critical complex eigenvalues coalesce at ③ on the real axis of the s-plane and become a pair of real eigenvalues. Then the pair of critical real eigenvalues diverge following the two arrows towards ④. As soon as the one that moves to the left reaches ④ at the origin, the SNB occurs. Since the load power cannot exceed the maximum loading level, the trajectory ends here at ④. The similar trajectory is also described in [97].

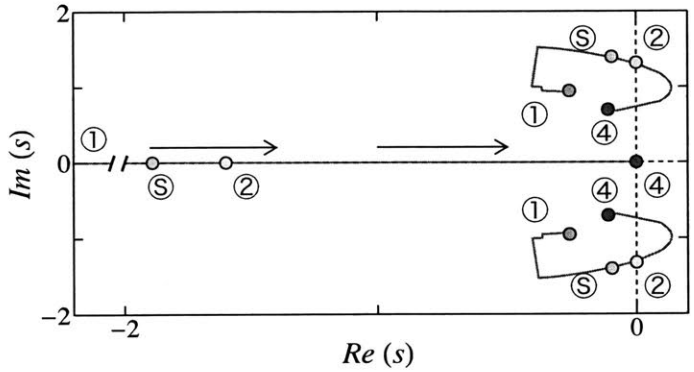

Figure 4-15: Critical eigenvalue trajectory under the load changes in the WSCC 3-machine, 9-bus system

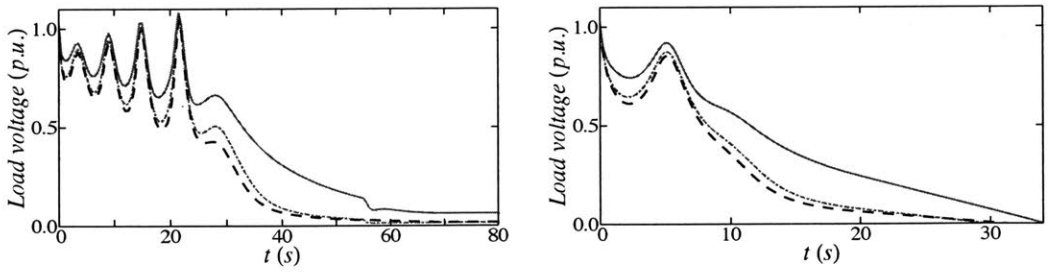

(a) $P_8 = 2\,p.u.$, Unstable

(b) Second Hopf bifurcation, Unstable

Figure 4-16: The load voltage evolutions in time-domain simulations at $P_8 = 2\,p.u.$ and the second Hopf bifurcation of the WSCC 3-machine, 9-bus system

For the WSCC 3-machine, 9-bus system and the considered scenario with $\tau_5 = 6.5\,s$, $\tau_6 = 5.9\,s$, $\tau_8 = 5.35\,s$; the critical eigenvalue trajectories, ①-Ⓢ-②-④ are plotted

in Figure 4-15. In this case, as the load level increases from zero to the maximum loading level, the critical eigenvalue trajectory starts at ① or the point at (−5.7, 0) which is far to the left, then follows the arrows direction to the origin or ④. The critical complex eigenvalue pair also crosses the imaginary axis to the right half plane then returns to the left half plane without coalescency. Along the trajectory the system encounters Hopf bifurcation twice. At ④ where the critical real eigenvalue reaches the origin, SNB happens. Interestingly, there is a small region between the second Hopf bifurcation and SNB, the system is stable. However, in that region, low damping causes the system oscillates under the effect of a disturbance. The corresponding time-domain simulation also indicates that the initial condition need to close to the equilibirum state values to ensure that the system will converge to that equilibirum. This implies that the equilibrium has a small stability region. The trajectories in Figure 4-14 and Figure 4-15 are the two typical transients from Hopf bifurcation to SNB that can be observed when scaling the loading level. They may be different in the region between Ⓢ and ④, but in the end, one single real eigenvalue reaches the origin at ④.

Effect of load power factors

Qualitatively, the load power factor does not change the trajectory of the critical eigenvalues of the system within S-SNB. It mostly pushes the point on the real axis where the critical complex eigenvalues pair merge to the right and widens the distance between the two points on the imaginary axis at ②. The effect on ③ is recorded in Table 4.5 for $\tau = 7.35\,s$.

Table 4.5: Effect of power factor on the critical eigenvalues

power factor	0.89 *lag*	0.98 *lag*	1.0	0.98 *lead*	0.89 *lead*
Re(s) @ ③	0.65	1.10	1.20	2.31	3.56

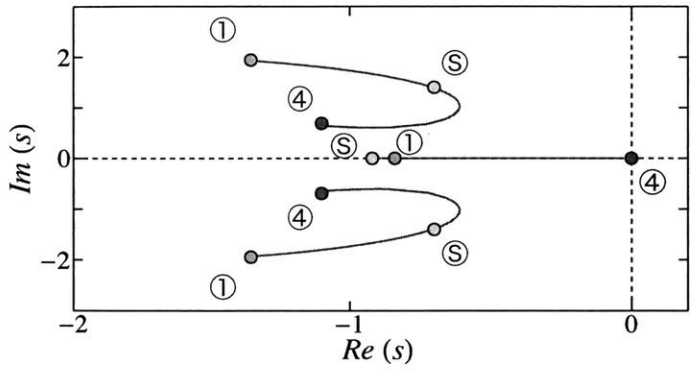

Figure 4-17: Critical eigenvalue trajectory under the load changes in the rudimentary system, $\tau = 1\,s$

Effect of the time constants of the loads

For $\tau = 1\,s$, the trajectory ①-Ⓢ-④ of critical eigenvalues of the system is plotted in Figure 4-17. In this case, Hopf bifurcation will not happen while increasing the loading level P_0, and all eigenvalues lie in the left half plane of the s-plane. At ④, the system encounters SNB or static voltage collapse. Moreover, the whole upper branch of the nose curve PV is stable up to SNB.

When the instant relaxation time of the load increases to a large enough value, for example $\tau > 7.35\,s$, the trajectory of the critical eigenvalues is similar to that in Figure 4-14 except point ③ on the real axis moves to the right. At the same time, Ⓢ also moves towards ② on the imaginary axis but it never reaches ②. This phenomenon can be explained as when the load time constant increases, the system may become unstable right after the robust stable point S. In this sense, if RSA cannot certify the system robust stability, the system is indeed non-robust stable.

From our simulations I found that, if other parameters of the system are kept unchanged, the system is prone to be unstable if the instant relaxation times of the loads increase. This phenomenon can be understood as the larger time constants of the loads add more delay to the system which in turn reduces the phase margin [40], finally causes the system to be unstable. In the s-plane, one can see that increasing

the loads time constants pushes the critical eigenvalues to move close to the imaginary axis. When the critical eigenvalues cross to the right-half plane, the system is likely unstable.

4.7 Conclusions

In this chapter I have addressed the problem of uncertainty of load dynamics and its effect on the stability of the system and in particular on the occurrence of Hopf bifurcation. RSA developed in this work allows to certify the stability of the power system without making any assumptions on the dynamic response of the load. Whenever the system is certified to be robust stable, the system is guaranteed to be stable for any dynamic responses of the loads involved. The algorithm relies on convex optimization and can be applied even to large-scale system models. The regions that are certified to be robust stable are surprisingly large for models considered in the thesis which suggest that Robust-Stability regime can be enforced in planning and operation without compromising efficiency and other economic factors.

Chapter 5

Conclusion & Future work

5.1 Conclusions

The inherent nonlinearity and the complexity of power systems make them fragile and vulnerable to disturbances and uncertainties. A severe consequence is a loss of stability which deemed responsible for major blackouts over last decades in many countries. Therefore, there is an urgent need to assess stability in the presence of uncertainties. This thesis proposes such robust stability assessment for three types on stability including long-term voltage, transient, and small-signal stability in Chapter 2, 3, and 4, respectively. Moreover, inner approximation techniques are developed to estimate the robust stability regions in either injection space or state space. In particular, Chapter 2 introduces a scalable algorithm for estimating the OPF feasibility subsets, and Chapter 3 presents a new approach to construct contraction regions and corresponding attraction basins.

The robust stability assessment techniques developed in this thesis primarily address the needs of a system operator in electrical power systems. The results, however, can be naturally extended to other nonlinear dynamical systems that arise in different fields such as biology, biomedicine, economics, neuron networks, and optimization.

5.2 Future work

For each stability problem considered above, the future extensions are discussed as follows. First, for OPF feasibility region estimation, an important open question considers what tighter bounds on the nonlinear residual terms one can use instead of box type bounds.

Concerning contraction analysis for DAE systems, in the future, I plan to extend our results to develop a more accurate characterization of the contraction of systems with strong time-scale separation and explore how the framework can be used for systematic decomposition of complex and large scale systems for distributed control/analysis purposes.

For robust small-signal stability assessment with load dynamic uncertainty, there are several ways of extending the algorithm that I plan to explore. First, I plan to extend the types of uncertainties that can be handled to uncertainty in static characteristic, load levels, and allow for using the range bounds on the time constants. Second, I plan to develop algorithms that certify the robust stability of whole regions in parameter space, eliminating the need for repeating the procedure for every operating point candidate. Finally, I am interested in applying the algorithm to practical problems like stability constraint remedial action design, stability constraint planning, and others.

More importantly, it is possible to certify robust stability in the presence of both uncertain dynamics and uncertain operating point if block diagonal base metric $Z_\star$ exist, i.e.

$$Z_\star^T J(\xi_\star) + J(\xi_\star)^T Z_\star \preceq 0. \tag{5.1}$$

Here we introduce the base parameter $\xi_\star = (\mathcal{T}_\star, \mathbf{x}_\star)$ where the subscript $\star$ denotes the nominal/base value. By fixing the base metric $Z_\star$, one can apply the SVD-based construction technique represented in Chapter 3 to characterize robust stability regions in the variable space. Moreover, the block diagonal structure ensures that the Lyapunov inequality will still hold as the dynamics characterized by the time

constants $\mathcal{T}$ change. Consequently, within such constructed stability regions, the system is guaranteed to be stable regardless its dynamics.

Bibliography

[1] F.L. Alvarado. Bifurcations in nonlinear systems-computational issues. In *Circuits and Systems, 1990., IEEE International Symposium on*, pages 922–925 vol.2, May 1990.

[2] Z. Aminzarey and E. D. Sontagy. Contraction methods for nonlinear systems: A brief introduction and some open problems. In *53rd IEEE Conference on Decision and Control*, pages 3835–3847, Dec 2014.

[3] P.M. Anderson, A.A.A. Fouad, Institute of Electrical, and Electronics Engineers. *Power System Control and Stability*. IEEE Press Power Systems Engineering Series. Ieee Press, 1977.

[4] D. Angeli. A lyapunov approach to incremental stability properties. *IEEE Transactions on Automatic Control*, 47(3):410–421, Mar 2002.

[5] Liviu Aolaritei, Saverio Bolognani, and Florian Dörfler. A distributed voltage stability margin for power distribution networks. *arXiv preprint arXiv:1612.00207*, 2016.

[6] Erin M Aylward, Pablo A Parrilo, and Jean-Jacques E Slotine. Stability and robustness analysis of nonlinear systems via contraction metrics and sos programming. *Automatica*, 44(8):2163–2170, 2008.

[7] Saverio Bolognani and Sandro Zampieri. On the existence and linear approximation of the power flow solution in power distribution networks. *IEEE Transactions on Power Systems*, 31(1):163–172, 2016.

[8] Bradley N Bond and Luca Daniel. Stable reduced models for nonlinear descriptor systems through piecewise-linear approximation and projection. *Computer-Aided Design of Integrated Circuits and Systems, IEEE Transactions on*, 28(10):1467–1480, 2009.

[9] Gabriel D Bousquet and Jean-Jacques E Slotine. A contraction based, singular perturbation approach to near-decomposability in complex systems. *arXiv preprint arXiv:1512.08464*, 2015.

[10] Stephen Boyd, Laurent El Ghaoui, Eric Feron, and Venkataramanan Balakrishnan. *Linear matrix inequalities in system and control theory*. SIAM, 1994.

[11] Corentin Briat. Linear parameter-varying and time-delay systems. *Analysis, Observation, Filtering & Control*, 3, 2014.

[12] F.L. Byc, B.B. Kobets, N.G. Nesterenko, and E.I. Zel'manov. An approach for decentralized evaluation of regimes in power systems. In *Fifth international conference on present day problems of power system automation and control, Gliwice*, pages 297–301, 1989.

[13] Mary B Cain, Richard P OâĂŹneill, and Anya Castillo. History of optimal power flow and formulations. *Federal Energy Regulatory Commission*, pages 1–36, 2012.

[14] Claudio A Cañizares and Steve Hranilovic. Transcritical and hopf bifurcations in ac/dc systems. *Proc. Bulk Power System Voltage Phenomena III âĂŤVoltage Stability and Security*, pages 105–114, 1994.

[15] A. Chakrabortty and Rensselaer Polytechnic Institute. *Estimation, Analysis and Control Methods for Large-scale Electric Power Systems Using Synchronized Phasor Measurements.* Rensselaer Polytechnic Institute, 2008.

[16] A. Chakrabortty and E. Scholtz. Time-scale separation designs for performance recovery of power systems with unknown parameters and faults. *Control Systems Technology, IEEE Transactions on*, 19(2):382–390, March 2011.

[17] S. Chen and O.P. Malik. Power system stabilizer design using μ synthesis. *Energy Conversion, IEEE Transactions on*, 10(1):175–181, Mar 1995.

[18] H. D. Chiang and C. Y. Jiang. Feasible region of optimal power flow: Characterization and applications. *IEEE Transactions on Power Systems*, PP(99):1–1, 2017.

[19] Hsiao-Dong Chiang. *Direct methods for stability analysis of electric power systems: theoretical foundation, BCU methodologies, and applications.* John Wiley & Sons, 2011.

[20] Hsiao-Dong Chiang and F.F. Wu. Stability of nonlinear systems described by a second-order vector differential equation. *Circuits and Systems, IEEE Transactions on*, 35(6):703–711, Jun 1988.

[21] J.H. Chow, F.F. Wu, and J.A. Momoh. *Applied Mathematics for Restructured Electric Power Systems: Optimization, Control, and Computational Intelligence.* Power Electronics and Power Systems. Springer, 2006.

[22] Carleton Coffrin, Hassan L Hijazi, and Pascal Van Hentenryck. The qc relaxation: A theoretical and computational study on optimal power flow. *IEEE Transactions on Power Systems*, 31(4):3008–3018, 2016.

[23] C. Concordia and S. Ihara. Load representation in power system stability studies. *Power Apparatus and Systems, IEEE Transactions on*, PAS-101(4):969–977, April 1982.

[24] R. Cooke and V.I. Arnold. *Ordinary Differential Equations*. Springer Textbook. Springer Berlin Heidelberg, 1992.

[25] Domitilla Del Vecchio and Jean-Jacques Slotine. A contraction theory approach to singularly perturbed systems with application to retroactivity attenuation. In *2011 50th IEEE Conference on Decision and Control and European Control Conference*, pages 5831–5836. IEEE, 2011.

[26] I. Dobson. An iterative method to compute a closest saddle node or hopf bifurcation instability in multidimensional parameter space. In *Circuits and Systems, 1992. ISCAS '92. Proceedings*, volume 5, May 1992.

[27] I. Dobson, F. Alvarado, and C.L. DeMarco. Sensitivity of hopf bifurcations to power system parameters. In *Decision and Control, 1992., Proceedings of the 31st IEEE Conference on*, pages 2928–2933 vol.3, 1992.

[28] Ian Dobson. Distance to bifurcation in multidimensional parameter space: Margin sensitivity and closest bifurcations. In *Bifurcation control*, pages 49–66. Springer, 2003.

[29] Ian Dobson and Hsiao-Dong Chiang. Towards a theory of voltage collapse in electric power systems. *Systems & Control Letters*, 13(3):253–262, 1989.

[30] Ian Dobson and Liming Lu. New methods for computing a closest saddle node bifurcation and worst case load power margin for voltage collapse. *Power Systems, IEEE Transactions on*, 8(3):905–913, 1993.

[31] Ian Dobson, Liming Lu, and Yi Hu. A direct method for computing a closest saddle node bifurcation in the load power parameter space of an electric power system. In *Circuits and Systems, 1991., IEEE International Sympoisum on*, pages 3019–3022. IEEE, 1991.

[32] Dobson, Ian. The irrelevance of electric power system dynamics for the loading margin to voltage collapse and its sensitivities. *Nonlinear Theory and Its Applications, IEICE*, 2(3):263–280, 2011.

[33] K. Dvijotham, H. Nguyen, and K. Turitsyn. Solvability regions of affinely parameterized quadratic equations. *IEEE Control Systems Letters*, 2(1):25–30, Jan 2018.

[34] K. Dvijotham and K. Turitsyn. Construction of power flow feasibility sets. *ArXiv e-prints*, June 2015.

[35] F. C. Schweppe E. Hnyilicza, S. T. Y. Lee. Steady-state security regions: The set theoretic approach. *Proc. 1975 PICA Conf.*, pages 347–355, 1975.

[36] M.K. El-Sherbiny and D.M. Mehta. Dynamic system stability part i - investigation of the effect of different loading and excitation systems. *Power Apparatus and Systems, IEEE Transactions on*, PAS-92(5):1538–1546, Sept 1973.

[37] Masoud Farivar and Steven H Low. Branch flow model: Relaxations and convexificationâĂŤpart i. *IEEE Transactions on Power Systems*, 28(3):2554–2564, 2013.

[38] Institute for Energy Research. History of electricitys.

[39] AA Fouad, F Aboytes, VF Carvalho, SL Corey, KJ Dhir, and R Vierra. Dynamic security assessment practices in north america. *Power Systems, IEEE Transactions on*, 3(3):1310–1321, 1988.

[40] G.F. Franklin, J.D. Powell, and A. Emami-Naeini. *Feedback control of dynamic systems*. Number v. 10. Pearson, 2010.

[41] David Gale. The game of hex and the brouwer fixed-point theorem. *The American Mathematical Monthly*, 86(10):818–827, 1979.

[42] David J Hill, Mk Pal, Xu Wilsun, Yakout Mansour, Co Nwankpa, L Xu, and R Fischl. Nonlinear dynamic load models with recovery for voltage stability studies. discussion. authors' response. *IEEE Transactions on Power Systems*, 8(1):166–176, 1993.

[43] I Hiskens. Significance of load modeling in power system dynamics. In *x symposium of specialists in electric operational and expansion planning*, 2006.

[44] IA Hiskens and J. Alseddiqui. Sensitivity, approximation, and uncertainty in power system dynamic simulation. *Power Systems, IEEE Transactions on*, 21(4):1808–1820, Nov 2006.

[45] IA Hiskens, M. A Pai, and T.B. Nguyen. Bounding uncertainty in power system dynamic simulations. In *Power Engineering Society Winter Meeting, 2000. IEEE*, volume 2, pages 1533–1537 vol.2, 2000.

[46] Guanji Hou and V. Vittal. Cluster computing-based trajectory sensitivity analysis application to the wecc system. *Power Systems, IEEE Transactions on*, 27(1):502–509, Feb 2012.

[47] Hou, Guanji and Vittal, Vijay. Trajectory sensitivity based preventive control of voltage instability considering load uncertainties. *Power Systems, IEEE Transactions on*, 27(4):2280–2288, 2012.

[48] JA Huang, A Valette, M Beaudoin, K Morison, A Moshref, M Provencher, and J Sun. An intelligent system for advanced dynamic security assessment. In *Power System Technology, 2002. Proceedings. PowerCon 2002. International Conference on*, volume 1, pages 220–224. IEEE, 2002.

[49] IEEE Task Force. Load representation for dynamic performance analysis [of power systems]. *Power Systems, IEEE Transactions on*, 8(2):472–482, May 1993.

[50] IEEE Task Force. Standard load models for power flow and dynamic performance simulation. *Power Systems, IEEE Transactions on*, 10(3):1302–1313, Aug 1995.

[51] M. Ilić and J. Zaborszky. *Dynamics and Control of Large Electric Power Systems*. A Wiley-Interscience publication. Wiley, 2000.

[52] Marija Ilic-Spong, J Thorp, and M Spong. Localized response performance of the decoupled q-v network. *IEEE transactions on circuits and systems*, 33(3):316–322, 1986.

[53] Information Trust Institute (ITI). Publically available power flow and transient stability cases.

[54] Rabih A Jabr. Radial distribution load flow using conic programming. *Power Systems, IEEE Transactions on*, 21(3):1458–1459, 2006.

[55] Charles R Johnson. Sufficient conditions for D-stability. *Journal of Economic Theory*, 9(1):53–62, 1974.

[56] D. Karlsson and D.J. Hill. Modelling and identification of nonlinear dynamic loads in power systems. *Power Systems, IEEE Transactions on*, 9(1):157–166, Feb 1994.

[57] E. Kaszkurewicz and A. Bhaya. *Matrix Diagonal Stability in Systems and Computation*. Birkhäuser Boston, 2000.

[58] U.G. Knight and U. G. Knight. *Power systems in emergencies: from contingency planning to crisis management*. John Wiley, 2001.

[59] Florian Knorn, Oliver Mason, and Robert Shorten. On linear co-positive lyapunov functions for sets of linear positive systems. *Automatica*, 45(8):1943–1947, 2009.

[60] P. Kundur, J. Paserba, V. Ajjarapu, G. Andersson, A. Bose, C. Canizares, N. Hatziargyriou, D. Hill, A. Stankovic, C. Taylor, T. Van Cutsem, and V. Vittal. Definition and classification of power system stability ieee/cigre joint task force on stability terms and definitions. *IEEE Transactions on Power Systems*, 19(3):1387–1401, Aug 2004.

[61] Prabha Kundur. *Power System Stability and Control*. New York, 1994.

[62] Javad Lavaei and Steven H Low. Convexification of optimal power flow problem. In *Communication, Control, and Computing (Allerton), 2010 48th Annual Allerton Conference on*, pages 223–232. IEEE, 2010.

[63] B.C. Lesieutre, P.W. Sauer, and M. A. Pai. Development and comparative study of induction machine based dynamic p, q load models. *Power Systems, IEEE Transactions on*, 10(1):182–191, Feb 1995.

[64] Bernard C Lesieutre, Daniel K Molzahn, Alexander R Borden, and Christopher L DeMarco. Examining the limits of the application of semidefinite programming to power flow problems. In *Communication, Control, and Computing (Allerton), 2011 49th Annual Allerton Conference on*, pages 1492–1499. IEEE, 2011.

[65] F. L. Lewis. Preliminary notes on optimal control for singular systems. *Unknown Journal*, pages 266–272, 1985.

[66] Hang Liu, A. Bose, and V. Venkatasubramanian. A fast voltage security assessment method using adaptive bounding. *Power Systems, IEEE Transactions on*, 15(3):1137–1141, Aug 2000.

[67] Winfried Lohmiller and Jean-Jacques E Slotine. On contraction analysis for non-linear systems. *Automatica*, 34(6):683–696, 1998.

[68] KA Loparo and F Abdel-Malek. A probabilistic approach to dynamic power system security. *IEEE transactions on circuits and systems*, 37(6):787–798, 1990.

[69] Steven H Low. Convex relaxation of optimal power flowâĂŤpart i: Formulations and equivalence. *IEEE Transactions on Control of Network Systems*, 1(1):15–27, 2014.

[70] Yuri V Makarov, Zhao Yang Dong, and David J Hill. A general method for small signal stability analysis. *Power Systems, IEEE Transactions on*, 13(3):979–985, 1998.

[71] Yuri V Makarov, David J Hill, and Zhao-Yang Dong. Computation of bifurcation boundaries for power systems: a new δ-plane method. *Circuits and Systems I: Fundamental Theory and Applications, IEEE Transactions on*, 47(4):536–544, 2000.

[72] Izumi Masubuchi, Yoshiyuki Kamitane, Atsumi Ohara, and Nobuhide Suda. HâĹđ control for descriptor systems: A matrix inequalities approach. *Automatica*, 33(4):669 – 673, 1997.

[73] J McCalley, S Asgarpoor, L Bertling, R Billinion, H Chao, J Chen, J Endrenyi, R Fletcher, A Ford, C Grigg, et al. Probabilistic security assessment for power system operations. In *Power Engineering Society General Meeting, 2004. IEEE*, pages 212–220. IEEE, 2004.

[74] F. John Meyer and K.Y. Lee. Improved dynamic load model for power system stability studies. *Power Engineering Review, IEEE*, PER-2(9):49–50, Sept 1982.

[75] Federico Milano. Power System Analysis Toolbox Reference Manual for PSAT, 5 2010.

[76] J.V. Milanovic and IA Hiskens. Effects of load dynamics on power system damping. *Power Systems, IEEE Transactions on*, 10(2):1022–1028, May 1995.

[77] Daniel K Molzahn, Vikas Dawar, Bernard C Lesieutre, and Christopher L DeMarco. Sufficient conditions for power flow insolvability considering reactive power limited generators with applications to voltage stability margins. In *Bulk Power System Dynamics and Control-IX Optimization, Security and Control of the Emerging Power Grid (IREP), 2013 IREP Symposium*, pages 1–11. IEEE, 2013.

[78] GK Morison, B Gao, and P Kundur. Voltage stability analysis using static and dynamic approaches. *Power Systems, IEEE Transactions on*, 8(3):1159–1171, 1993.

[79] K. Morison, H. Hamadani, and Lei Wang. Practical issues in load modeling for voltage stability studies. In *Power Engineering Society General Meeting, 2003, IEEE*, volume 3, pages 1392–1397 Vol. 3, July 2003.

[80] K. Morison, L. Wang, and P. Kundur. Power system security assessment. *Power and Energy Magazine, IEEE*, 2(5):30–39, Sept 2004.

[81] H.D. Nguyen and K. Turitsyn. Robust stability assessment in the presence of load dynamics uncertainty. *Power Systems, IEEE Transactions on*, PP(99):1–16, 2015.

[82] Hung Nguyen, D. and Konstantin Turitsyn. Voltage multistability and pulse emergency control for distribution system with power flow reversal. *arXiv preprint arXiv:1407.1355*, 2014.

[83] Hung D Nguyen, Krishnamurthy Dvijotham, Suhyoun Yu, and Konstantin Turitsyn. A framework for robust steady-state voltage stability of distribution systems. *arXiv preprint arXiv:1705.05774*, 2017.

[84] Nguyen, Hung D and Turitsyn, Konstantin S. Appearance of multiple stable load flow solutions under power flow reversal conditions. In *PESGM*. IEEE, 2014.

[85] Ontario Hydro . Voltage stability/security assessment and on-line control: Volumes 1-4, May 1, 1993.

[86] S.S. Oren. Risk management vs. risk avoidance in power systems planning and operation. In *PESGM 2007. IEEE*, pages 1–3, June 2007.

[87] Thomas J Overbye and Christopher L De Marco. Voltage security enhancement using energy based sensitivities. *Power Systems, IEEE Transactions on*, 6(3):1196–1202, 1991.

[88] TJ Overbye. Effects of load modelling on analysis of power system voltage stability. *International Journal of Electrical Power & Energy Systems*, 16(5):329–338, 1994.

[89] AD Patton. A probability method for bulk power system security assessment, i-basic concepts. *IEEE Transactions on Power Apparatus and Systems*, (1):54–61, 1972.

[90] Power Systems Engineering Research Center. Estimation of synchronous generator parameters from on-line measurements. *PSERC Publication 05-36*, 2005.

[91] P.B. Reddy and I.A. Hiskens. Limit-induced stable limit cycles in power systems. In *Power Tech, 2005 IEEE Russia*, pages 1–5, June 2005.

[92] I.C. Report. Excitation system models for power system stability studies. *Power Apparatus and Systems, IEEE Transactions on*, PAS-100(2):494–509, Feb 1981.

[93] A. Rudkevich. Locational assessment of resource adequacy and co-optimization of generation and transmission expansion. the FERC Technical Conference on Increasing Real-Time and Day-Ahead Market Efficiency through Improved Software, June 26, 2012.

[94] Björn S Rüffer, Nathan van de Wouw, and Markus Mueller. Convergent systems vs. incremental stability. *Systems & Control Letters*, 62(3):277–285, 2013.

[95] Giovanni Russo, Mario di Bernardo, and Jean-Jacques E Slotine. A graphical approach to prove contraction of nonlinear circuits and systems. *IEEE Transactions on Circuits and Systems I: Regular Papers*, 58(2):336–348, 2011.

[96] Andrija T Saric and Aleksandar M Stankovic. Applications of ellipsoidal approximations to polyhedral sets in power system optimization. *IEEE Transactions on Power Systems*, 23(3):956–965, 2008.

[97] P.W. Sauer and A. Pai. *Power System Dynamics and Stability.* Prentice Hall, 1998.

[98] S.C. Savulescu. *Real-Time Stability Assessment in Modern Power System Control Centers.* IEEE Press Series on Power Engineering. Wiley, 2009.

[99] Steffen Schulz. Four lectures on differential-algebraic equations. Technical report, Department of Mathematics, The University of Auckland, New Zealand, 2003.

[100] Olivier Sename, Peter Gaspar, and József Bokor. *Robust control and linear parameter varying approaches: application to vehicle dynamics*, volume 437. Springer, 2013.

[101] John W Simpson-Porco. A theory of solvability for lossless power flow equations–part i: Fixed-point power flow. *IEEE Transactions on Control of Network Systems*, 2017.

[102] John W Simpson-Porco. A theory of solvability for lossless power flow equations–part ii: Conditions for radial networks. *IEEE Transactions on Control of Network Systems*, PP(99):1–1, 2017.

[103] John W Simpson-Porco, Florian Dörfler, and Francesco Bullo. Voltage collapse in complex power grids. *Nature communications*, 7, 2016.

[104] Jean-Jacques E Slotine. Modular stability tools for distributed computation and control. *International Journal of Adaptive Control and Signal Processing*, 17(6):397–416, 2003.

[105] Jean-Jacques E Slotine, Weiping Li, et al. *Applied nonlinear control*, volume 60. Prentice-Hall Englewood Cliffs, NJ, 1991.

[106] Kiyotsugu Takaba, Naoki Morihira, and Tohru Katayama. A generalized lyapunov theorem for descriptor system. *Systems & Control Letters*, 24(1):49 – 51, 1995.

[107] C.W. Taylor, N.J. Balu, and D. Maratukulam. *Power System Voltage Stability*. EPRI PES series. McGraw-Hill Education, 1994.

[108] Dy-Liacco Tomas Enciso. Control of power systems via the multi-level concept, 1968.

[109] Thierry Van Cutsem and Costas Vournas. *Voltage stability of electric power systems*, volume 441. Springer, 1998.

[110] V.P. Vasin. Regions of power system operating point existence and their analytic estimates. *internal report of Energoset'proekt (in Russian)*, 1985.

[111] D. Del Vecchio and J. J. E. Slotine. A contraction theory approach to singularly perturbed systems. *IEEE Transactions on Automatic Control*, 58(3):752–757, March 2013.

[112] V. Venkatasubramanian, H. Schattler, and J. Zaborszky. Voltage dynamics: study of a generator with voltage control, transmission, and matched mw load. *Automatic Control, IEEE Transactions on*, 37(11):1717–1733, Nov 1992.

[113] George Verghese, Bernard Lévy, and Thomas Kailath. A generalized state-space for singular systems. *IEEE Transactions on Automatic Control*, 26(4):811–831, 1981.

[114] M Vidyasagar. On matrix measures and convex liapunov functions. *Journal of Mathematical Analysis and Applications*, 62(1):90 – 103, 1978.

[115] M. Vidyasagar. *Nonlinear Systems Analysis*. Society for Industrial and Applied Mathematics, second edition, 2002.

[116] Vijay Vittal, Wenzheng Qiu Mustafa Khammash, Chuanjiang Zhu, Rod Holland Peter Young, and Christopher DeMarco. Robust control of large scale power systems. *PSERC Publication 02-43*, 2002.

[117] Cong Wang, Andrey Bernstein, Jean-Yves Le Boudec, and Mario Paolone. Existence and uniqueness of load-flow solutions in three-phase distribution networks. *IEEE Transactions on Power Systems*, 2016.

[118] Felix F Wu and Sadatoshi Kumagai. Steady-state security regions of power systems. *Circuits and Systems, IEEE Transactions on*, 29(11):703–711, 1982.

[119] Hansheng Wu and K. Mizukami. Stability and robust stabilization of nonlinear descriptor systems with uncertainties. In *Proceedings of 1994 33rd IEEE Conference on Decision and Control*, volume 3, pages 2772–2777 vol.3, Dec 1994.

[120] Le Xie, Yang Chen, and Huaiwei Liao. Distributed online monitoring of quasi-static voltage collapse in multi-area power systems. *Power Systems, IEEE Transactions on*, 27(4):2271–2279, Nov 2012.

[121] Le Xie, J Ilic, and MD Ilic. Novel performance index and multi-layered information structure for monitoring quasi-static voltage problems. In *PESGM, 2007. IEEE*, pages 1–7. IEEE, 2007.

[122] Wilsun Xu and Y. Mansour. Voltage stability analysis using generic dynamic load models. *Power Systems, IEEE Transactions on*, 9(1):479–493, Feb 1994.

[123] S. Yu, H. D. Nguyen, and K. S. Turitsyn. Simple certificate of solvability of power flow equations for distribution systems. In *2015 IEEE Power Energy Society General Meeting*, pages 1–5, July 2015.

[124] Yuan Zhou and V. Ajjarapu. A fast algorithm for identification and tracing of voltage and oscillatory stability margin boundaries. *Proceedings of the IEEE*, 93(5):934–946, May 2005.